IMAGE ANALYSIS OF CORROSION PIT INITIATION ON ASTM TYPE A240 STAINLESS STEEL AND ASTM TYPE A 1008 CARBON STEEL

A THESIS

SUBMITTED TO THE FACULTY OF THE
UNIVERSITY OF MINNESOTA
BY

H M ZULKER NINE

IN PARTIAL FULFILLMENT OF THE REQUIREMENTS
FOR THE DEGREE OF
MASTER OF SCIENCE

ADVISOR: DR. BRIAN HINDERLITER, P.E, CHP

February 2016

ACKNOWLEDGEMENT

I want to express my deepest gratitude to my supervisor, Dr. Brian Hinderliter, a respectable scholar; whose encouragement, guidance, and support from the beginning to the end enabled me to develop an understanding of the subject and also for giving me the privilege of working under his supervision. The knowledge and skills that I have learned from him especially those wonderful conversations about research, coursework and overall life, will be motivating me continuously in my future endeavors.

Also thankful to Dr. Hongyi Chen for her encouraging advice and organized class lectures, which helped me a lot to channel my thoughts into different projects.

Finally special thanks to Dr. Elizabeth Hill, for agreeing to serve on the thesis committee.

H M Zulker Nine

ABSTRACT

The adversity of metallic corrosion is of growing concern to industrial engineers and scientists. Corrosion attacks metal surface and causes structural as well as direct and indirect economic losses. Multiple corrosion monitoring tools are available although those are time-consuming and costly. Due to the availability of image capturing devices in today's world, image based corrosion control technique is a unique innovation. By setting up stainless steel SS 304 and low carbon steel QD 1008 panels in distilled water, half-saturated sodium chloride and saturated sodium chloride solutions and subsequent RGB image analysis in Matlab, in this research, a simple and cost-effective corrosion measurement tool has identified and investigated. Additionally, the open circuit potential and electrochemical impedance spectroscopy results have been compared with RGB analysis to gratify the corrosion. Additionally, to understand the importance of ambiguity in crisis communication, the communication process between Union Carbide and Indian Government regarding the Bhopal incident in 1984 was analyzed.

Table of Contents

List of Figures

List of Tables

Chapter 1: Introduction

1.1. Corrosion in general

In modern society, human lives are significantly intruded by the adversity of corrosion. Perhaps we come close to corrosion at first hand when we find our heating pipe or gas pipe or the automobile in our driveway, whose loan has not yet been paid off has become the victim of corrosion. From our driveway to the large oil rigs in the ocean; from a backyard heating pipe to the long intercontinental pipelines; from the cooking utensils to the shuttle in outer space, corrosion invades everywhere. To combat corrosion, government, and industries in every nation have taken many measures. Billions in various currencies are spent worldwide to prevent corrosion. Research shows that industrial countries spend on average 5% of nation's income on corrosion prevention and maintenance [4]. To prevent corrosion and raise public awareness, corrosion professionals and scientists are studying and developing cutting edge technologies, practicing effective management strategies for decades.

1.2. Thesis objective

The primary objective is to identify a simple camera based computational tool and compare with electrochemical measurement technique to estimate the corrosion damage for a given metal in a particular environment. There are several corrosion monitoring techniques used widely in industry; radiographic testing, electromagnetic testing, ultrasonic testing, and guided wave testing are few of those. All these methods require the presence of an expert in the field and are costly. Interestingly, the easy access to optical cameras offers a low-cost corrosion monitoring tool in addition to standard evaluation protocols that are used by trained professionals.

In this study, ASTM type A 240 stainless steel (SS 304) and ASTM type A 1008 low carbon steel (QD 1008) were investigated under distilled water, half-saturated sodium chloride (NaCl) and saturated sodium chloride (NaCl) solutions. After analyzing the captured images, results were plotted to correlate with electrochemical results.

Despite having a corrosion prevention process, corrosion can attack in industrial operation and can cause tremendous crisis. Industrial accidents push the organization to their limit

and compel them to deal with the crisis. However, managing crisis requires different sets of techniques and communication is one of those. While exploring literatures, the case study of crisis communication by Union Carbide after the chemical explosion at one of their plant in Bhopal, India was found intriguing as it revealed the importance of an effective communication process which includes ambiguity. Additionally, due to the humid sub-tropical climate of Bhopal, the possibility of the presence of various salts including sodium chloride relates its environment with the corrosion experiments of this study.

Therefore, as a secondary objective, crisis management through effective communication will be explored using the case of Union Carbide chemical explosion in Bhopal, India.

1.3. What is corrosion?

Corrosion is the degradation of a material due to its chemical reaction with the surrounding environment. It is a natural process, and this degradation implies the deterioration of the physical properties in the form of weakening of the material due to loss of cross-sectional area, cracking due to hydrogen embrittlement or degradation due to sunlight exposure [16]. These materials can be metals, polymers or composites-mechanical mixtures of two or more materials with different properties. Structural alloys merely corrode from exposure to moisture in the environment however the process can be strongly affected due to the presence of certain chemical substances.

Metallic corrosion is chemical in nature whereas many non-metallic materials such as ceramics are chemically nonreactive, and they degrade by physical breakdown, mechanical wear, and erosion. The corrosion of polymers is a bit different than the rest, and failure often occurs due to cracking and brittleness [17]. Corrosion can be local, in a form of a pit or crack, or it can extend to the entire surfaces.

1.4. Corrosion on metallic surface

Metallic corrosion involves the destructive attack on the metal by chemical or electrochemical reaction with its environment. Except few precious metals (Gold, Platinum, and Silver) most of the metals are found as minerals or ores in nature which are more stable oxide forms. They are then extracted to metallic form for commercial use. The

unstable character of the metallic form initiate the chemical reaction between the metals and surrounding aqueous and non-aqueous solutions [1]. This chemical reaction is the outcome of both oxidation and reduction reactions in the electrolyte solutions. In an oxidation reaction, the metal leaves electron and becomes positively charged metallic ions whereas in reduction reaction solution substance (most of the time H^+) receives the electron and turns into atomic form. Energy is transferred in these reactions, and the corrosion rate is determined by the equilibrium of these two reactions. Let us consider the reaction between iron (Fe) and sulphuric acid (H_2SO_4)

$$\text{Fe} + H_2SO_4 \rightarrow \text{Fe}SO_4 + H_2$$

Now in the solution of sulfuric acid, electron will be transferred, and the ionic form of the above equation can be written as,

$$Fe + 2H^+ + SO_4^{2-} \rightarrow Fe^{2+} + SO_4^{2-} + H_2$$

Eliminating SO_4^{2-} the reaction stands down to

$$Fe + 2H^+ \rightarrow Fe^{2+} + H_2$$

Thus, the corrosion reaction can be separated by anodic and cathodic reactions.

$$Fe \rightarrow Fe^{2+} + 2e^- \qquad \text{Anodic/Oxidation reaction}$$

$$2H^+ + 2e^- \rightarrow H_2 \qquad \text{Cathodic/Reduction reaction}$$

Metals are the vital resources for almost all types of commercial productions. The dependency on different metallic resources has made today's industry more diverse. Due to the high industrial importance, this study focuses on both stainless and low carbon steel.

Steel, which is the alloy of iron and other metals, is widely used in industries because of the chemical durability, mechanical properties, weldability and heat resistant properties [6]. According to the World Steel Association, worldwide crude steel production in August 2015 was 132.3 million tons [18]. Steels are aggressively used in transportation, building and infrastructure, energy, cooking utensils, watches, guns, wires, medical device, reinforced concrete and many more places. The different application of steel often puts the

unintentional risk of corrosion attack and due to the hidden corrosion initiation, the identification of corrosion damage can be quite challenging.

1.5. Cost of corrosion

1.5.1. Economic

As a naturally occurring phenomenon, corrosion impacts both directly and indirectly in our life. The degradations and damages caused by corrosion are spread from the home appliance, water pipeline, automobiles to large scale infrastructure and affect substantially to individual's life. A study reveals that in 2001, the annual per capita corrosion cost in the United States was $970 per person [4].

The severity of economic damages due to corrosion could be better understood if it is compared to the financial losses from natural disasters. Natural disaster is one of the significant sectors that inhibits the economic growth in the US each year by damaging lives, infrastructures, transportations, electricity and overall daily works. From 1980 to 2003, in this 23 years, the estimated losses in the United States due to the natural disaster were $350 billion (averaging $15 billion annually) [22]. However, the 2-year breakthrough study, released by U.S. Federal Highway Administration (FHWA) shows that the annual direct cost due to only metallic corrosion is $276 billion which is approximately 3.1% of the country's gross domestic product (GDP) [4]. Moreover from a global perspective, worldwide direct corrosion cost is in between 1.3 to 1.4 trillion euro that is around 3% of world's GDP [6].

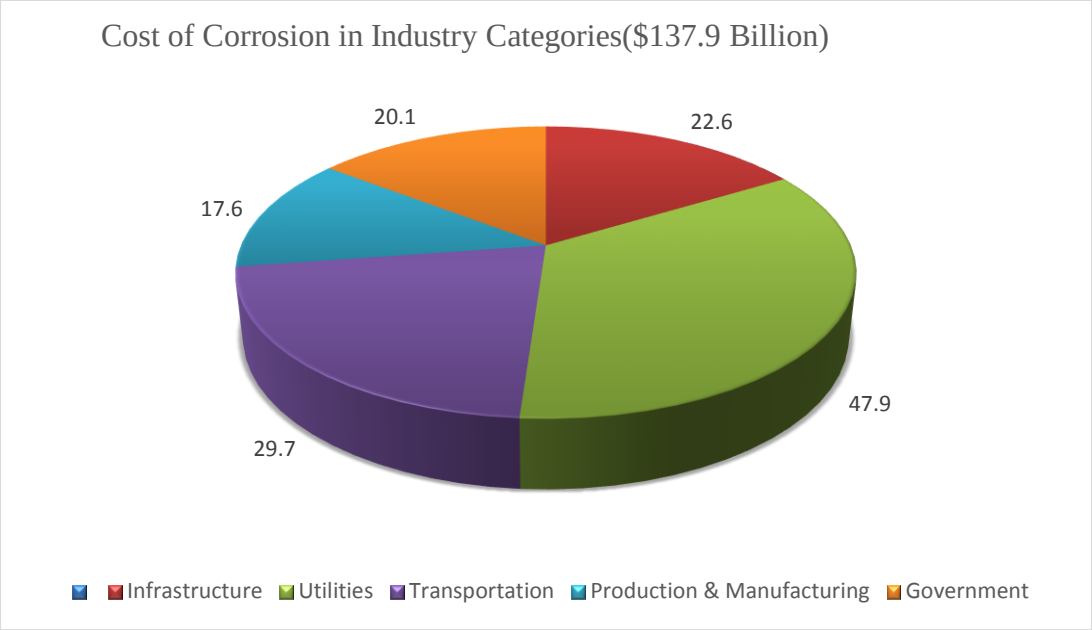

Figure 1.1: Sector-wise direct corrosion cost distribution in the United States. Recreated from data provided in [4]

Figure 1.1 demonstrates direct corrosion cost across the five top industrial categories of US economy with a total value of $137.9 billion. From this figure, the cost of corrosion was extrapolated to the overall US economy ($8.79 trillion) for an annual cost of corrosion of $276 billion. However, this figure only shows the direct cost of corrosion, while the indirect costs are more severe probably even greater and are summarized in next section.

1.5.1.1. Plant downtime

The economic loss due to inoperable plant is higher than the repair cost. Especially in a large power plant or a continuous production facility, every minute count and is considered as profit. The attack of corrosion in these type of scenarios can sometimes cost millions of dollars per day.

1.5.1.2. Loss of product

Corrosion causes leaking in pipelines, tanks, containers result in tremendous losses of high priced liquid products. Also, due to leaking the surrounding environment also faces the threat of contamination, if the product is hazardous. The lost products cannot often be recovered and put the companies into a financially risky situation.

1.5.1.3. Loss of efficiency

Due to corrosion products, metallic surfaces deteriorate and loses efficiency as well. For example the efficiency of heat transfer in a tube and the pumping capacity of a pipeline significantly affected due to corrosion attack.

1.5.1.4. Contamination

Corrosion products threaten the environment and the surrounding lives greatly with contamination. The majority of the corrosion contamination can be traced to the leaks from tanks and pipelines containing oil, gas, chemicals, sewage, colored dyes, etc. For example, the presence of high levels of bacteria in the oil supplied from Pembina Oilfield of North Central Albert, Canada to Montreal was due to the corroded pipeline [23]. In most of the cases sulfate reducing bacteria produces the pit and perforation in a carbon steel heavy pipe [24]. These types of leaking harm the marine lives adversely and can cause the death of marine fauna.

In a nuclear power plant, the stress corrosion cracking and deposition of activated corrosion products are the two biggest corrosion challenges. Radioactive nuclear wastes are transported through the pipeline, and strict corrosion inspection is required to prevent any form of leaking.

1.5.1.5. Overdesign

Sometimes in a remote and isolated places, where much information is not available, engineers and designers make overdesign of equipment and pipeline to prevent failure due to corrosion attack. As corrosion is often a naturally slow process, it requires periodic checking and interpretable information. But in a severe condition, like long pipeline through thousands of miles of ice, river or ocean, extra precautionary overdesign can ensure safety. But this overdesign cost the company huge amount of wasted resources as well as capital. Moreover, additional resources might be spent to meet different federal regulations.

1.5.2. Human life and safety

Besides the economic impact, corrosion causes a significant toll on human life and safety. There have been quite some incidents over the last century in many places due to corrosion and caused catastrophic accidents.

1.5.2.1. Chemical plant explosion in Bhopal, India 1984

By far regarding death, injury and long-term health issues, the explosion of a chemical plant, Union Carbide India Limited (UCIL) in Bhopal, India in 1984 was the worst. The plant was established to produce fertilizers and insecticides and was part of India's Green Revolution [7]. The design flaw and management problem were the ultimate reasons for the disaster. It is reported that the steel pipes containing water, were corroded and water leaked into methyl isocyanate (MIC) tanks. Iron came with water as a corrosion product and acted as a catalyst for the explosion [44]. The sign of corrosion was evident in many pieces of equipment of the plant. The aftermath was a massacre.

Figure 1.2: Deteriorating section of the MIC plant, decades after the gas leak (By Simone.lippi at it.wikipedia [CC BY-SA 2.0 (http://creativecommons.org/licenses/by-sa/2.0)], from Wikimedia Commons) [25]

According to the Madhya Pradesh Government of India, approximately 4000 were dead due to the toxic gas release and 500,000 were injured both permanently and temporarily. Additionally, another 8000 died as a consequence of toxicity within few years [25]. After a long and tedious legal action, the parent company Union Carbide, USA paid $470 million for the damages caused by the Bhopal explosion in 1989. A number of laws were enacted since the incident, and it became one of the tragic events in history.

Perhaps if the workers had a simple way to monitor that pipeline corrosion; a camera to capture the image and send to the management, it could have prevented the disaster.

1.5.2.2. Sinking of the Tongan inter-island ferry, 2009

In 2009, the inter-island ferry "MV Princess Ashika" in Tonga, a Polynesian sovereign state; sank just after a month of commissioning. All the 68 passengers and four crew members died. The investigation found that the entrances on the ferry were unable to close entirely due to corrosion and was advised not to sail. Poor management along with corrosion attack caused the deaths of many innocent people.

1.5.2.3. Berlin Hall collapse, 1980

In 1980, the spectacular Berlin Congress Hall, a sign of friendship between USA and Germany collapsed due to the failure of corrosion prevention. It was built in 1957 and was a unique architecture with a curved canopied concrete panel. In this type of panel, a metal or plastic duct forms the framework and high strength steels are inserted into the duct and are fixed at one end. After that, the concrete is placed and hardened, while the other free end is pulled in tension and anchored. Grout is used to fill the duct to allow load sharing between concrete and steel. The steel is protected from active corrosion by high alkaline concrete and grout.

Figure 1.3: Previous and Post images of Berlin Congress Hall By Berthold Werner (Own work) [GFDL (http://www.gnu.org/copyleft/fdl.html) or CC-BY-SA 3.0 (http://creativecommons.org/licenses/by-sa/3.0)], via Wikimedia Commons [26]

The post analysis of the collapse discovered that the steels were not placed correctly, therefore, they were not properly surrounded by concrete. Due to this factor, the passivation

didn't work all over the surface, and the supports were subject to cracking after several years. One person died in that accident, and five were injured.

1.5.2.4. Failure of Aloha airline flight, 1988

In 1988, the flight 243 of Aloha Airlines, from Hilo to Honolulu in Hawaii experienced explosive decompression inside the flight at 24,000 feet [7]. The explosion tore off a portion of the cockpit, and the flight control went loose. Although the crew managed to land the plane safely, a flight attendant was swept overboard from 24,000 feet and assumed dead with eight others were injured. US National Transportation Safety Board concluded the investigation that, the accident was due to metal fatigue by crevice corrosion [27].

In addition to the examples mentioned above, in 1967 a bridge collapsed at Pt. Pleasant, West Virginia resulted in the death of 46 people. The reason was stress corrosion cracking. Also in 1986 due to the corrosion attack on welded liquid gasoline pipeline in Minnesota caused massive fire damage and two were dead [1].

These are only a few examples of the many fatal accidents resulted by corrosion. In many cases the management showed negligence to identify and address corrosion or administrative bodies were not sufficiently concerned or proper tools or technologies were not available. Even in modern days similar or bigger accidents are happening in industries due to lack of easily accessible corrosion monitoring tools. Due to the availability of image capturing devices all around, engineers and workers could utilize those methods in corrosion monitoring if an image-based monitoring tool is available. Therefore, it is expected that the primary focus of this research will initiate an important step in this field.

1.6. Corrosion measurement

1.6.1. Corrosion measuring standards

Many organizations have contributed to set a structured, and acceptable corrosion measurement procedure, out of which, American Society for Testing and Materials (ASTM) and National Association of Corrosion Engineers (NACE) have extensive explanations.

1.6.1.1. ASTM corrosion standard

ASTM has developed an extensive standard protocol for corrosion and wear monitoring. Some relevant standards are mentioned in following Table 1.1.

Table 1.1: ASTM corrosion standards [52]

Standard	Designation	Title
Atmospheric Corrosion	G33-99 (2015)	To record data from atmospheric corrosion tests of metallic-coated steel specimens
	G50-10(2015)	Standard to conduct atmospheric corrosion tests on metals
	G84-89(2012)	Standard for measurement of time of wetness on surfaces exposed to wetting conditions as in atmospheric corrosion testing
	G91-11	Standard practice to monitor atmospheric SO_2 deposition rate for atmospheric corrosion evaluation
	G92-86(2015)	Standard for characterization of atmospheric test sites
	G101-04(2015)	Standard for estimating atmospheric corrosion resistance of low-alloy steels
	G116-99(2015)	Standard for conducting wire-on-bolt test for galvanic corrosion
	G140-02(2014)	Standard test method for determining atmospheric chloride deposition rate by wet candle method.
Natural water corrosion	G52-00(2011)	Standard practice for exposing and evaluating metals and alloys in surface seawater.
		Standard guide for crevice corrosion testing of iron

	G78-15	base and nickel base stainless alloys in seawater and other chloride-containing aqueous environments
Laboratory corrosion tests	G16-13	Standard guide for applying statistics to analysis corrosion data
	G46-94(2013)	Standard to examine and evaluate pitting corrosion
	G48-11(2015)	Standard test method for pitting and crevice corrosion resistance of stainless steel and alloys by using ferric chloride solution
	G112-92(2015)	Standard for conducting exfoliation corrosion tests in aluminum alloys

The above table represents a few among the many standards of ASTM corrosion and wear standard.

1.6.1.2. NACE corrosion standard

NACE has developed their corrosion standards, and some of the relevant standards are mentioned in below Table 1.2.

Table 1.2: NACE corrosion standards [53]

Item Number	Designation	Title
21017	SP0775-2013	Standard for installation, preparation, analysis and interpretation of corrosion coupons in oilfield
21026	RP0281-2004	Standard method to evaluate panel coating in atmospheric exposures.
21035	RP0287-2002	Standard to measure surface profile of abrasive blast-cleaned steel surface by using a replica tape

21061	RP0193-2001	Standard for external cathodic protection of on-grade carbon steel storage tank bottoms
21091	SP0200-2008	Standard for steel cased pipeline practices
21097	ANSI/NACESP0502-2010	Standard direct assessment methodology for pipeline external corrosion
21166	SP0112-2012	Standard for corrosion management of atmospherically exposed reinforced concrete structure

1.6.2. Corrosion measurement techniques- a literature review

Industrial engineers and corrosion scientists have been investigating different cost efficient and simple corrosion monitoring and measurement techniques for decades. The extensive literature search resulted in a considerable quantity of research articles published on corrosion measurement techniques. In the following sections, few of those advanced methods will be summarized.

1.6.2.1. Visual inspection

Among various optical corrosion inspection techniques, using of 'coupons' and 'probes' are two efficient and cheap corrosion monitoring methods and widely used in industry.

Predetermined in shape, size and surface, coupons are made of metal that exhibits chemical similarity with any process equipment as shown in Figure 1.4 [51]. After inserting the coupons into the process stream, they are taken out to access the weight and corrosion rate to measure the physical damage of process equipment due to corrosion attack.

Like coupons, 'probes' are also widely used corrosion measuring devices. Probes have an electrical connection that allows them to link with electronic instruments of the process equipment shown in Figure 1.5. Probes provide quantitative data that can be translated to much useful information like reduction of wall thickness etc.

1.6.2.2. Spectroscopic measurements

Corrosion products can be characterized using spectroscopic techniques like Raman Spectroscopy, Fourier Transform Infrared Spectroscopy (FTIR), X-ray diffraction (XRD) and Infrared Photography, etc. Metallic corrosion produces chemical compounds of different nature. These compounds have different spectral characteristics based on solar irradiance spectrum (300 to 2500 nm) [28]. Solar spectrum has three main categories; ultraviolet range (300-400 nm), visible light range (400-700 nm) and near infrared (700-2500 nm).

It is interesting to mention that in their comprehensive research work, Ronen Levinson, Paul Berdahl, and Hashem Akbari experimented with 87 samples of coating pigments (iron oxide, chrome oxide, cobalt aluminate, chrome titanate, etc.) and characterized their optical properties i.e. reflectance, transmittance, and absorption. As we know, the most common corrosion products of stainless steel exposed to the aqueous and atmospheric environment are iron (III) oxide i.e. Fe_2O_3 and based on stainless steel composition chrome oxide. Now in this article, the researchers predicted the reflectance and found a good match with the measured reflectance in visible solar spectrum range for Fe^{3+} oxides having reddish color while Cr^{3+} oxides are showing green color [39]. Fe_2O_3 is known as hematite that is a mineral, brown to red in color and is considered as the main ore of iron [11]. Researcher David M. Sherman and David Waite from MIT analyzed the electronic spectra of Fe^{3+} oxides, and they found the visible and near-UV absorption spectra of different iron oxides in Figure 1.6

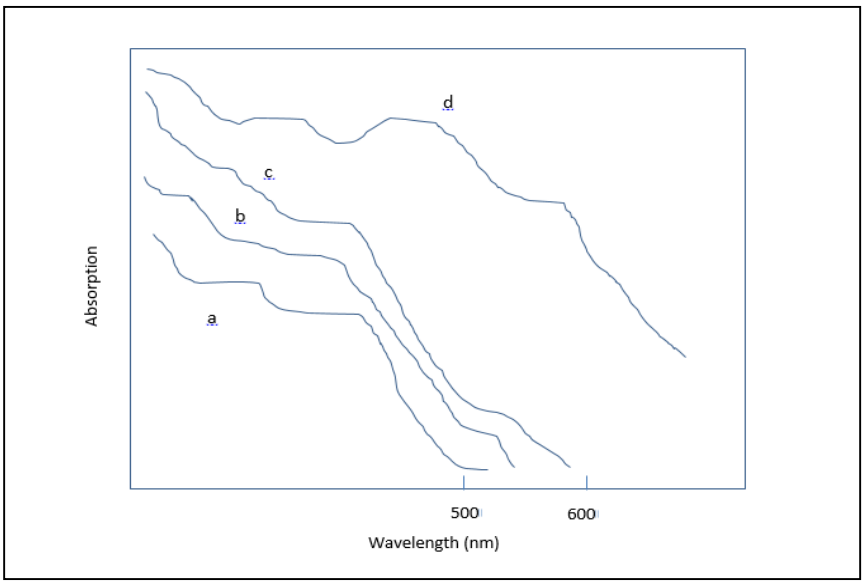

Figure 1.6: Visible and near-UV absorption spectra of (a) goethite (b) lepidocrocite (c) maghemite and (d) hematite. Recreated from [10]

It is clear from the above figure that, the spectrum of hematite appeared as a distinct feature in the visible light zone.

Researcher Jeong-Seb Han and Jin-Hwan Park from South Korea, have estimated corroded area on steel by measuring the temperature distribution at the surface, through an infrared camera [29]. This technique is known as Infrared thermography in which the sample is heated or cooled, and the possible defects can be visible from the localized temperature regions on the surface. Additionally, they were able to identify and quantify iron oxides from the 3-D analysis of the temperature.

In another article, to investigate the red mud, researcher Sara J Palmer and Ray L. Frost used ultra-violet (UV), visual and near infrared (NIR) diffuse reflectance spectroscopic approach at Queensland University of Technology, Brisbane, Australia. Red mud (RM) is an insoluble residue that is found after Bayer process refinement [30]. The composition of red mud is largely iron oxides, hematite (Fe_2O_3), goethite (FeOOH), boehmite [γ-AlO (OH)], other aluminum hydroxides, calcium oxides, titanium oxides and alumino-silicate minerals [31][32]. In their experiments, they also identified the existence of hematite by Raman spectroscopy.

Researcher C. Rémazeilles and Ph. Refait tried to characterize Fe (II) hydroxides by using Fourier Transform Infrared Spectroscopy (FTIR) as Fe (II) hydroxides rapidly oxidized to the most common form of corrosion product, Fe (III) oxyhydroxides [33].

1.6.2.3. Electrochemical measurements

Many researchers focused on the electrochemical nature of corrosion and investigated the corrosion behavior using different electrochemical techniques. Electrochemical measurements have been used for over 40 years. In between 1940 and 1960, this method was slowly progressing, but it got momentum after 1970's when Solatron (UK) and Princeton Applied Research (US) of automated EIS instruments were introduced [34].

Researcher K. Darowicki, S. Krakowiak, and P. Slepski investigated the full electrochemical impedance spectroscopy under a potentiodynamic condition to evaluate pitting corrosion in Stainless Steel grade 304L and were able to detect the correlations and dependencies of charge transfer among passive, metastable and pitting states [35].

Researcher M. Lez, M. Mitoraj, E. Godlewska and M. Jakubowska from AGH University of Science and Technology, Poland have used electrochemical noise measurement technique to compare the corrosion behavior of three chemically different materials: Aluminum, Iron and Iron aluminide (Fe_3Al) in distilled water, 4 wt% NaCl solution, 4 wt% NaCl with acetate buffer and 4 wt% NaCl with carbonate buffer solutions. The result of deviation of potential vs. deviation of current shows that the higher values of noise resistance indicate better resistance to corrosion which was also confirmed by microscopic examination [36].

In their article, researchers Jianyu Xiong, Mike Yongjun Tan and Maria Forsyth from Deakin University, Australia presented the potentiodynamic polarization results of corrosion attack on weldments of Stainless Steel grade 316 and 2205. The electrochemical polarization study revealed that SS2205 weldment was less resistant to pitting corrosion compare to SS316 weldment [37].

Stainless Steel is normally corrosion resistant and has good weldability. However during the welding process, the microstructure of stainless steel can be changed and make them

susceptible to localized corrosion i.e. pitting corrosion, intergranular corrosion and stress corrosion cracking [38].

1.6.3. Image analysis as a corrosion measurement tool

In the previous section, different electrochemical and spectral analysis of corrosion measurement techniques were discussed. However, image analysis based on textural features is of immense interest to the contemporary corrosion researchers. Different image processing tools and algorithms to process visual data and pixel values are being investigated to get better results. As an engineering management graduate student, I have become interested in exploring the technical details of image processing based corrosion measurement to find a more cost-efficient solution than laboratory-based chemical analysis. Due to the availability of cell phone camera or any simple image capturing device the image-based analysis could be a cheap, useful tool in field operation to estimate corrosion while components are still in service.

In visible light range, Red, Green, and Blue known as RGB are the three primary color features of any image. Corrosion damages on the metallic surface can be quantified by analyzing these RGB color spectrums. Several researchers investigated corrosion phenomena through RGB analysis.

Researcher Iwaya K, Yamamoto H measured red and green ratios (R/G) on images to quantify the water content of wheat [55]. Besides, green and red ratios (G/R) also been used to measure leaf necrosis and chlorosis of bamboo [56].

D.Itzhak, I. Dinstein, and T. Zilberberg investigated the pitting probability in AISI 304L stainless steel with the help of computerized image processing and found to be 9.73%. They scanned the images of the sample and estimated the ratio of the pitted area over the total area to find the probability [61].

E.N. Codaro et al. used light microscopy image analysis to quantitatively characterize the pitting corrosion morphologies on Aluminum and Aluminum-Titanium alloys [62]. They studied different shapes of the pit and identified few stable sizes by using shape descriptor.

R. M. Pidaparti, B. Hinderliter, and D. Maskey investigated the surface corrosion growth on stainless steel 304 under distilled water, Na2SO4 and NaCl solutions [2]. They have used cutoff-range RGB analysis method where they chose few ranges from 8-bit (0 to 255) color ratios and quantified the corrosion pit growth in Matlab.

This article was an inspiration for my approach of RGB analysis. However, in my sets of experiments, the histogram of each red, green and blue image was used to find a proper Gaussian fit and quantify peaks in different ranges. The fundamental principle is to identify the growth of different sets of corrosion peaks that reflect on various color ranges i.e. red, green and blue.

Chapter 2: Types of corrosion

2.1. Passivity

In some metallic corrosion like Fe, Ni, Cr, Ti the rate of corrosion decreases after some critical potential (Ep) as shown in Figure 2.1 despite high anodic driving force this is called passivity.

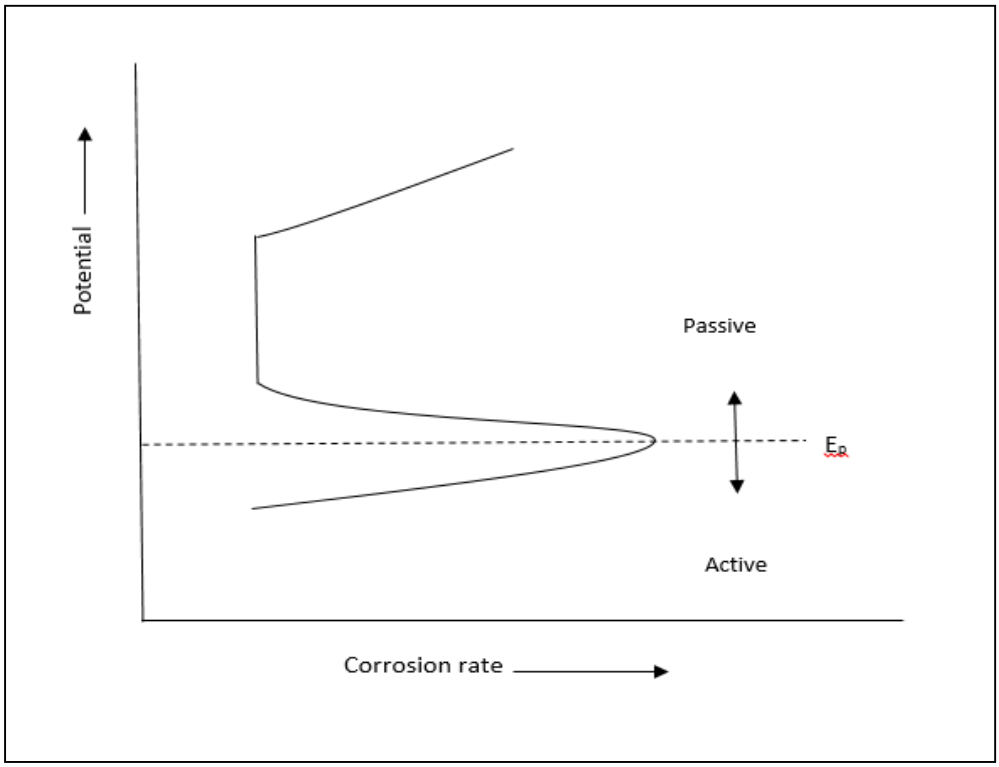

Figure 2.1: Passivity. Recreated from [40]

Below Ep, the metallic alloy corrodes at a high rate. However, due to the formation of a thin protective hydrated oxide layer which acts as a barrier to the anodic reaction the corrosion rate seizes. Based on the potential or oxidizing power of the solution, metal might exist in the active or passive zone. This protective layer eventually breaks down and causes different localized corrosion like pitting, crevice and embrittlement by stress corrosion cracking [1].

Metal shows different electrochemical behavior due to passivity. In this study, the effect of passivity on both stainless, and low carbon steel in various solutions was noticed, and the result section discusses that in details.

2.2. Classification of corrosion

To understand the corrosion aspects and mechanisms to details, knowledge of various forms of corrosion is essential. The following Table 2.1 briefly classifies different corrosions.

Table 2.1: Types of corrosion

Corrosion Type	Brief description	Examples
Uniform Corrosion	A uniform and regular removal of metal from the surface	Atmospheric corrosion
Galvanic Corrosion	When two dissimilar alloys are coupled in a corrosive electrolyte, galvanic corrosion occurs. In this case, one alloy is corroded while the other is protected from corrosion.	At the joint of flanges in a pipeline
Crevice Corrosion	An alloy corrosion occurs in the crevice with the contact of second materials.	In a bolt, with the presence of nut or washer
Pitting Corrosion	When the protective film barrier breaks, localized corrosion leads to pitting corrosion	The pitting corrosion formed on steel surface
Environmentally Induced Cracking	Environmental cracking refers to a corrosion cracking caused by a combination of conditions that can specifically result in Stress corrosion cracking or corrosion fatigue or hydrogen embrittlement	Examples are in the nuclear industry are cracks in stainless steel piping systems and stainless steel valve stems
Hydrogen Damage	This is a process resulting in a decrease of the toughness or ductility of a metal due to the presence of atomic hydrogen	During the electroplating process of metals at high temperature, this type of corrosion can happen
Intergranular Corrosion	This corrosion occurs at the grain boundary due to impurities or deployment of passivation elements	During heat treatment process of austenitic stainless steel
De-alloying	Preferential corrosion can happen due to de-alloying of an alloy which is comparatively active than the solution	The graphite corrosion in cast iron

Erosion Corrosion	When corrosive fluid due to high velocity, physically erodes the protective film and leaving it to corrode fast, is known as erosion corrosion	Cavitation

Due to the growth of the passive film on the surface, stainless steel is highly susceptible to pitting corrosion. Most failures occur in stainless steel in neutral to acid solutions with the presence of chloride ions. Therefore, the chemical and marine industries have immense interest in understanding and exploring pitting corrosion on stainless steel under chlorides environment; as a result pitting corrosion is discussed in next section.

2.2.1. Pitting corrosion

Pitting corrosion is a process of causing a deep localized attack on metal surfaces, including perforations of thin-walled structures. The reason to concentrate on pitting of passive metals is its outstanding practical importance for safety considerations. In contrast to uniform corrosion, whose rate is frequently predictable from vast experience, pitting corrosion proceeds at an unexpected and high rate of localized metal dissolution [17]. Based on the alloy metallurgy and the surrounding environmental chemistry, pits form differently. It can be shallow, elliptical, deep, undercut or subsurface. Figure 2.2 shows some typical pit morphologies, and Figure 2.3 shows a shallow pit causing surface penetration in stainless steel 304.

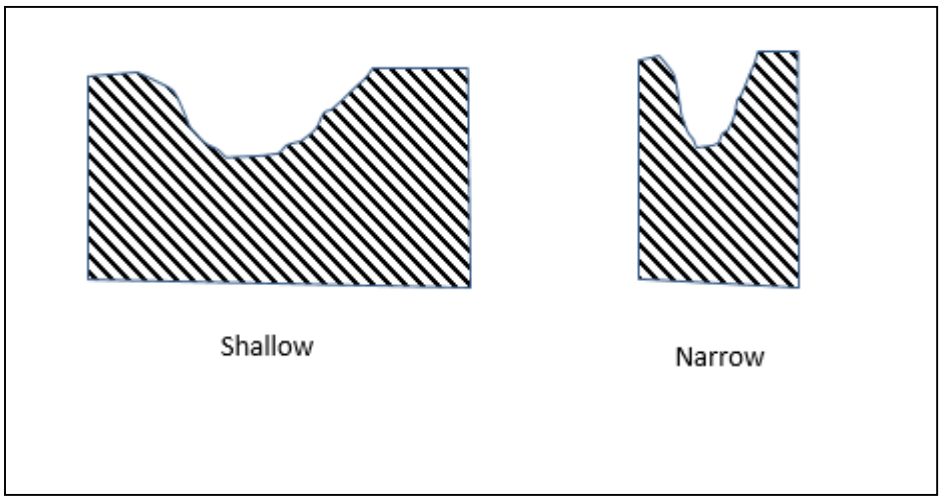

Figure 2.2: Variations of cross sectional shape of pits. Recreated from [41]

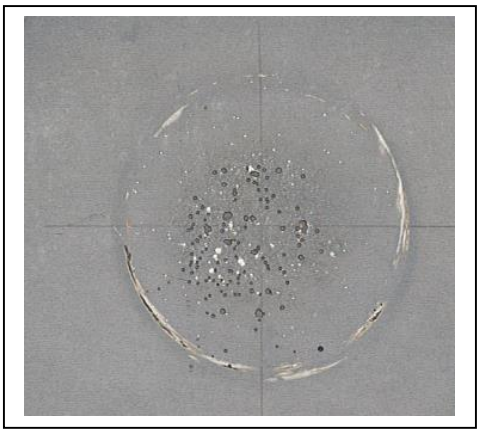

Figure 2.3: Shallow type pit formed in SS 304

On the metal surface, critical pitting potential, E_{pit} and the presence of aggressive chlorides ions are the two primary initiators of pitting corrosion. E_{pit} is the corrosion resistance potential, and higher E_{pit} value represents higher nobility of the metal. However in acidic solution, chloride increases the potentiodynamic or potentiostatic current at all potentials primarily at E_{pit}, as shown in Figure: 2.4 and causes low overvoltage anodic dissolution within the corrosion pits. Pitting is autocatalytic in nature, and it continues to grow as more and more positively charged metal ions are attracted to the environment. The chemical composition of the alloy is also responsible for extraordinary pitting growth. For

example, MnS inclusion in stainless steel alloy accelerates the protective layer breakdown and promotes pitting corrosion [42].

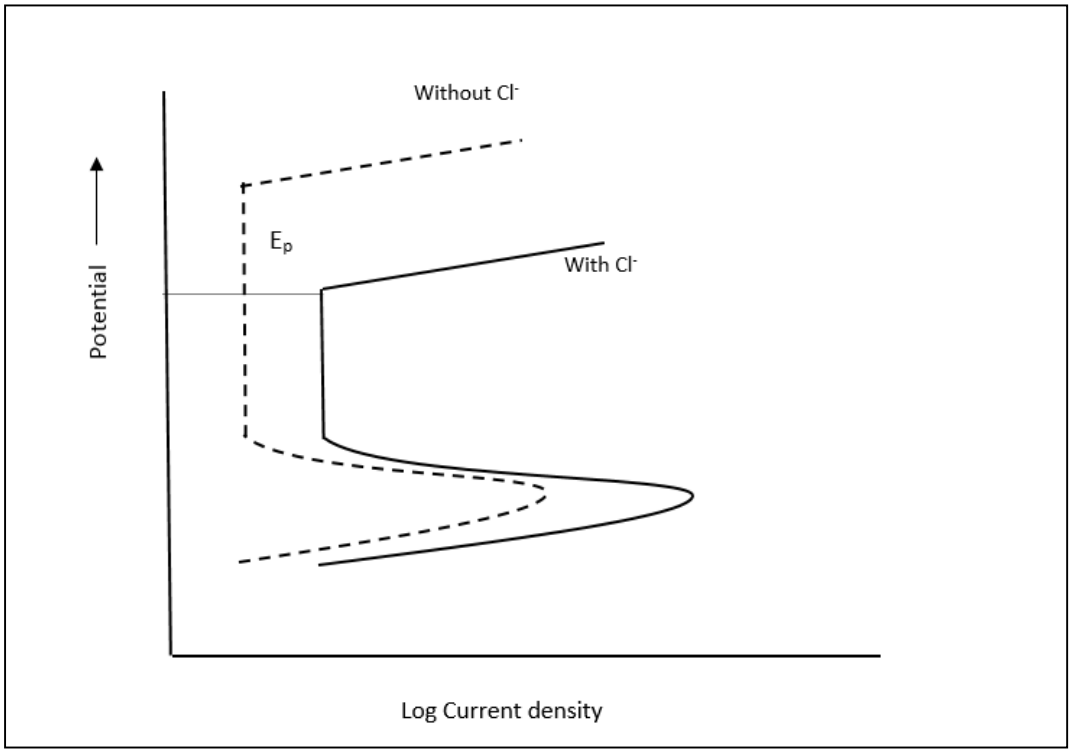

Figure 2.4: Critical pitting potential, E_{pit} determination from anodic polarization. Recreated from [1]

Pitting initiates aggressively yet silently on the surface. Sometimes it remains undetected for a long period and only visible when leaking results in from the metal surface. Although scientists have not understood the actual mechanism and the interaction process of chlorides entirely however, modern techniques show some insights into the chemical reactions.

2.2.2. Mechanism of pitting corrosion

Chloride plays the big role in pitting mechanism. The negatively charged Cl^- ions are attracted to the positively charged metal surface and the Cl^- concentration increases with the potential increases to E_{pit}. Electron microscopic observation shows the thick accumulation of chloride salt "islandistilled" on the metal surface even at below E_{pit} [1]. As a result, a high chloride and low pH environment are developed underneath the island by a hydrolysis reaction.

$$Fe^{2+} + 2H_2O + 2Cl^- \rightarrow Fe(OH)_2 + 2HCL \ldots\ldots(1)$$

In the absence of Cl^- ions the passive film on surface dissolves slowly as Fe3+

$$FeOOH + H_2O \rightarrow Fe^{3+} + 3OH^-$$

However, in the presence of Cl^- this passive hydrated film of FeOOH liberates Fe^{3+} as outer displacement

$$FeOOH + Cl^- \rightarrow FeOCl + OH^-$$

$$FeOCl + H_2O \rightarrow Fe^{3+} + Cl^- + 2OH^- \ldots\ldots(2)$$

Reaction (2) removes the passive film at a preferred pitting site until a pit is initiated [1]. These reactions are autocatalytic; the acidic chloride solution further increases the anodic dissolution and continues concentrating chloride in the pit that produce an insoluble cap of $Fe(OH)_3$ corrosion products. At the same time, Fe^{2+} are diffused out of the pit and oxidized to Fe^{3+} and the reactions go on and on.

From the above mechanism, it is well understood that chloride plays a significant role in corrosion initiation process, and it accelerates the reaction. However, due to the metal composition chloride attacks differently. Chapter 5 discusses the growth of various corrosion peaks in distilled water, half saturated and saturated chloride solutions.

Chapter 3: Corrosion experiment

In this chapter the experimental procedure, apparatus and instructions are discussed. For this corrosion experiment we have used stainless steel 304 and low carbon steel A1008 grade panels.

3.1. List of Materials:

1. SS 304 stainless steel (ASTM A 240 grade) panel (152mm x 76mm x 0.81 mm) manufactured by Q-Lab as shown in Figure 3.1. Chemical composition is as below

Table 3.1: Chemical composition of AISI 304 type stainless steel [1]

ASTM specification	AISI designation	Type	Composition (%)							
			Fe	C	Mn	P	S	Si	Cr	Ni
A 240	304	SS	65-70	0.08	2.00	0.045	0.03	1.00	18.00 - 20.00	8.00-10.50

2. QD 1008 low carbon steel (ASTM A1008 grade) panel (152mm x 76mm x 0.51 mm) as shown in Figure 3.2. Chemical composition is as below

Table 3.2: Chemical composition of AISI 1008 type low carbon steel [50]

ASTM specification	AISI designation	Type	Composition (%)				
			Fe	Mn	C	S	P
A 1008	1008	QD	99.31-99.7	0.30-0.50	0.10	0.05	0.04

3. Distilled water
4. Half-saturated sodium chloride solution
5. Saturated sodium chloride solution
6. KEYENCE VHX-100 digital microscope as shown in Figure 3.3
7. ECM 8^{TM} Electrochemical Multiplexer as shown in Figure 3.4
8. Gamry Framework (data acquisition software)
9. Gamry Echem Analyst
10. Ag/AgCl reference electrode
11. 3M 600 and 1000 grit sand paper.

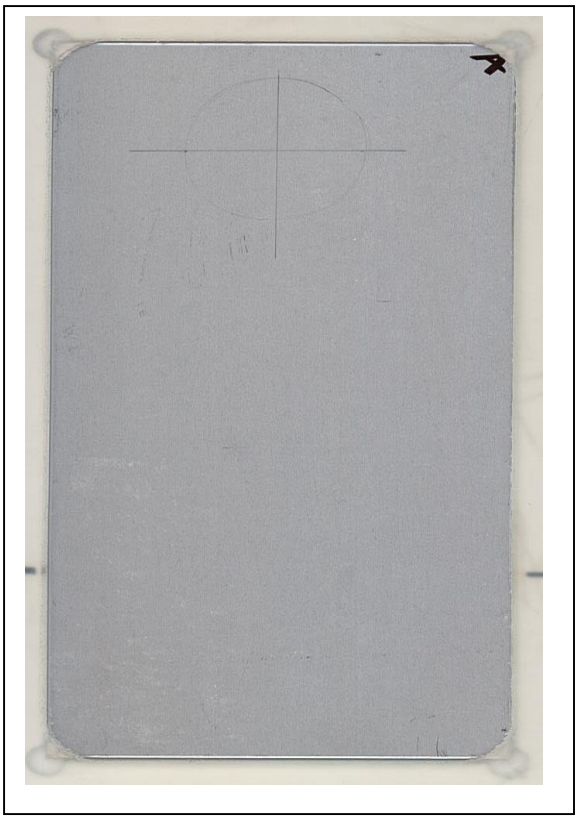

Figure 3.1: SS 304 panel

Figure 3.2: QD A1008 panel

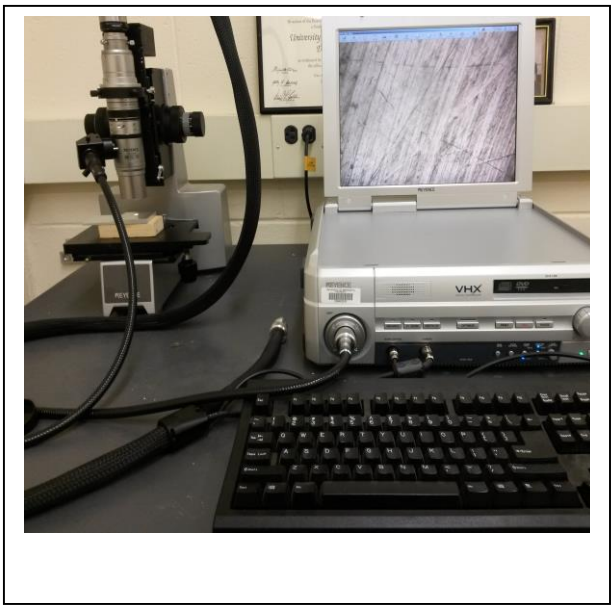

Figure 3.3: Keyence Digital Microscope

Figure 3.4: Gamry ECM 8^{TM} Multiplexer

3.2. Preparation

3.2.1. Panel preparation

1. Before starting the procedures, panels were cleaned with 300 grit sand paper followed by 1000 grit sand paper to remove any sign of surface corrosion.
2. After that, the panels were cleaned with distilled water.
3. It was ensured that the panels were dry before starting the experiment.

3.2.2. Solution preparation

4. 200 ml distilled water were poured into a bottle and kept separately for experiment.
5. 35.7-gram laboratory sodium chloride salts were mixed with 200 ml distilled water to prepare 200 ml half-saturated sodium chloride solution and was poured into a bottle.
6. 71.4-gram laboratory sodium chloride salts were mixed with 200 ml distilled water to prepare 200 ml saturated sodium chloride solution and was poured into a bottle.

3.2.3. Electrochemical cell preparation

7. In Gamry Framework data acquisition software, open circuit potential (OCP) and Electrochemical Impedance Spectroscopy (EIS) settings were selected for all experiments.
8. Out of eight (8) channels in a multiplexer, two (2) were used to connect the panel setup.
9. In every step of preparation, hand gloves were used to prevent any oil or salt contamination on the panel surface.

3.3. Experiment procedure

1. The panel and the bottom of the multiplexer were separated by using Teflon to prevent electrochemical interaction between them as shown in Figure 3.5.
2. Using customized set up, each panel, was set for the experiment.
3. Periodically each panel was removed from the solution

Figure 3.5: Customized experiment set up

Figure 3.6: Corroded solution

4. After taking the panels out of the solution, they were cleaned with distilled water and let dry for 15 minutes.
5. Each panel was put on the customized Teflon frame, and the experimental area was observed under the digital microscope.
6. The microscope was set at 100x magnification, and the images were taken with default lighting setup.
7. After taking the images, the panels were put back to the solutions again.
8. Procedures 1 to 7 were repeated until the panels were entirely corroded and the solution became cloudy with corrosion products shown in Figure 3.6
9. The images were imported into Matlab.

Chapter 4: Image analysis algorithm

The images taken by the digital microscope were imported in Matlab and were examined through histogram analysis to identify the growth of corrosion peaks. Before explaining the details of it, the flow chart of algorithm has been mentioned below:

4.1. Flowchart of the algorithm

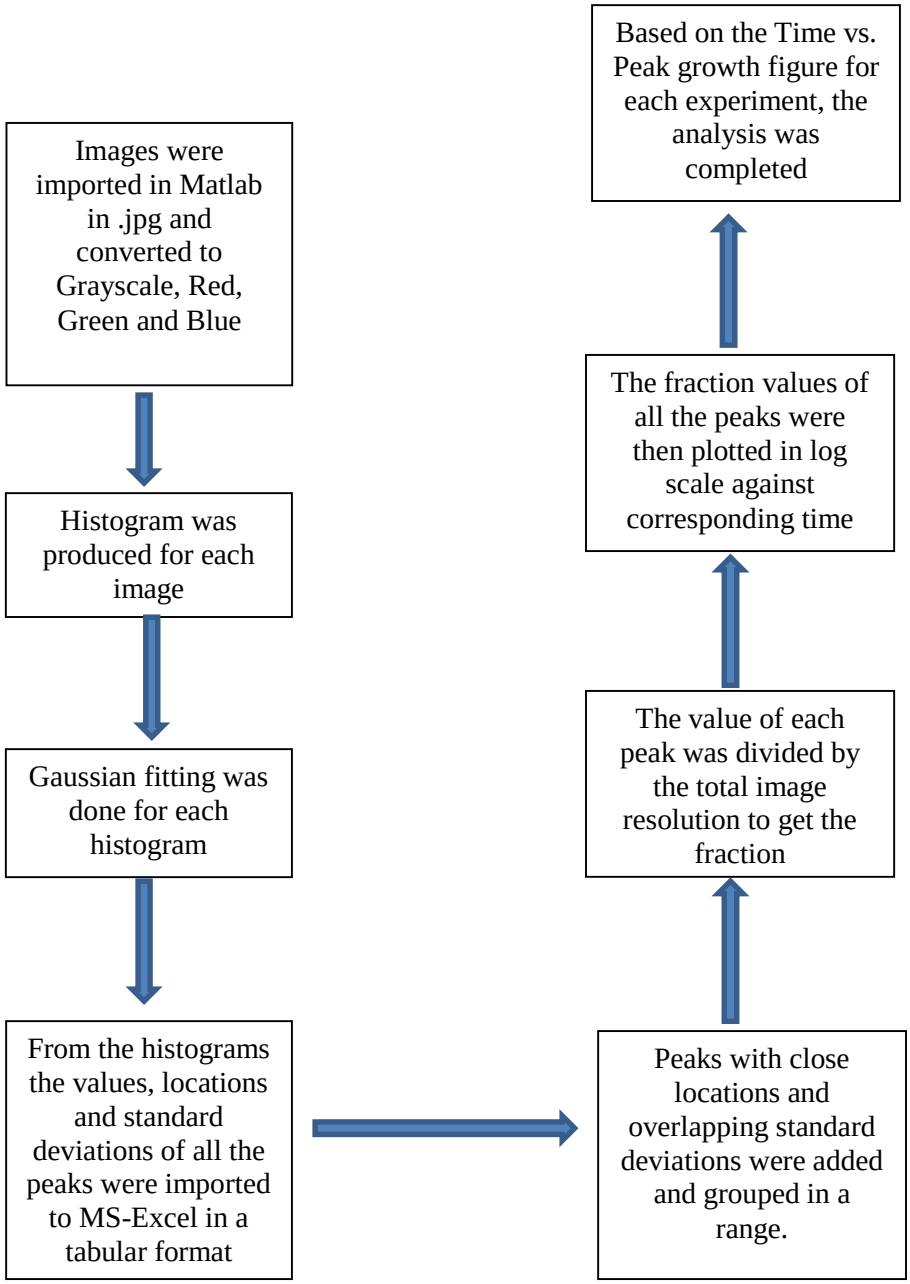

Figure 4.1: Flowchart of algorithm

4.2. Details of the algorithm

Step 1: A code was developed to take the images in Matlab as input and convert them into grayscale, red, green and blue images as shown in Figure 4.2. All the images were of 1600 x1200 resolution and .jpg format. As any image is an arrangement of a matrix, 'strcat' command was used to concatenate the corresponding elements of the image matrix. After that, 'imread' command took the image as an input. To convert to grayscale image, 'rgb2gray'command was used. A coded loop was developed to get the R, G & B values. All images were stored in the drive location by using 'imwrite' command. Finally, one set of grayscale, red, green and blue images are shown below.

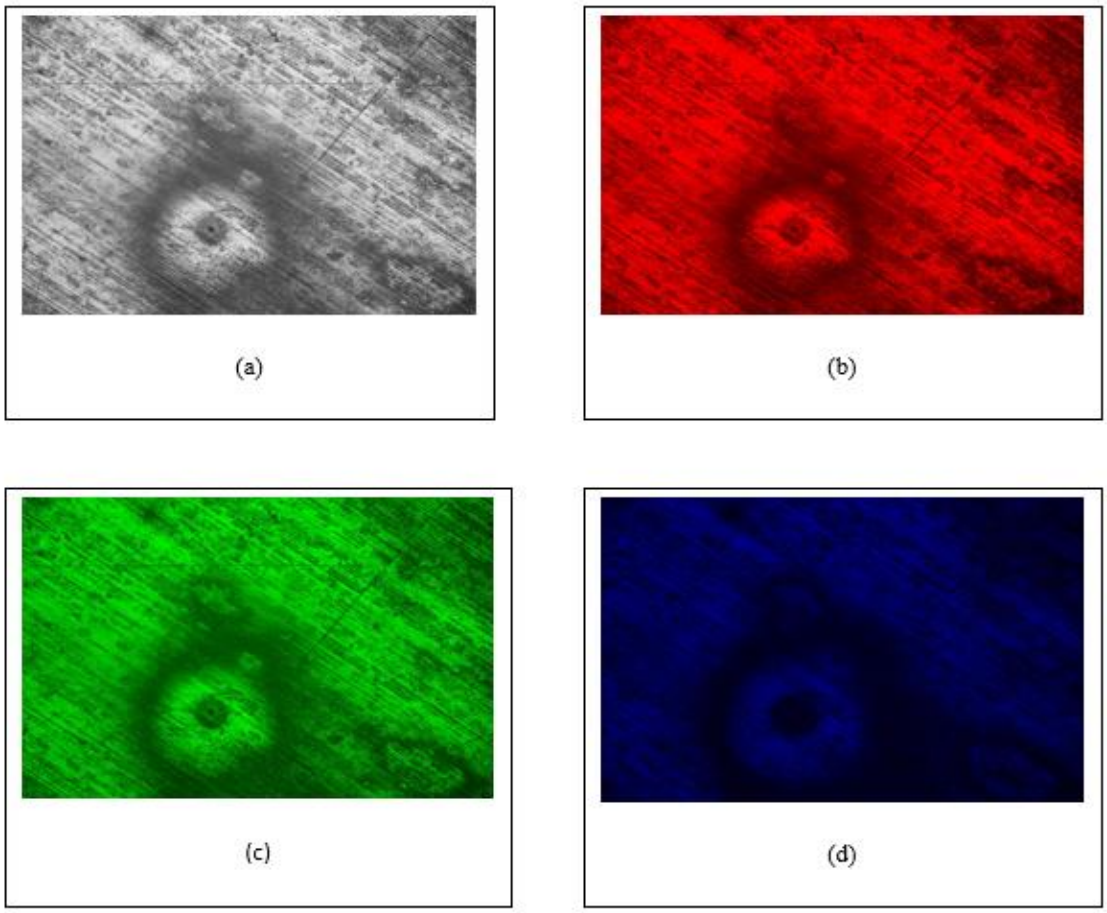

Figure 4.2: (a) Grayscale, (b) Red, (c) Green and (d) Blue images

Step 2:

In this step, the histogram was produced for each grayscale, red, green and blue image through a Matlab code. The 'imread' command used to take an image as input and 'imhist' command was used to create a histogram of the image. Figure 4.3 shows a snapshot of histogram for a grayscale image.

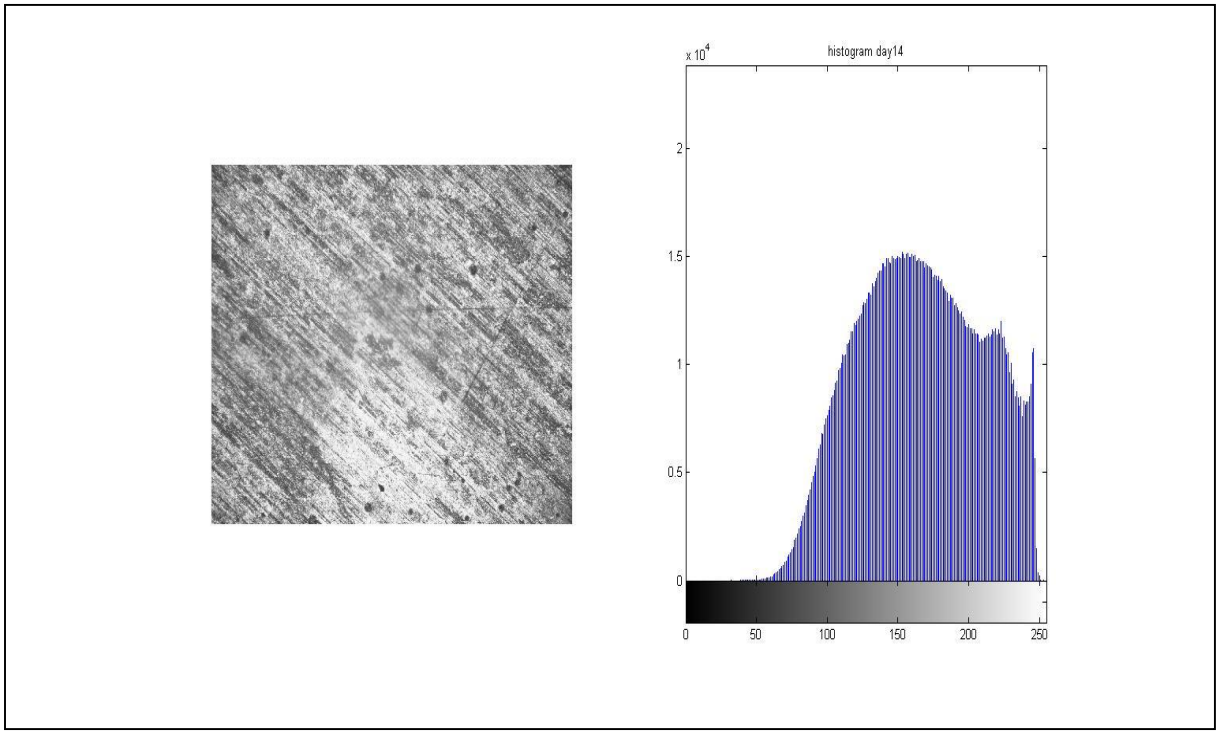

Figure 4.3: Histogram of a Grayscale image

Step 3: In this step, by using curve fitting tool 'cftool' in Matlab, Gaussian fitting was done for each histogram. The Gaussian function can be explained by the following formula.

$$F(x) = a * e^{\frac{-(x-b)^2}{2c^2}}$$

Here,

a= height of the curve's peak or amplitude;

b= position of the center of the peak or mean;

c= standard deviation or Gaussian RMS width.

Because of the bell shaped nature of the histogram, the Gaussian curve was applied to measure the peak height, mean and width. The objective is to identify and measure the growth of different peaks for each grayscale, R, G and B image. The histogram analysis shows the significance of peak growth due to corrosion damage.

Figure 4.5 shows the snapshot of 'cftool' used in Matlab for Gaussian fitting.

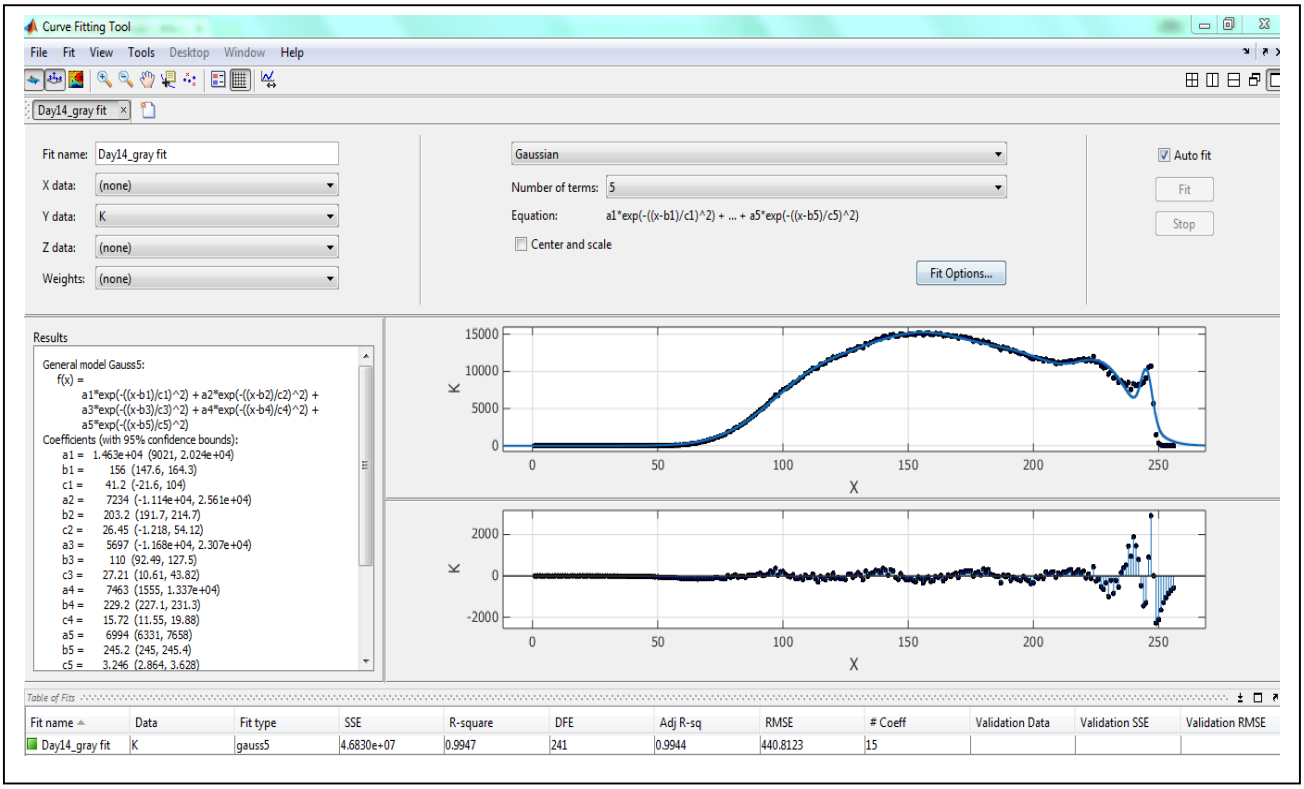

Figure 4.5: Curve fitting tool for Gaussian fit.

The curve fitting tool is an interactive tool and allows up to 8 Gaussian fits. The results section on the left as shown in Figure 4.5 delivers the values for a, b and c. Based on the R-square value the appropriate Gaussian fit was chosen for each histogram. The X axis represents the color intensity range (0-255) for 8-bit grayscale and Y-axis shows the different height of the peaks over the color ranges.

Step 4: After getting the values of amplitude (a), the location of the center or mean (b), and standard deviation (c); those were imported into Microsoft Excel and were arranged according to the value of mean (b).

Time (day)	a1	b1	c1	a2	b2	c2
0	56530	76.23	1.986	13340	68.68	1.076
0.01	60170	76.24	2.06	15290	68.73	1.15
0.02	80140	76.49	1.627	29220	68.34	7.47
0.03	90610	76.31	2.01	29190	69.01	8.09
0.04	88730	76.56	1.66	27660	69.3	7.02
0.06	80180	76.37	1.30	28890	77.73	2.04
0.08	73650	76.34	1.77	21920	76.82	0.23
0.1	82990	76.48	1.85	27480	73.64	3.076
0.12	75870	76.43	1.86	27960	73.52	3.211
0.14	57040	76.4	1.83	24730	74.09	4.123
0.16	40380	76.38	1.79	24390	74.27	4.184
0.18	35330	76.35	1.78	23530	74.26	4.196
0.22	37280	76.39	1.71	23740	74.33	4.06
0.3	32410	76.25	1.93	23700	73.21	4.77
2	71700	75.95	2.77	18820	71.85	1.332

Figure 4.6: A snapshot of data arrangement in Excel

Figure 4.6 shows the arrangement of peaks, means and standard deviations that were generated from the Gaussian fit. The first column represents the time duration for the images of each panel. Columns a_1, b_1, $c_1 \ldots a_n$, b_n, c_n represent different peaks, means and standard deviations of an image at any given time. For example, in column b1, all the peaks that have means close to 75 or 76 and are within the range of standard deviation.

Step 5: Peaks with overlapping standard deviation and or close means were grouped together in this step. A separate excel table was made for each data set similar to Figure 4.7

Time	Peaks in 50 to 80	Peaks in 140 to 170	Peaks in 191 to 230	Peaks in 231 to 245
0	0	4594	29941	0
1	3050	5306	23992	0
2	3141	4181	25157	0
3	3208	4225	23746	0
4	3095	4765	29685	0
5	3281	4845	28187	0
6	3162	3676	29688	0
7	3105	4621	26998	0
8	3100	5149	26819	0
9	2997	3611	27994	0
10	5115	7199	26520	0
11	5005	7793	28945	7484
12	4950	6979	28639	0
13	5187	7047	29626	3809
14	4423	7369	21973	0

Figure 4.7: Grouped data as per mean and standard deviation

Step6: The value of peaks in each cell similar to Figure 4.7 was divided by the total image resolution i.e. 1920000 pixels (1600*1200) to measure the ratio of each set of peaks compared to the entire image. It also gives a good estimation of the growth pattern of the peaks. Figure 4.8 shows one set of example.

Time	Peaks in 50 to 80	Peaks in 140 to 170	Peaks in 191 to 230	Peaks in 231 to 245
0	0.00000	0.00239	0.01559	0.00000
1	0.00159	0.00276	0.01250	0.00000
2	0.00164	0.00218	0.01310	0.00000
3	0.00167	0.00220	0.01237	0.00000
4	0.00161	0.00248	0.01546	0.00000
5	0.00171	0.00252	0.01468	0.00000
6	0.00165	0.00191	0.01546	0.00000
7	0.00162	0.00241	0.01406	0.00000
8	0.00161	0.00268	0.01397	0.00000
9	0.00156	0.00188	0.01458	0.00000
10	0.00266	0.00375	0.01381	0.00000
11	0.00261	0.00406	0.01508	0.00390
12	0.00258	0.00363	0.01492	0.00000
13	0.00270	0.00367	0.01543	0.00198
14	0.00230	0.00384	0.01144	0.00000

Figure 4.8: Peaks are divided by the value of total image resolution

Step 7 and 8: In these two steps, Time vs. Peak growth figures for all the images were created and analyzed. Chapter 5 discusses these in details

Chapter 5: Results and discussion

5.1. Experimental panels

Six panels were used to conduct the overall corrosion experiments, and they are summarized in below table.

Table 5.1: Number of experimental panels

Panel	No. of panel in Distilled water experiment	No. of panel in Half-saturated sodium chloride solution	No. of panel Saturated sodium chloride solution
Stainless Steel SS 304	1	1	1
Carbon Steel QD 1008	1	1	1

5.2. Results

5.2.1. Stainless steel in distilled water experiment

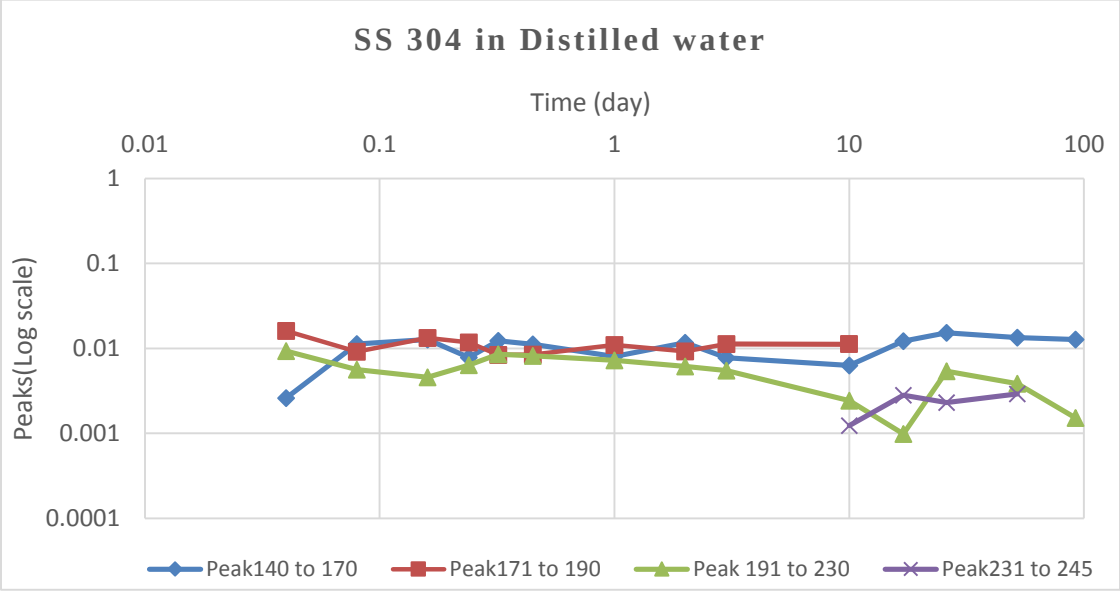

Figure 5.1: Time vs. Peak growth of SS304 in distilled water (Grayscale)

The above figure shows the growth of different peaks in the grayscale image over time for SS 304 panel. The panel is not entirely corroded yet. Nonetheless, the progress of three months has been considered to present in this research. From the chemical composition of

SS 304 stainless steel, we know the strong presence of Fe and Cr along with a moderate existence of Mn, which results in the formation of Fe_2O_3, Cr_2O_3, and MnO in distilled water solution. The grayscale image shows a consistent growth of the peaks equivalent to 0.01 value in log scale. From the grayscale image, a growing trend of the peaks in 140 to 170 intensity followed by 171-190 range is noticeable. To understand the growth of different peaks in Red, Green and Blue images, the RGB image analysis have presented below.

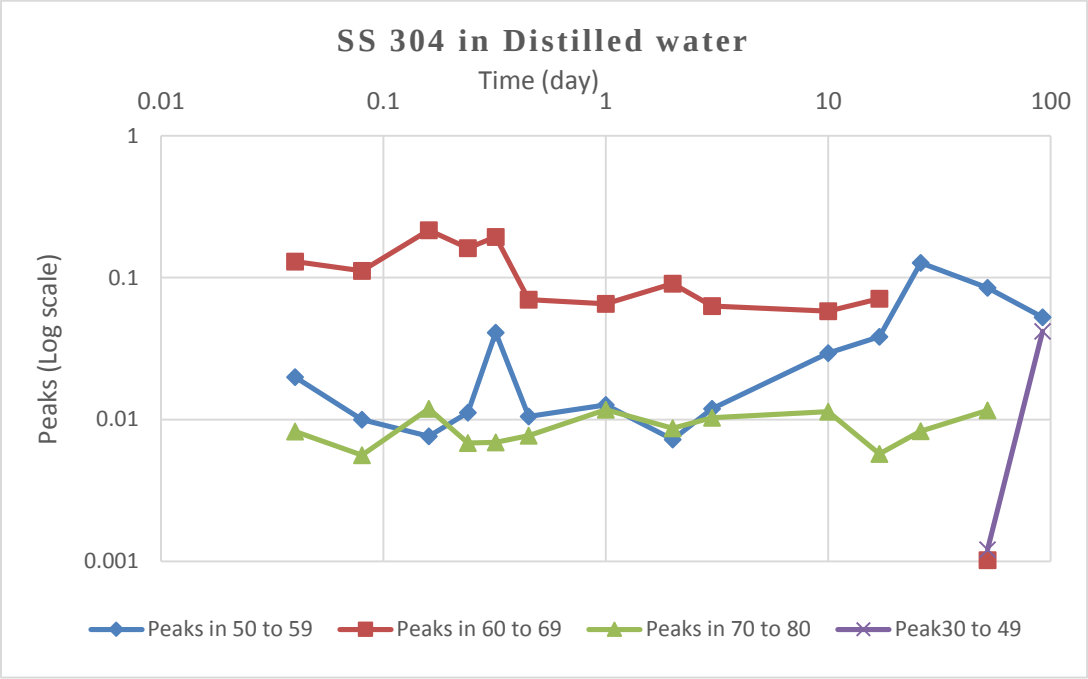

Figure 5.2: Time vs. Peak growth of SS 304 in distilled water (Red)

Figure 5.2 shows the morphological analysis of different peaks based on various light intensities in the red image. From the literature review, we know that Fe^{3+} oxides i.e. Fe_2O_3 is red in color and is responsible for the growth of different sets of peaks in red image. For example, in 30 to 49 color range, peaks started to grow from 0.001 to almost 0.1 value in Log scale. It means in this dark area peaks rose nearly 100%. Peaks in 50 to 59, 60 to 69 and 70 to 80 ranges also show a growing trend.

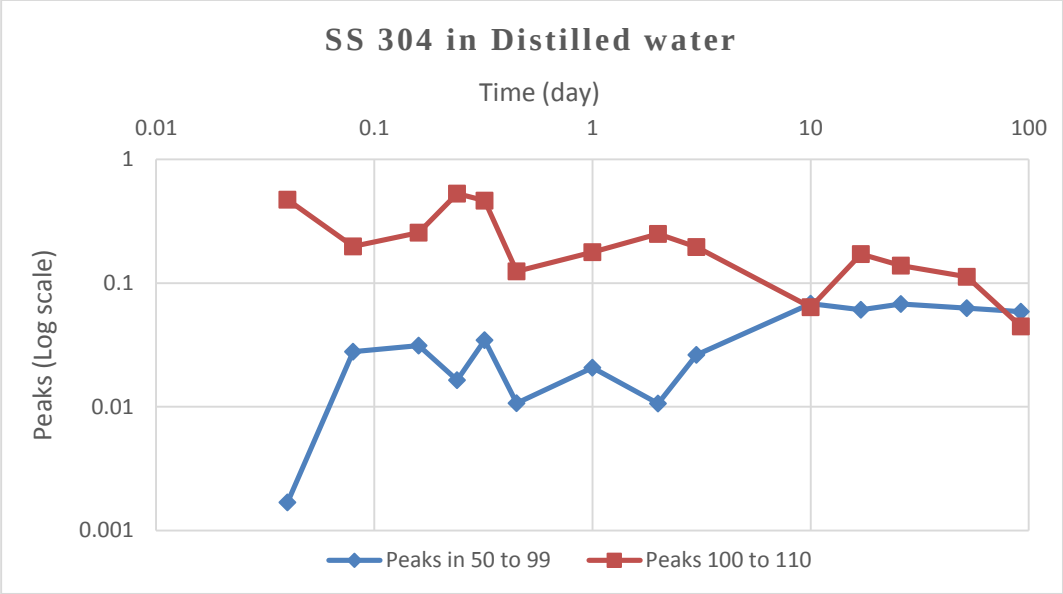

Figure 5.3: Time vs. Peak growth of SS 304 in distilled water (Green)

In Figure 5.3 two sets of peaks are visible at 50-99 and 100-110 ranges. These peaks are due to the formation of Cr_2O_3 and MnO [39] [54]. These peaks are of high amplitude values and at 100-110 ranges the peaks went over log 0.1. The overall upward and downward trend indicates the effect of protective oxide layers at different times.

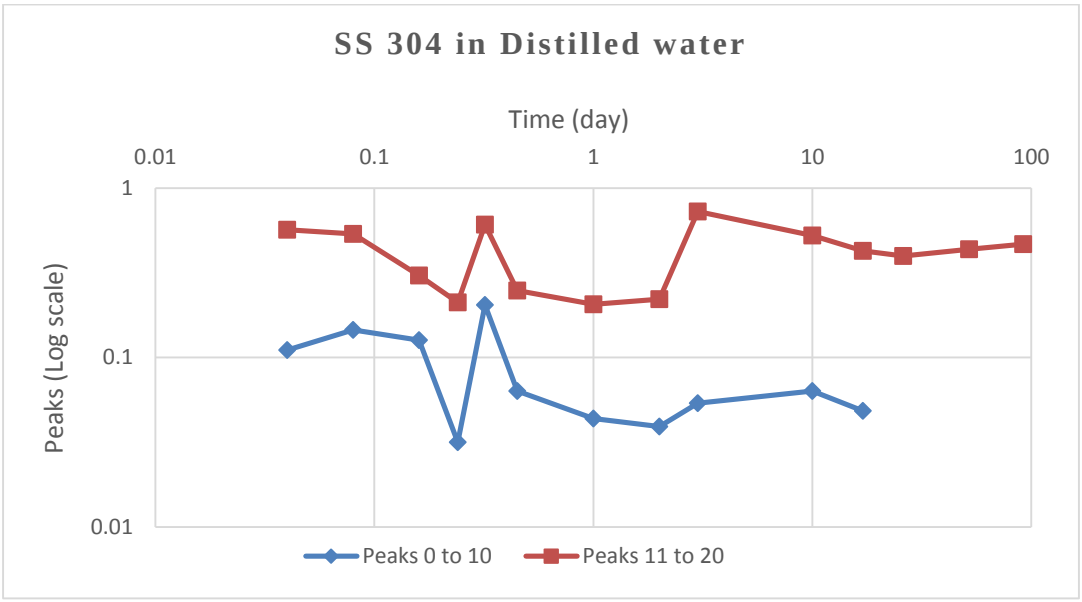

Figure 5.4: Time vs. Peak growth of SS 304 in distilled water (Blue)

The blue image shows the growth of two sets of peaks in 0-10 and 11-20 intensities and the peaks at 11-20 have high values almost close to Log 1 representing high corrosion pit formation.

After conducting the corrosion experiment for over 92 days, the panel was corroded and the solution became cloudy with corrosion products. The panel was taken out from the set up.

5.2.2. Stainless steel in half-saturated sodium chloride (NaCl) solution experiment

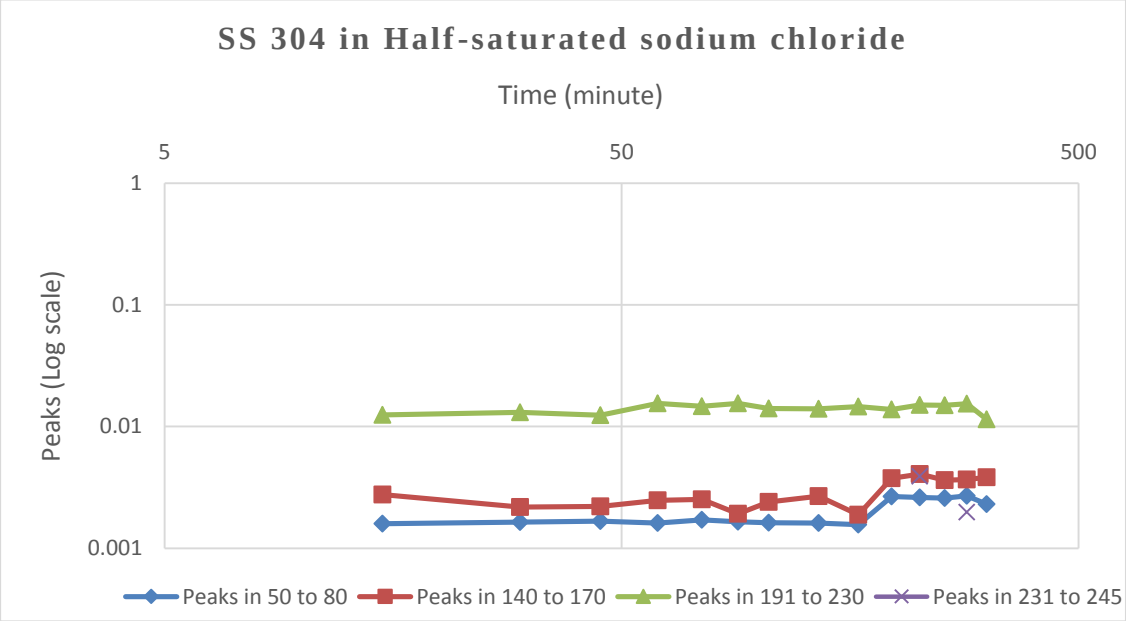

Figure 5.5: Time vs. Peak growth of SS 304 in half saturated NaCl (Grayscale)

Stainless steel in chloride solution is attacked by several corrosion accelerating chloride products along with oxides. The presence of Cr_2O_3, $CrCl_2$, $CrCl_3$ $(H_2O)_x$; x=1, 5, 6, $FeCl_2$, $FeCl_3$, MnO, Ni (II) chlorides creates a perfect corrosive environment, and the process gets faster compared to distilled water experiment. Figure 5.5 shows the continuous and steady growth of peaks in 191 to 230 intensities followed by 140 to 170. Peaks growing in 50 to 80 ranges are also increasing with time. To get a better understanding, the RGB images of SS 304 in half saturated NaCl have analyzed below.

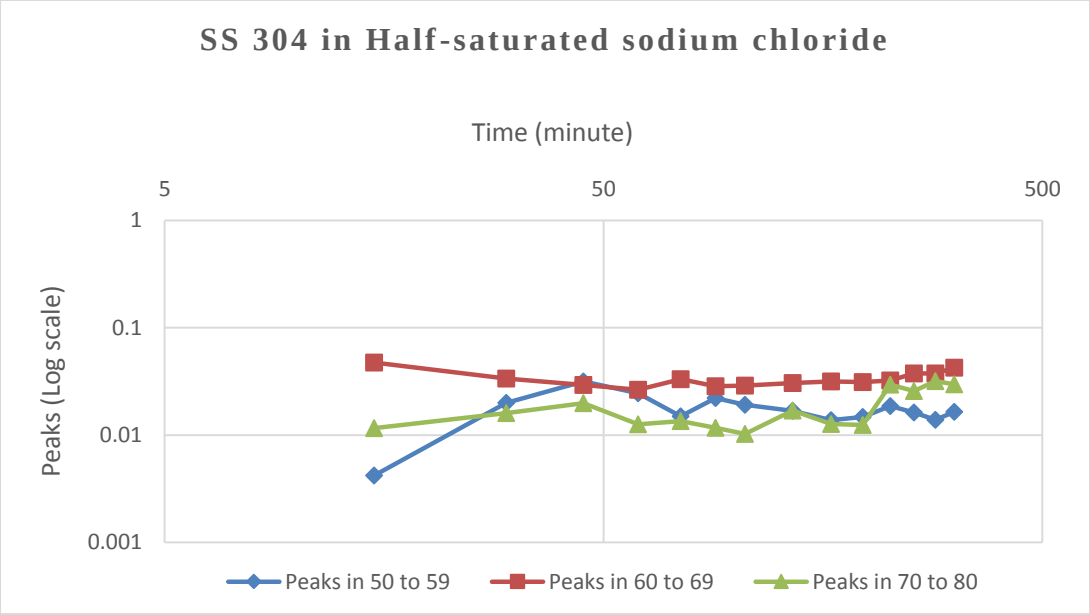

Figure 5.6: Time vs. Peak growth of SS 304 in half saturated NaCl (Red)

The presence of Fe_2O_3 accelerates the corrosion process and from Figure 5.6, we see the significant growth of peaks in 60 to 69 intensity along with 50 to 59 and 70 to 80 ranges. The overall trend in the red image is increasing in nature with over log 0.01 value.

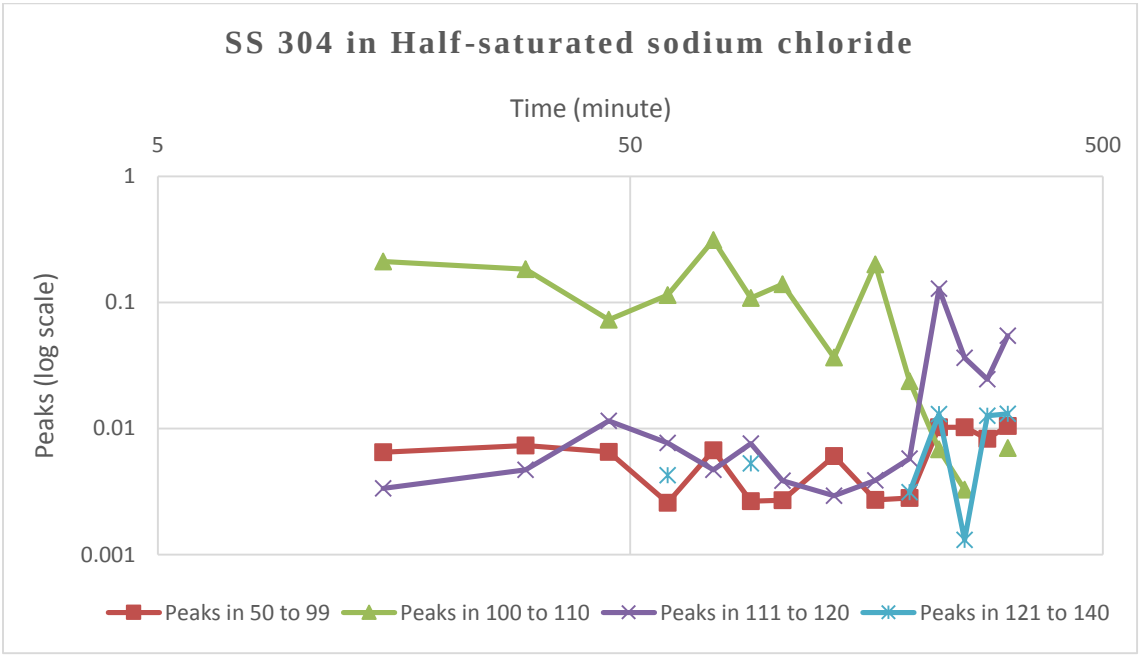

Figure 5.7: Time vs. Peak growth of SS 304 in half saturated NaCl (Green)

The green image, Figure 5.7 shows the existence of different sets of peaks. In chloride environment, the formation of several compounds like Cr_2O_3, $CrCl_2$, $CrCl_3$ $(H_2O)_x$; x=1, 5, 6, $FeCl_2$, $FeCl_3$, MnO, Ni (II) chlorides, etc. cause the high growth of peaks [12],[16],[17]. As a result, peaks are visible in 50 to 99, 100 to 110, 111 to 120 and 121 to 140 show the increasing trend at the end. This image displays the significant contribution of greenish colored corrosion products into the overall chemical process.

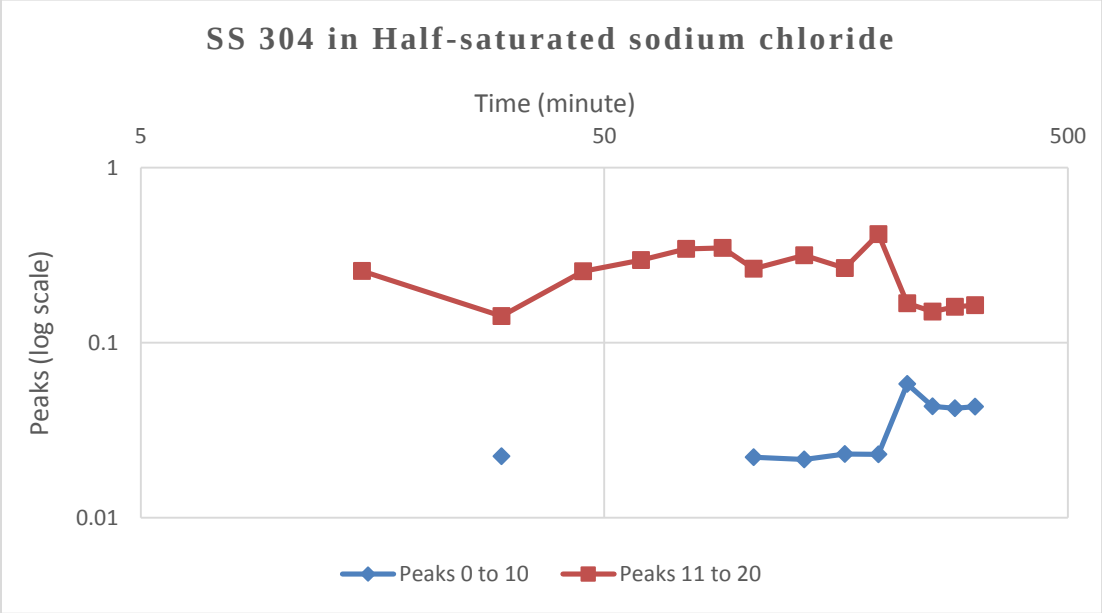

Figure 5.8: Time vs. Peak growth of SS 304 in half saturated NaCl (Blue)

Figure 5.8 displays the aggressive growth of one set of peaks at 11 to 20 with values more than log 0.1.

The solution became cloudy with corrosion products after conducting the experiment for 315 minutes and the panel was taken out.

5.2.3. Stainless steel in saturated sodium chloride (NaCl) solution experiment

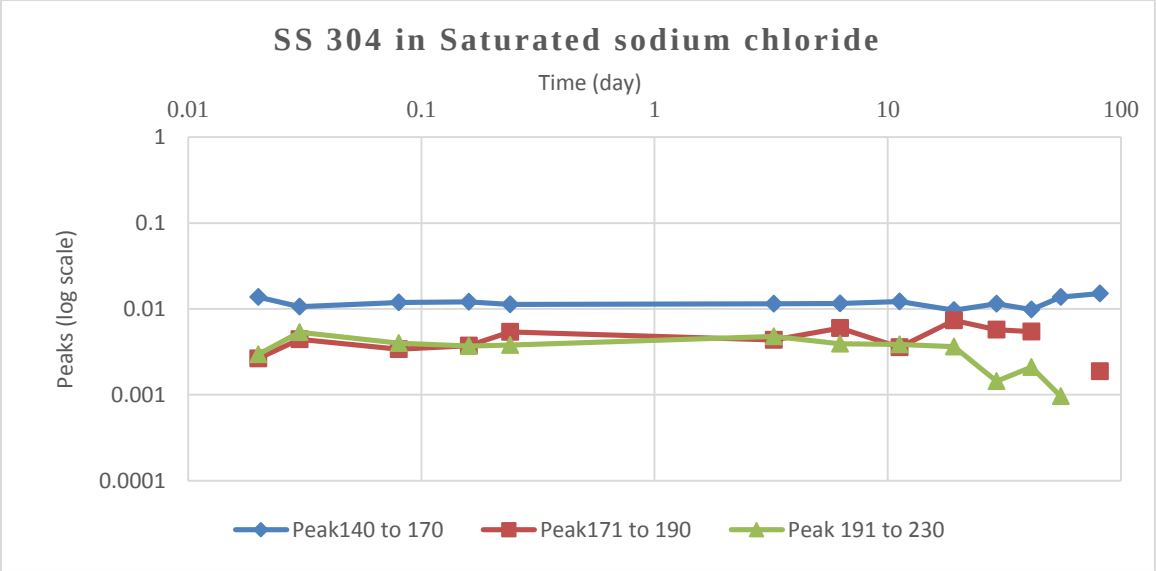

Figure 5.9: Time vs. Peaks of SS 304 in saturated NaCl solution (Grayscale)

The grayscale image shown in Figure 5.9 depicts the growth of various peaks. In 140 to170 range, the peaks are dominating with log 0.01 values. Peaks in two other ranges; 171 to 190 and 191 to 230 are also following a similar trend. Unlike half saturated NaCl experiment, in saturated NaCl solution, peaks in 191 to 230 range are lower than log 0.01 value and show a decreasing trend. The RGB image analysis explains the growth of peaks in details.

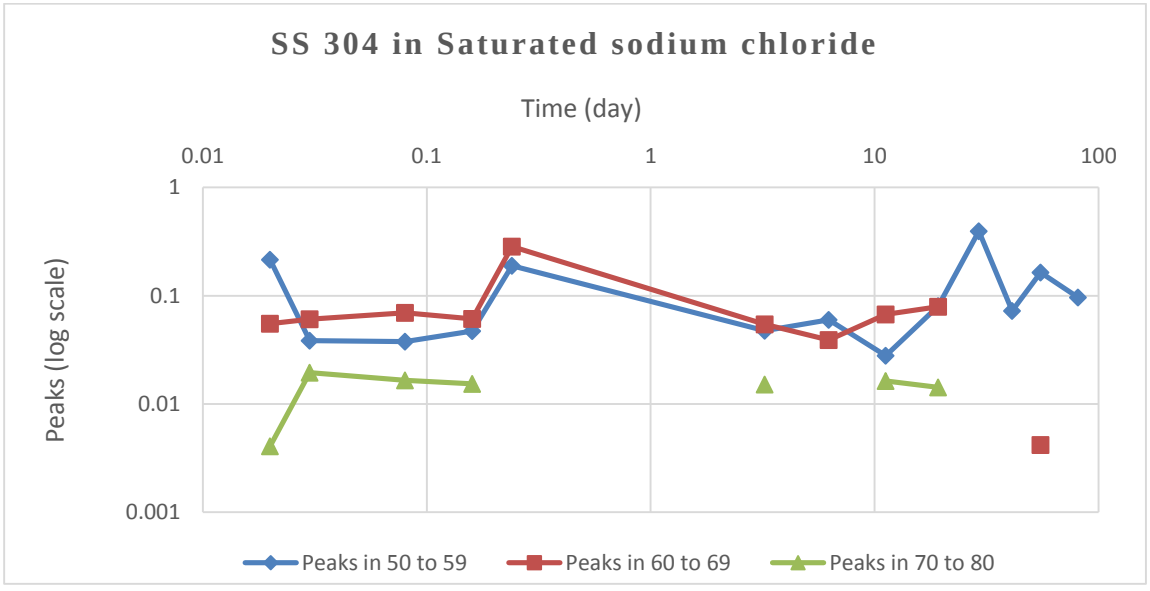

Figure 5.9: Time vs. Peaks of SS 304 in saturated sodium chloride solution (Red)

In Figure 5.9, three sets of peaks are visible in 50 to 59, 60 to 69 and 70 to 80 color intensities. However, in saturated NaCl solution, peaks look more dominant i.e. close to log 0.1 value than half saturated experiment. Therefore, the formation of Fe_2O_3 perhaps contributing more in corrosion process compared to half saturated chloride experiment. The overall trend shows increasing.

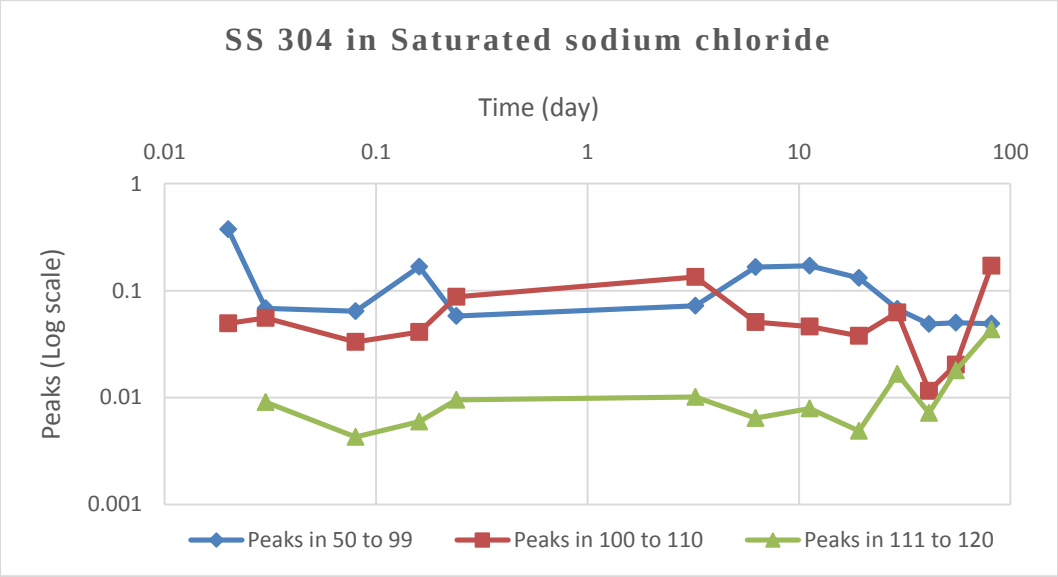

Figure 5.10: Time vs. Peaks of SS 304 in saturated sodium chloride solution (Green)

Similar to the green image from half saturated NaCl experiment, several sets of peaks are noticeable in Figure 5.10. The chloride ions contribute to the formation of different corrosion product i.e. $CrCl_2$, $CrCl_3$ $(H_2O)_x$; x=1, 5, 6, $FeCl_2$, $FeCl_3$, MnO, Ni (II) Chlorides etc. to accelerate the corrosion process in 50 to 99, 100 to 110 and 111 to 120 intensity ranges. An overall growing trend in the green image shows the major contribution of greenish colored corrosion products into the overall chemical process.

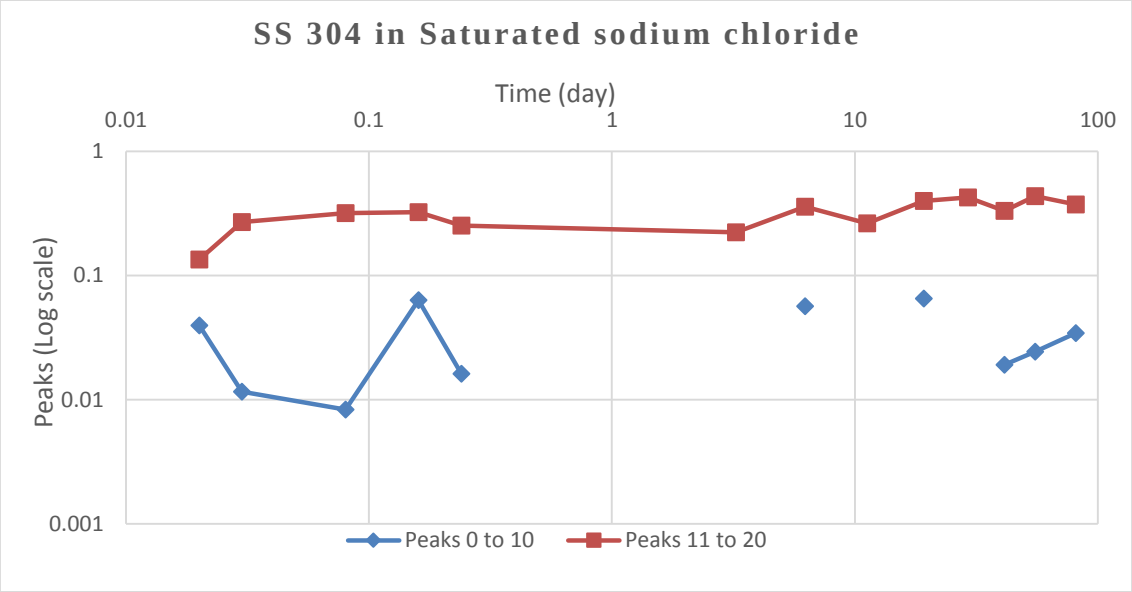

Figure 5.11: Time vs. Peaks of SS 304 in saturated sodium chloride solution (Blue)

Similar to distilled water and half saturated NaCl experiments, in saturated NaCl experiment, shown in Figure 5.11, peaks in 11 to 20 color intensity are dominating and continuously growing with over log 0.1 value.

The experiment was stopped after 81 days when the panel was corroded completely, and the solution became cloudy.

5.2.4. A comparison of images of SS 304 experiments

The following Table 5.2 shows a comparison of three sets of experiments of SS 304 in distilled water, half saturated NaCl and saturated NaCl solutions.

Table 5.2: Comparison of SS 304 panel in distilled water, Half-saturated NaCl & Saturated NaCl solutions

	SS304 in Distilled water	SS304 in Half-saturated sodium chloride	SS304 in Saturated sodium chloride
Duration of experiment	92+ days	315 minutes	81+ days
Dominating peaks	Red	Red and Green	Red and Green
Main corrosion products	Fe_2O_3	Cr_2O_3, $CrCl_2$, $FeCl_3$, $CrCl_3.nH_2O$, MnO	Fe_2O_3,Cr_2O_3, $CrCl_2$, $FeCl_3$, $CrCl_3.nH_2O$, MnO

From the above table, it is clear that SS 304 shows better corrosion resistance in distilled water than chloride solutions. Interesting to notice that SS 304 corrodes slowly in saturated solution compared to the half-saturated chloride solution. The reason is NaCl dissolution rate decreases with the increase in saturation [67] as a result, less chloride ions are available in saturated solution result in slower reaction rate.

Moreover, the dominance of red (R) image in all three experiments also deserves extra attention. Therefore, one major set of peaks (50 to 59 ranges) from the three red images of SS304 experiments has been selected as shown in Figure 5.12.

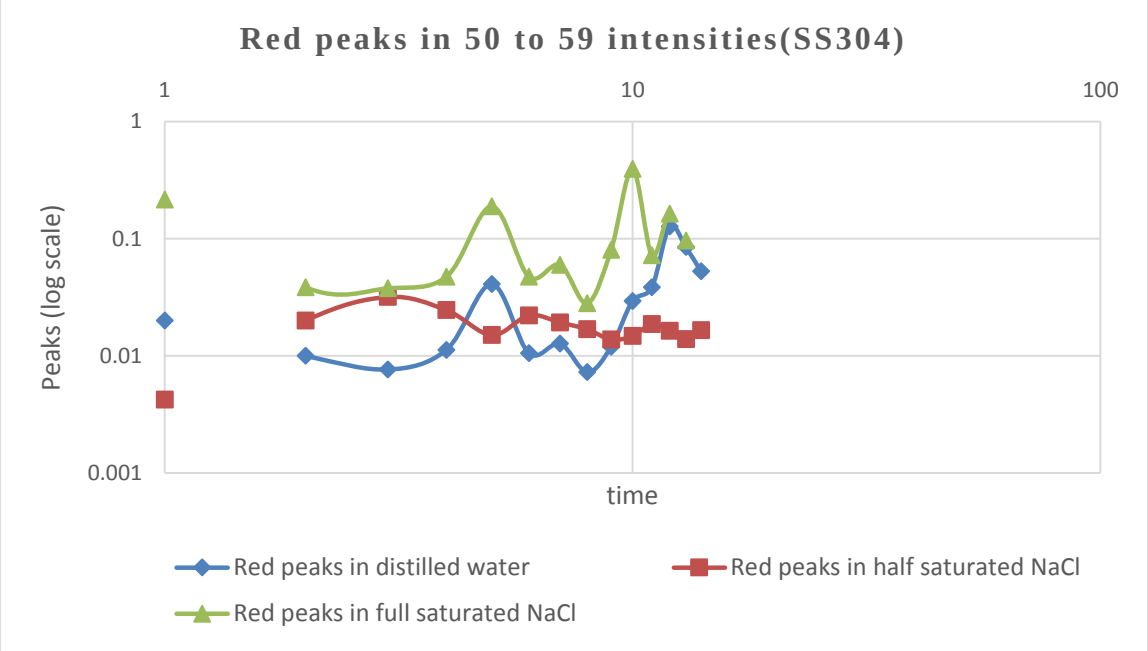

Figure 5.12: Comparison of peaks in 50 to 59 intensities in SS 304 experiments

The figure shows that peaks in 50 to 59 color intensities are growing continuously in half-saturated chloride solution; as a result SS304 is corroding quickly in this solution while peaks in distilled water and saturated chloride solutions are showing up and down then distilled. Perhaps the protective oxide layers are inhibiting the growth of different peaks at different intervals and as a result, peaks are showing upward and downward shapes.

However, to understand the internal corrosion phenomenon, it is necessary to investigate the electrochemical behavior of the chemical reactions. In the next two sections,

the open circuit potential and electrochemical impedance spectroscopy have been discussed.

5.2.4.1. Open circuit potential of SS 304

Open circuit potential (OCP) indicates the corrosion potential of the metal compared to the reference electrode in the absence of electrical connection. It is an excellent way to understand the presence of passivity and protective layers of a pitting corrosion reaction and can be used to measure the corrosion rate. Below figure shows the comparison of different corrosion potentials of SS 304 in three solutions. Here, the potentials were measured in volt (V) against Ag/AgCl reference electrode and by setting up in Gamry Framework data acquisition software.

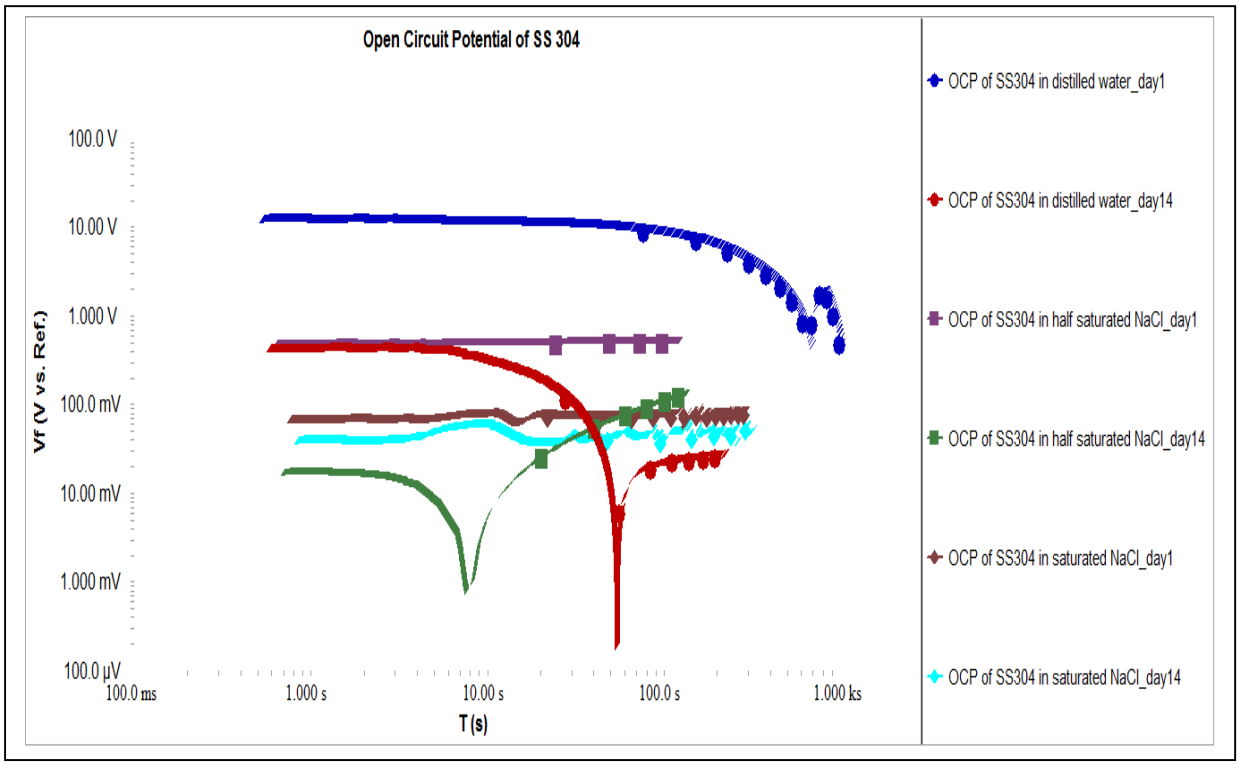

Figure 5.13: Open circuit potentials of SS 304 in distilled water, half saturated NaCl & saturated NaCl solutions

From the Figure 5.13, it is evident that almost all potentials are positive which indicate the good corrosion resistance nature of SS 304. In distilled water the initial potential is high enough i.e. 10 V to resist corrosion attack for a longer period. This resistance is due to the

oxide layer formation [57] although the rest of the potentials show that, SS 304 has little corrosion resistance in half saturated and saturated chloride solutions.

Open circuit potential result displays the similarity with RGB analysis. The high corrosion resistance of SS304 in distilled water compared to the chloride solutions is evident in both analysis.

5.2.4.2 Electrochemical impedance spectroscopy (EIS) of SS 304

Impedance measures the ability of a circuit to resist the flow of electrical current. However, unlike resistance, impedance depends on three fundamental nature of a circuit: resistor, capacitor, and inductor. Impedance is expressed by 'Z'. The relationships are as below

Z=R; when the circuit behaves as resistor (R)

Z=$j\omega L$; where ω is frequency and L is inductor

Z=$\frac{1}{j\omega C}$ where C is capacitor

From the above relationships; the impedance of a resistor does not depend on frequency. The impedance of an inductor will increase with the increase in frequency, and the impedance of a capacitor decreases with the increase in frequency. Based on these relationships, the EIS of SS 304 in distilled water and chloride solutions have been discussed below.

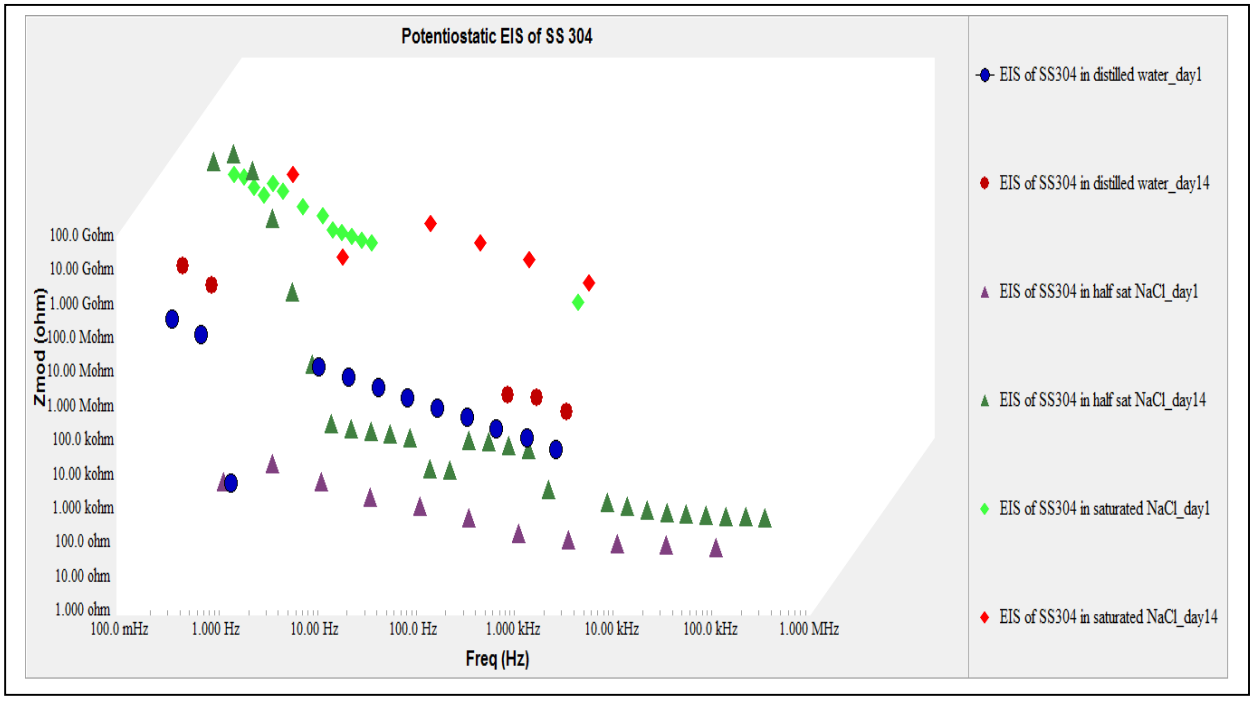

Figure 5.14: Electrochemical impedance spectroscopy of SS 304 in distilled water, half saturated NaCl & saturated NaCl solutions

In Figure 5.14, the impedance (Z) in distilled water solution, decreased slowly with the increase of frequency (Hz) which indicates the high corrosion resistance of SS304 in distilled water solution due to the formation of protective oxide layers. On the other hand, in both half saturated and saturated chloride solutions, the resistance dropped quickly.

The EIS result also shows cohesion with RGB and OCP results. Therefore, from the optical and electrochemical behavior of corrosion, it can be said that SS 304 shows high corrosion resistance in distilled water although the formation of Fe_2O_3 initiates the pitting attack. The existence of Fe_2O_3 is identified from the red image analysis, and peaks have been found in 50 to 59, 60 to 69 and 70 to 80 color intensities. The presence of chloride ions has accelerated the corrosion process in both half saturated and saturated NaCl solutions. Different sets of chloride compounds have exhibited strong presence in the green image primarily in 50 to 99, 100 to 110 and 111 to 120 intensities.

5.2.5. Carbon steel in distilled water experiment

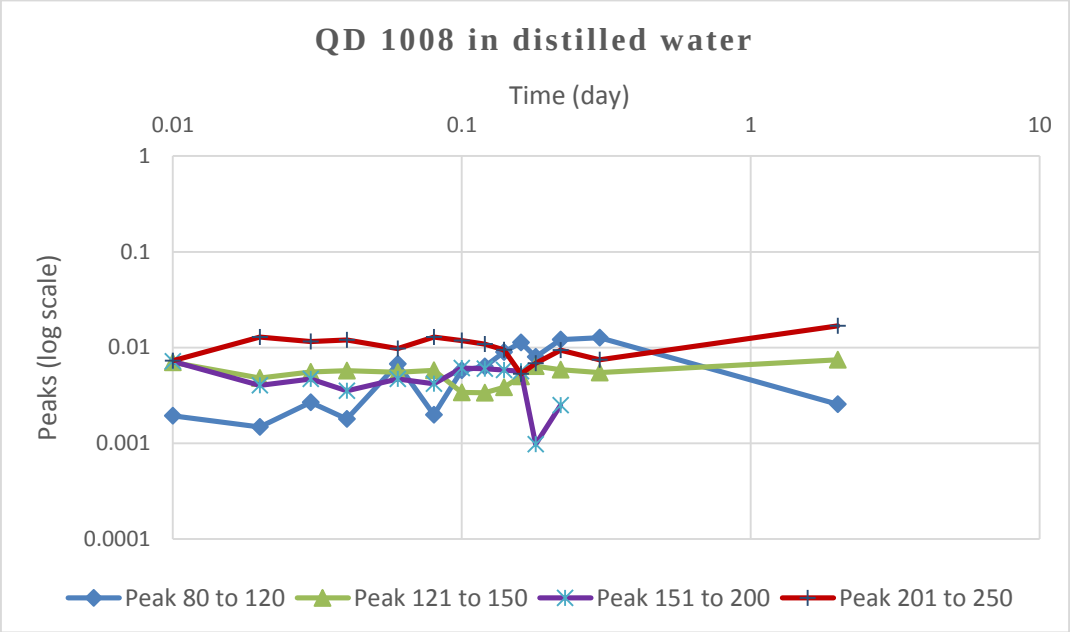

Figure 5.15: Time vs. Peaks growth of QD 1008 in distilled water (Grayscale)

Low carbon steel QD 1008 contains 99% iron (Fe) which makes it more vulnerable to corrosion attack than stainless steel. Also, a high concentration of Fe initiates the formation of Fe_2O_3 in distilled water experiment and act as primary corrosion product. The grayscale image as shown in Figure 5.12 displays the continuous growth of different sets of peaks close to log 0.01 value in 80 to 120, 121 to 150, 151 to 200 and 201 to 250 color intensities. However, to investigate the growth of different peaks in details the RGB images have been analyzed in below.

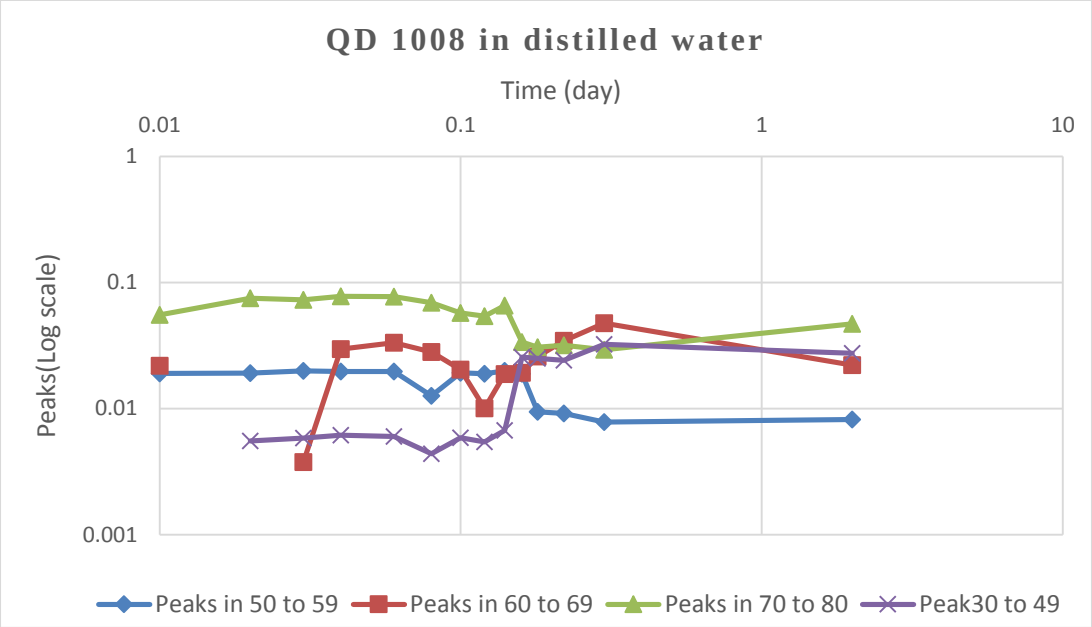

Figure 5.16: Time vs. Peaks growth of QD 1008 in distilled water (Red)

From the red image shown in Figure 5.16 the presence of four sets of peaks in 50 to 59, 60 to 69, 70 to 80 and 30 to 49 intensities is visible. Compared to the SS304 in distilled water experiment, in low carbon steel, the peaks have increased consistently. The protective oxide layer formed in QD 1008 is not strong enough to inhibit corrosion attack and as a result, corrosion product like Fe_2O_3 forms and initiates pitting on the metal surface.

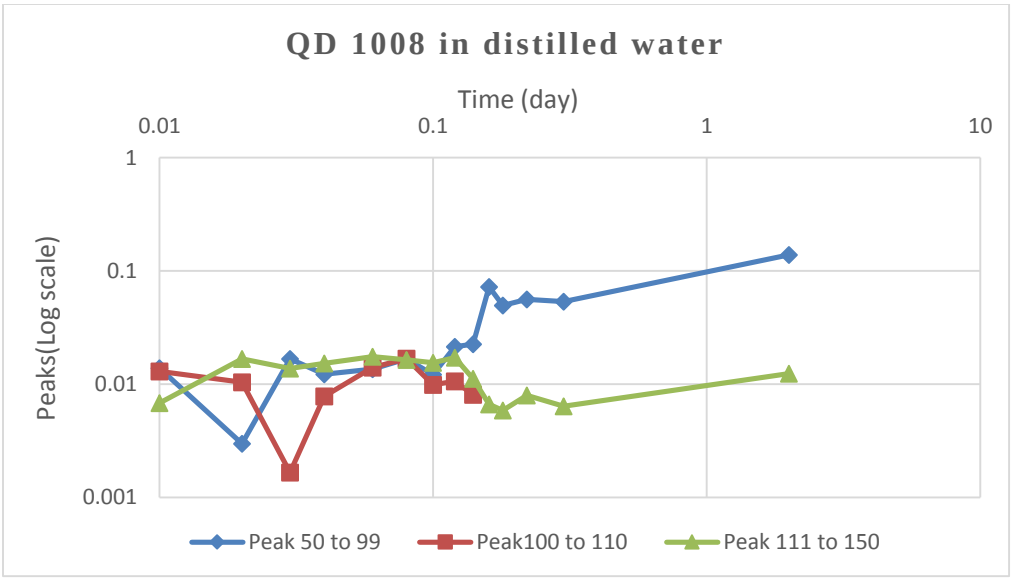

Figure 5.17: Time vs. Peaks growth of QD 1008 in distilled water (Green)

Figure 5.17 shows the growth of peaks in 50 to 99, 100 to 110 and 111 to 150 intensities in the green image.

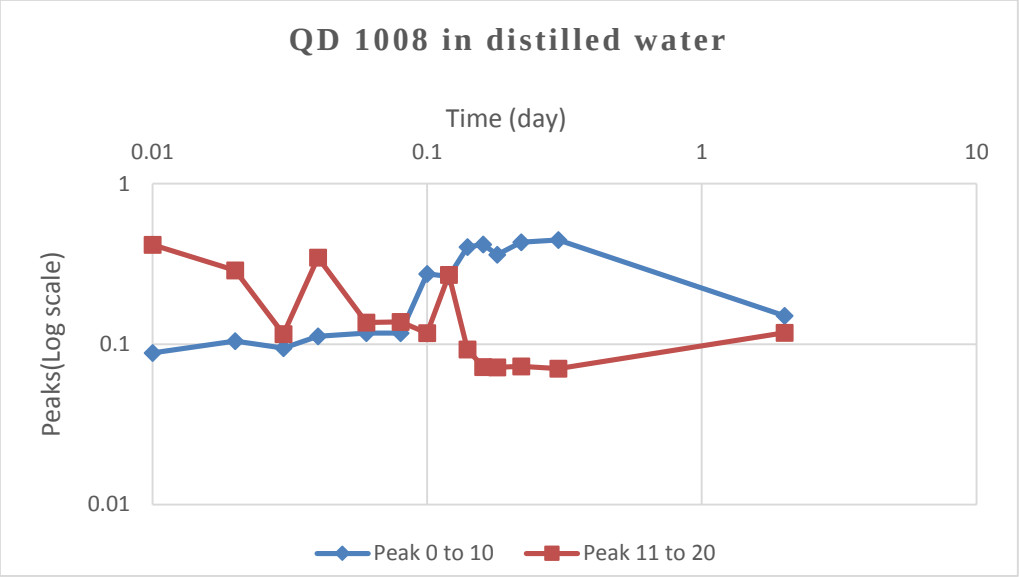

Figure 5.18: Time vs. Peaks growth of QD 1008 in distilled water (Blue)

From Figure 5.18 we see that in the blue image, peaks in 0 to 10 intensity look dominating compared to peaks in 11 to 20.

After 2 days the panel was taken out as the solution became full of corrosion products and the panel was corroded.

5.2.6. Carbon steel in half-saturated sodium chloride (NaCl) solution experiment

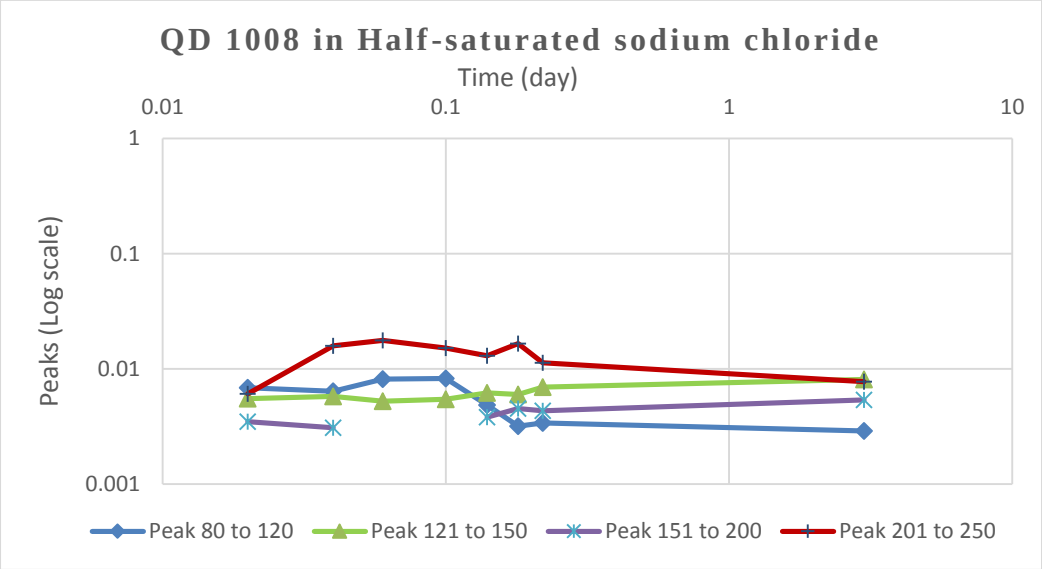

Figure 5.19: Time vs. Peaks growth of QD 1008 in half saturated NaCl (Grayscale)

The grayscale image in Figure 5.19 shows the increase of peaks in different intensities. The presence of chloride ions accelerates the corrosion process along with iron oxides. However, the RGB image analysis gives more insights about the growth of peaks.

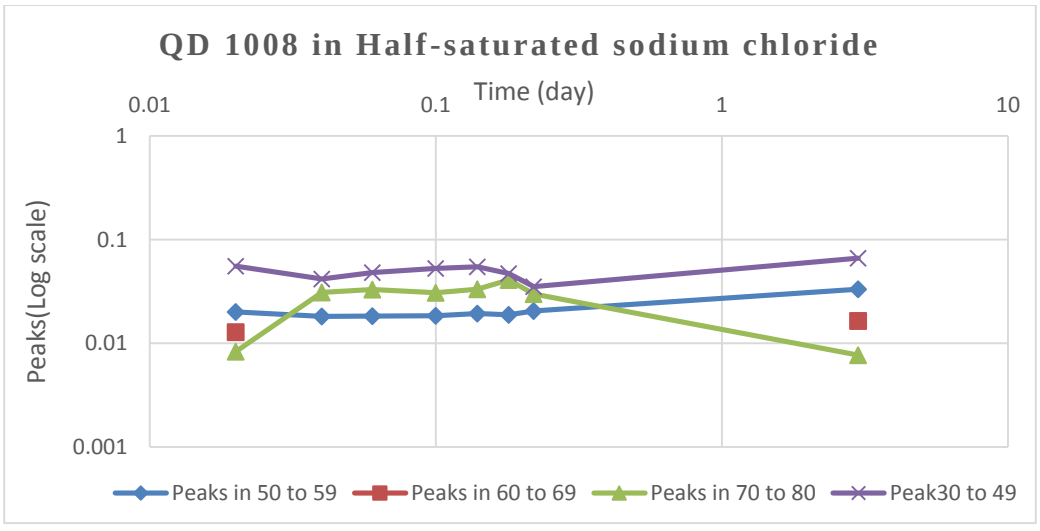

Figure 5.20: Time vs. Peaks growth of QD 1008 in half saturated NaCl (Red)

Peaks are growing consistently in the red image in 30 to 49, 50 to 59, 60 to 69 and 70 to 80 ranges as shown in Figure 5.20. The presence of chloride ions contributes to the growth

of $FeCl_2$, $FeCl_3$, along with Fe_2O_3 corrosion initiating compounds. Red image shows a consistent and steady growth of peaks due to a thin protective layer of oxides and the panel was corroded in a short time.

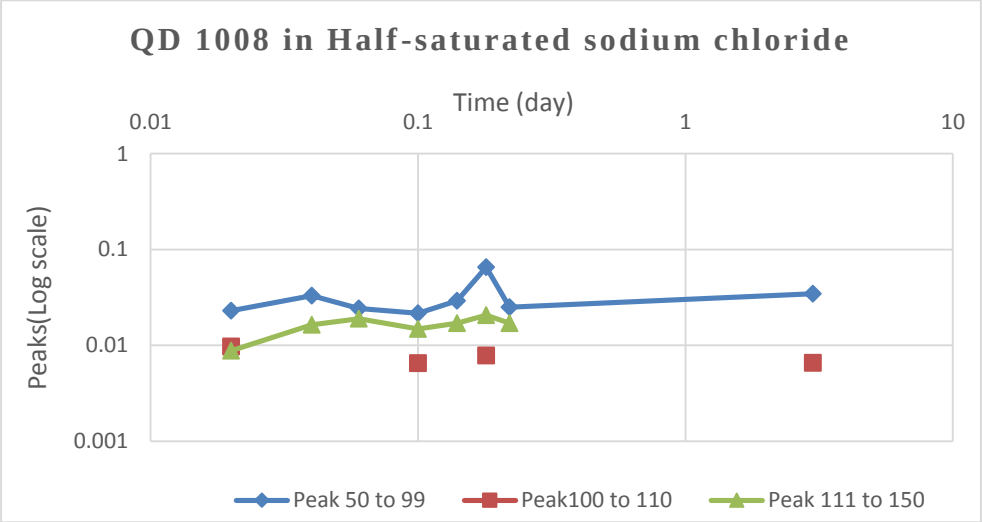

Figure 5.21: Time vs. Peaks growth of QD 1008 in half saturated NaCl (Green)

The green image as shown in Figure 5.21 displays the growth of peaks primarily in 50 to 99 and 111 to 150 color intensities. However unlike red image, only two sets of peaks are visible here.

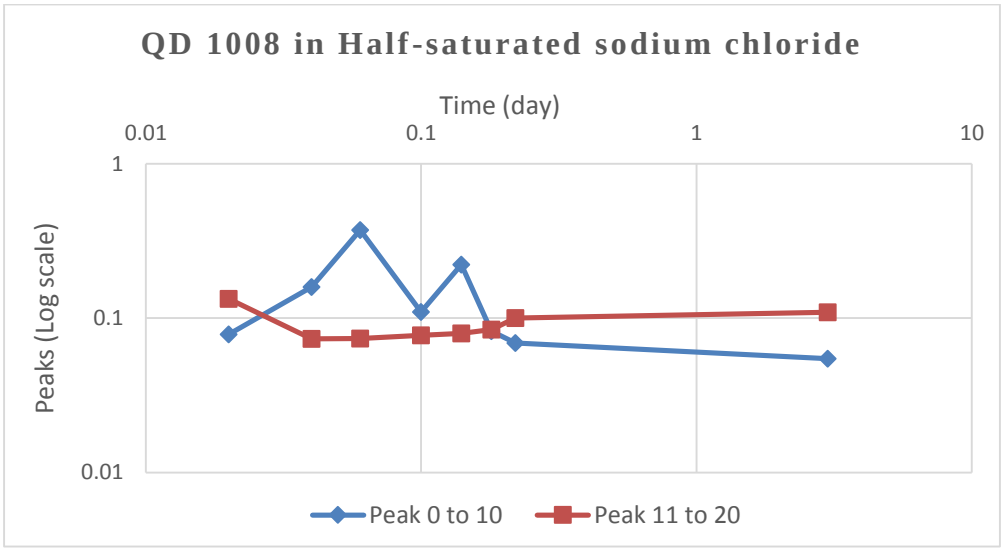

Figure 5.22: Time vs. Peaks growth of QD 1008 in half saturated NaCl (Blue)

Blue image shows the development of two sets of peaks in 0 to 10 and 11 to 20 ranges as illustrated in figure 5.22 and peaks display a continuous growth.

The experiment ended after 3 days when the solution became full of corrosion product.

5.2.7. Carbon steel in saturated sodium chloride (NaCl) solution experiment

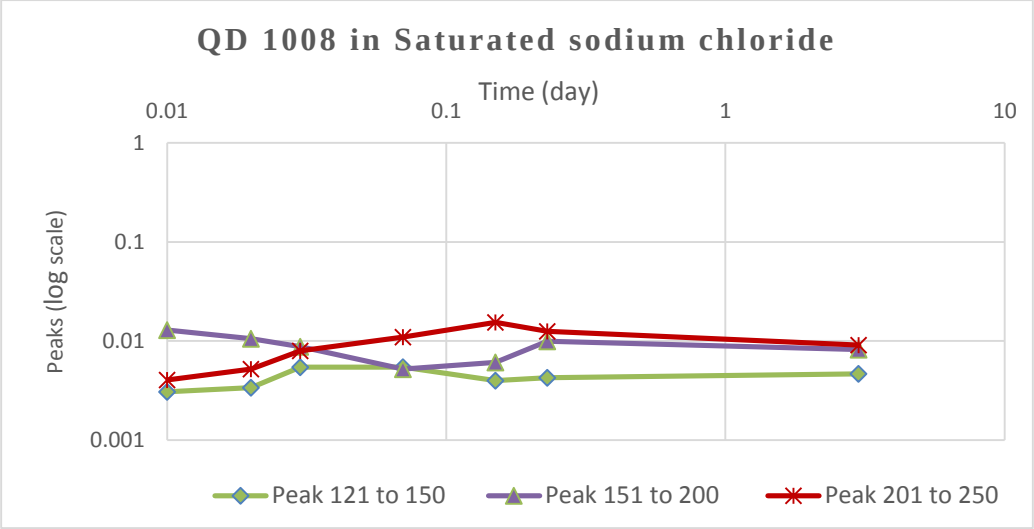

Figure 5.23: Time vs. Peaks growth of QD 1008 in saturated NaCl (Grayscale)

Three sets of peaks are visible in 121 to 150, 151 to 200 and 201 to 255 intensities showing a steady growth over time as shown in Figure 5.23. The presence of chloride ions plays a vital role along with iron (iii) oxide. RGB image analysis will be helpful to get more insights and are presented below.

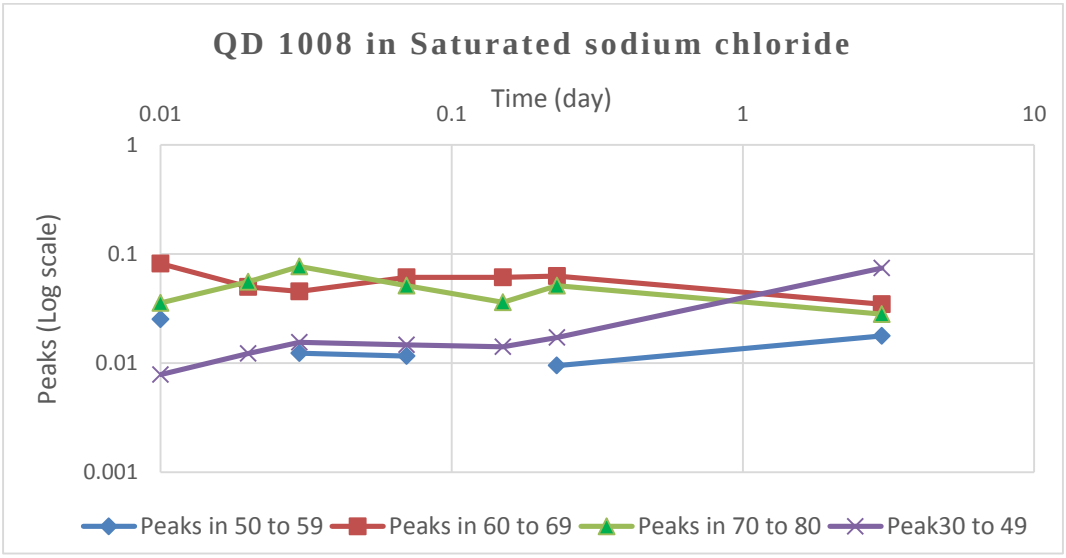

Figure 5.24: Time vs. Peaks growth of QD 1008 in saturated NaCl (Red)

In Figure 5.24 four sets of peaks are growing in 30 to 49, 50 to 59, 60 to 69 and 70 to 80 intensities; show the domination of corrosion products on the metal surface. Active chloride ions mix with iron and form $FeCl_2$ and $FeCl_3$, which initiate the corrosion attack in saturated sodium chloride solution.

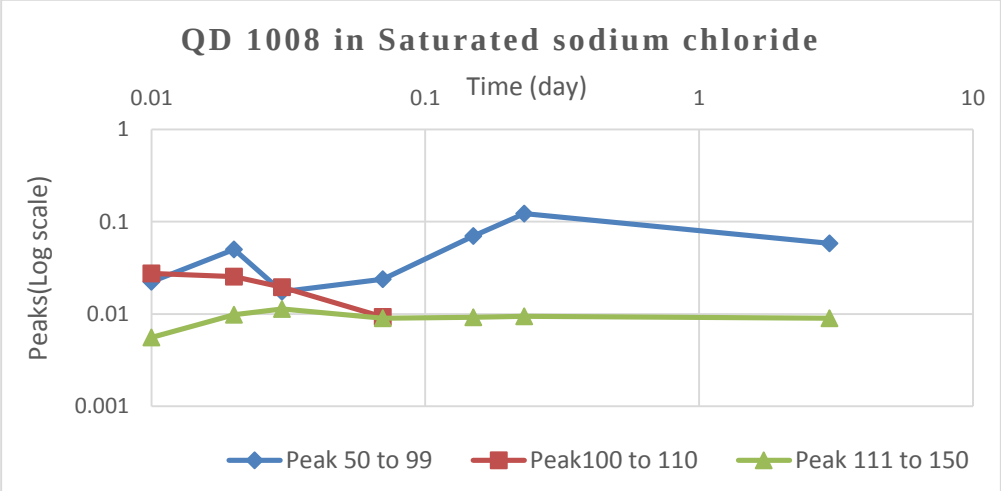

Figure 5.25: Time vs. Peaks growth of QD 1008 in saturated NaCl (Green)

Figure 5.25 displays three sets of peaks in 50 to 99, 100 to 110 and 111 to 150 intensities growing steadily.

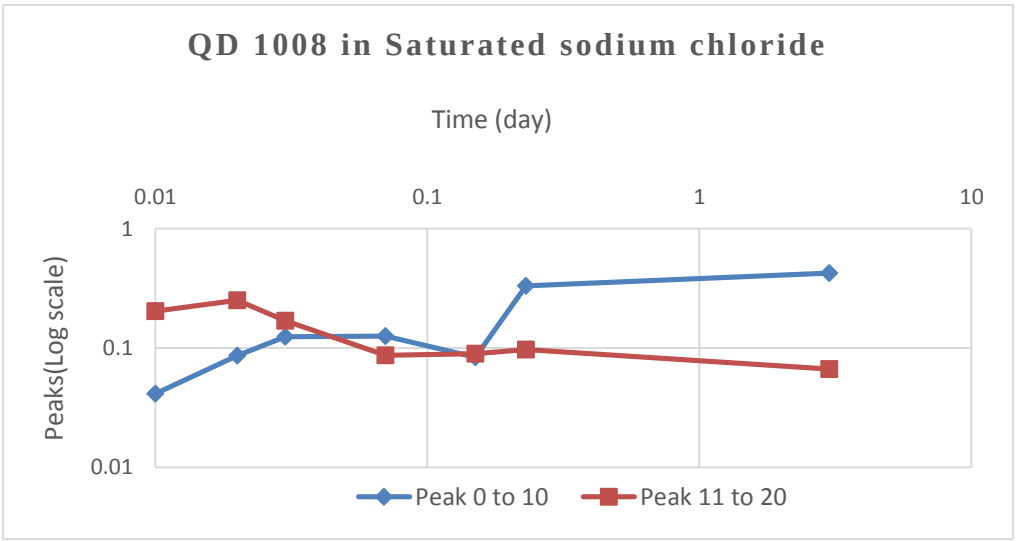

Figure 5.26: Time vs. Peaks growth of QD 1008 in saturated NaCl (Blue)

In the blue image, peaks in 0 to 10 and 11 to 20 intensities are showing an increasing trend as shown in Figure 5.26.

Finally, the panel was corroded after 3 days, and the solution became full of corrosion products.

5.2.8. A comparison of images of QD 1008 experiments

The following Table 5.3 displays a comparison of the three sets of experiment of QD 1008 in distilled water, half saturated NaCl and saturated NaCl solutions.

Table 5.3: Comparison of QD 1008 panel in distilled water, half saturated NaCl & saturated NaCl solutions

	QD 1008 in distilled water	QD 1008 in half - saturated sodium chloride	QD 1008 in saturated sodium chloride
Duration of experiment	2 days+	3 days	3 days
Dominating peaks	Red	Red	Red
Main corrosion products	Fe_2O_3	Fe_2O_3, $FeCl_2$ and $FeCl_3$	Fe_2O_3, $FeCl_2$ and $FeCl_3$

The comparison table clearly shows that low carbon steel QD 1008 was corroded within a short time than stainless steel. The presence of higher iron component and absence of other alloys has made QD 1008 vulnerable to corrosion attack.

Additionally, the dominance of red (R) image in all three experiments also deserves extra attention. Therefore, one major set of peaks (70 to 80 ranges) from the three red images of QD 1008 experiments has been selected as shown in Figure 5.27.

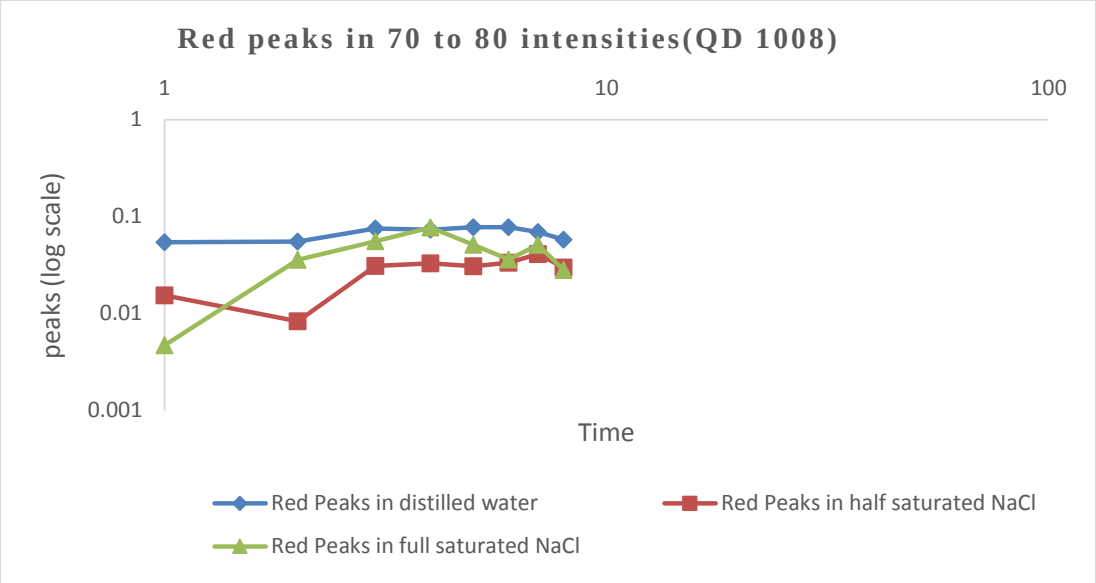

Figure 5.27: Comparison of peaks in 70 to 80 intensities in QD 1008 experiments

From the Figure 5.27 it is evident that in low carbon steel QD 1008, peaks are growing steadily in 70 to 80 intensities. High concentration of iron and absence of other alloys made QD 1008 susceptible to pitting attack. Moreover, the protective oxide layers on low carbon steel are thin and can not sustain longer. As a result pit forms easily and quickly.

The electrochemical behavior of the corrosion reactions are necessary to explore and in the following sections, open circuit potential, and electrochemical impedance spectroscopy results will be discussed and analyzed.

5.2.8.1. Open circuit potential of QD 1008

The open circuit potential (OCP) as shown in Figure 5.28 measures the potential of QD 1008 in distilled water, half saturated and saturated sodium chloride solutions compared to Ag/AgCl reference electrode.

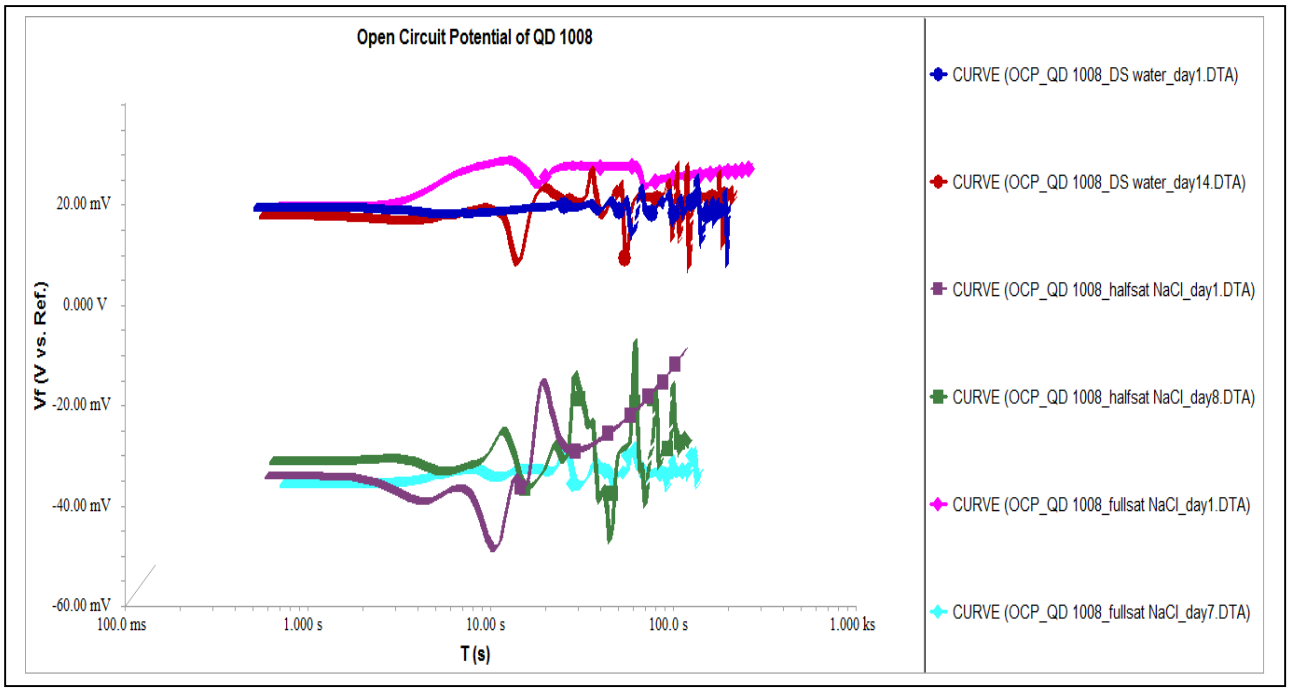

Figure 5.28: Open circuit potentials of QD 1008 in distilled water, half saturated NaCl & saturated NaCl solutions

The OCP result shows small potential for all three experiments of QD 1008. In distilled water, carbon steel showed better corrosion resistance (20mV) than in other two solutions. However, 20mV is a low potential and indicates the thin protective layer in distilled water experiment. On the other hand, the corrosion potentials in half saturated and saturated NaCl are significantly small and close to -40mV indicating the poor oxide protection.

Open circuit potential result shows similitude to the RGB analysis. Poor oxide protection and accelerated pitting attack are the main characteristics of QD 1008 in distilled water, half saturated and saturated NaCl solutions.

5.2.8.2 Electrochemical impedance spectroscopy (EIS) of QD 1008

Similar to SS 304, to understand the electrochemical behavior of the solutions, the electrochemical impedance spectroscopy for each of the experiments of QD 1008 was studied and is discussed below.

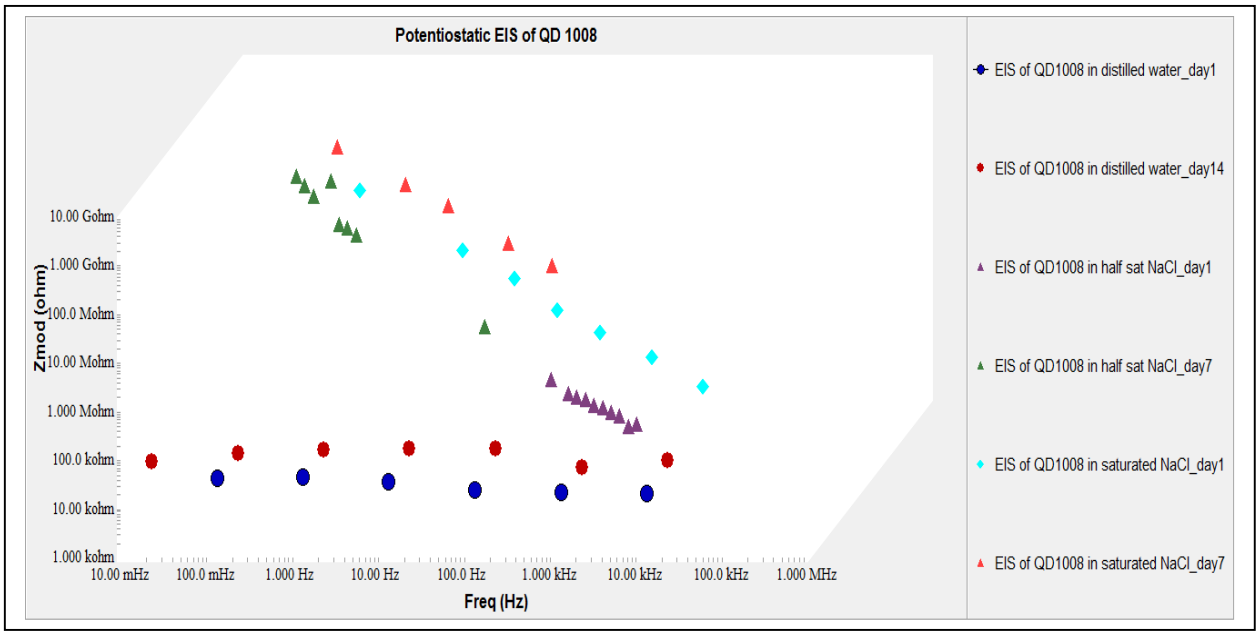

Figure 5.29: Electrochemical impedance spectroscopy of QD 1008 in distilled water, half saturated NaCl & saturated NaCl solutions

The EIS curve showed in Figure 5.29, exhibits interesting features. Although in distilled water solution, the impedance remains almost same, the small magnitude can be correlated with the thin oxide layers. On the other hand, in both chloride solutions, the impedance fell rapidly which also can be correlated with the discontinuous layer of oxides.

QD 1008 performed poorly compared to SS 304 in distilled water and chloride solutions. Due to the presence of a large amount of iron and lack of alloy materials, low carbon steel is vulnerable to corrosion pitting attack and the RGB analysis, OCP result and EIS result validate the poor performance.

Chapter 6 Analysis of Bhopal crisis in light of communication ambiguity

6.1. Flashback from Bhopal

Mentioned in chapter 1, the chemical explosion of Union Carbide India Limited (UCIL) in 1984 at Bhopal, India caused by both technical and management failures revived the importance of crisis management among the academia and business world. When the corroded steel pipe instigated the leaking and allowed iron to come into contact with water which later got mixed with methyl isocyanate (MIC), it triggered the explosion. 45 tons of gas, foam and chemical mixtures escaped to the atmosphere [45]. Numerous studies and research have been conducted to understand the reasons, contexts, and consequences of the incident. It was evident that the whole incident came as a shock to the parent company, Union Carbide and there was miscommunication between Carbide's top management and their Indian subsidiary regarding the disaster. The official committee did not even have a precise estimation of the victim right after the crisis. The company had to face numerous lawsuits and paid $470 million as demurrage [45].

Crisis challenges the strategic strength of an organization. It pushes to the limit, and forces management to protect different stakeholders. However, in protecting its interest and shifting the blame to external parties, an organization often fails to include ambiguity in their communication process. Ambiguity in communication is the possibility of different options; interpreting situation from a different angle. When ambiguity addresses the interests of the various groups, it could bring a healthy perspective in crisis management [63].

Analyzing the communication ambiguity is an effective way to evaluate an organization's actions during the crisis. Ulmer and Sellnow identified three questions: the question of evidence, the question of intent, and the question of locus while they analyzed the crisis communication in tobacco industry [65]. These questions investigate the ambiguity in the communication process during the crisis and scrutinize the actions of the internal stakeholders over externals. The question of evidence focuses on the organization's communication ability to shift responsibility based on evidence; the question of intent investigates the communication success in clarifying intention and finally, the question of locus analyzes the credibility in shifting the blame to some external parties in times of crisis

communication. However, in Bhopal context, much could not be discussed regarding locus, as no external suppliers played a vital role in UCIL's operation and the subsequent incidents.

The following sections discuss the question of evidence and question of intent.

6.2. Questions of ambiguity

6.2.1. Question of evidence

When a crisis occurs, the organization's product, service, and actions become crucial in the eye of various stakeholders. Before facing the legislative agencies and the government, the organization tries to collect evidence of the incident through scientific and legal investigations. Most of the time such investigations prefer to protect the interests of few stakeholders over others. Internal investigations also try to present ambiguous interpretations of available evidence which often confuse the customers and different communities. Ulmer & Sellnow argues that this ambiguity of evidence is constructive if it can shift the responsibility to external stakeholders by new perspective, balanced relationships with various groups, and finally, if it is within the ethical boundary [63].

6.2.2. Question of intent

Crisis reveals different communication gaps between the organization and its stakeholders. As a part of the operating environment, the organization is required to maintain a healthy conformity with the surroundings. However, during crises, when it fails to show concern for the community, and exhibits irresponsible actions, this compliance breaks. Therefore, the overall intention of the organization falls under question in the eyes of media and consumers. In this circumstances, a rhetoric clarification with sufficient ambiguity can ensure trust among different groups. Additionally, to maintain an ethical practice, the organization should be aware of the interests of external audiences particularly those who suffered.

In Bhopal, communication occurred through various channels. Union Carbide dealt the crisis with the Indian government until 1999, when Dow Chemical bought UC for $8.89 billion stock [49]. Due to the nature of the crisis, Dow Chemical also had to resolve few issues for the next few years. However, for a better perspective, the communication

between UC and the Indian government have been analyzed in the following section. Applying the question of evidence and question of intent some of Union Carbide's actions during the crises will be dissected.

6.3. Analysis of crisis management of Union Carbide

6.3.1. Question of evidence

Despite owning 50.9 percent shares of UCIL, UC was blamed mainly for the tragedy. 145 federal and state suits were filed against them, including a civil suit by the Indian government in Federal District Court in New York City. To respond legal suits and media pressure, Union Carbide took different initiatives. However, they were not successful to shift few blames due to lack of documented evidence. It was reported that there were slums around the Bhopal plant, and a large number of people living in those slums were the direct victims of MIC contamination [45]. Right after the incident, Union Carbide could blame the Indian government for allowing those slums if they had any documented communication. A documented evidence could create ambiguity in the legal suits and open other possibilities.

The initial investigation was also delayed for three months due to the bureaucratic blockage imposed by the Indian government and it took almost two years for UC to verify interview, and witness documents as the access were limited [64]. According to B. Browning, retired Vice President of EHS program at Union Carbide,

"*We did not have answers to such basic questions as, "What caused the disaster?" or even, "What happened?" In this information vacuum, we reaffirmed a standing procedure -- no speculation" [64, p.6]*

Union Carbide could hold the Indian government responsible for the communication obstacles and present the evidence in media. This allegation could open a new perspective in overall crisis management.

However, later in 1987, Union Carbide succeeded in one case to depict the local government's obstruction in building a rehabilitation center at Bhopal; when CBS covered the story in an episode of "60 Minutes" in 1987 [64].

The analysis shows an overall poor communication channel between UC and Indian government regarding several issues. Union Carbide could have shared some responsibilities if they had documented evidence which could create a healthy ambiguity in the overall communication process and enable them to deal with the crises in a better way.

6.3.2. Question of intent

Perhaps the biggest failure of Bhopal crisis was Union Carbide's intention, which was under serious question. There were series of events that went against internal stakeholder's interest and as they tried to prioritize those, it gave a negative impression to Indian government and media. With a good intention, Union Carbide offered $5 million for relief and $200 million to settle as compensation package right away [64]. However, the $5 million was refused by the Indian government and was later used by the Red Cross team. On the other hand, information was leaked that, the company was insured for $200 million, so the settlement offer failed to earn sympathy from the Indian community [45]. Moreover, the prime minister of India, Indira Gandhi was assassinated one month before the gas leak, and several political tensions were also rising in locality [64], which put the victims and their well-wishers in an insecure climate. It was a common thought that Union Carbide did not care for the victims rather than saving themselves.

In additions, in between 1978 and 1983, several toxic spills incidents were reported and weren't addressed properly by UCIL [47]. This negligence was unexpected from a global chemical company and was seen as an ethical compromise.

It is true that crises put the organization into a difficult situation. However, by applying communication ambiguity organization can be benefited and clear their intention. Union Carbide failed in taking these advantages; instead of staying away from serious allegations they could have confronted those with an action plan. The relationship dynamics between Union Carbide and Indian government did not seem transparent nor was the authority delegation. Overall the company demonstrated poor communication channel regarding the question of intent.

6.4. Final thoughts

Bhopal incident had a severe impact on Union Carbide. The overall growth of Union Carbide started to collapse and gradually its worldwide operation shrank. Post-crisis analysis of Bhopal incident reveals multiple defects in operation and management at UCIL. It is evident that earlier corrosion detection could have prevented the technical failure. Climatically, Bhopal is similar to West Virginia, USA where UC had another facility; both have a humid and sub-tropical climate. However, the operation and maintenance standards were not similar [47]. The importance of periodic preventive maintenance was not perceived seriously in many developing countries like India in 1984. Several leaking incidents were reported in Bhopal and were overlooked by the local management [47]. Furthermore, the field maintenance personnel were not familiarized with high-tech corrosion monitoring tools. Perhaps if they had access to an easily operable camera based corrosion monitoring tool, the detection could have been easier. Also, water contains different salts in humid sub-tropical climate, and salt water contains a higher amount of iron which is a corrosion triggering element. Hence, Union Carbide could also investigate the salt concentration in Bhopal as a preventive measure.

Prevention is better than cure; however, during the crisis, the cure comes in the form of management effectiveness. The way Union Carbide mismanaged the post-explosion public affairs, points finger to the lack of proper communication. By incorporating ambiguity in the communication process, UC could formulate a successful strategy to address all stakeholders.

Finally, an engineering manager acts as a bridge between the technical part and the management and often during a crisis, he/she has to protect interests of various stakeholders. This case study analysis could motivate an engineering manager to utilize communication ambiguity to balance those interests in crisis.

Chapter 7: Conclusion

The primary purpose of this research is to identify a simple and affordable camera-based technology to understand the corrosion behavior of stainless steel SS 304 and low carbon steel QD 1008 in distilled water, half-saturated sodium chloride and saturated sodium chloride solutions. By setting up six panels in those solutions, the objective was tried to achieve. SS 304 showed high corrosion resistance compared to QD 1008. From the RGB image analysis results, it is evident that, for both SS304 and QD 1008, Fe_2O_3 played a significant role as a corrosion initiating product in both distilled water and chloride solutions. The red image displayed four sets of peaks, growing due to the Fe_2O_3. The presence of chloride ions also initiated few compounds like $FeCl_2$, $FeCl_3$, $CrCl_2$, $CrCl_3$ $(H_2O)_x$; x=1, 5, 6. Additionally, the red image analysis has identified 30 to 49, 50 to 59, 60 to 69 and 70 to 80 color intensities on grayscale (0 to 255) as a probable location to investigate for peaks growth. In the case of green image, 50 to 99, 100 to 110 and 111 to 150 are suitable locations for peaks to grow. The OCP and EIS studies also comply with the RGB analysis and conclude that, both SS 304 and QD 1008 exhibit better corrosion resistance in distilled water than chloride solutions. The electrochemical results have helped to understand the strength of protective oxide layers in different solutions.

As a secondary objective, this study has analyzed the communication ambiguity of Union Carbide in light of the chemical explosion at Bhopal, India. Ambiguity plays a positive part in crisis communication and helps the organization to share responsibilities, clarify intentions as well as shift blame under ethical boundaries. It creates opportunities for different explanations of any crisis incident. However, the analysis shows that Union Carbide failed to take the benefits of ambiguity in their communication process with Indian Government. The inclusion of communication ambiguity will help future engineers and business leaders as they often get consumed by the technical details; whether it is a corrosion attack on a continuous flow pipeline or a malfunction of a safety valve in a process plant, and overlook the bigger goal.

Finally, the collected data tables, images, and the Matlab codes are provided in Appendices and hope these will be beneficial in future studies.

Chapter 8: Future work

Due to the limitations of time and few resources, some potential future works are discussed below.

1) In this research, only one panel was used for each set of experiment. The number of panels could be increased to get more validated results.
2) From the master's research work of Yan Fang; a graduate student of Mechanical & Nuclear Engineering at Virginia Commonwealth University, under the supervision of Dr. Brian Hinderliter, the idea of developing a Matlab code similar to the flood-fill algorithm to quantify the growth of corrosion pits on the metallic surface can be investigated.
3) Additionally, the algorithm could be developed to locate the coordinate of different corrosion pits.
4) In this research work some literature from solar spectrum were cited. The research works on those articles, or similar concepts could be beneficial to quantify Fe^{3+}, Cr^{3+} oxides, and chlorides along with other compounds.
5) The peaks in different color intensities change based on gloss and can provide various results. To streamline the results, statistical methods can be applied to predict the weighted combination of trends of different peaks. Finally, better corrosion results will be achieved.

Bibliography

[1] D. A. Jones, *Principles and Prevention of Corrosion.* Macmillan Publishing Company, New York, 1996.

[2] R. M. Pidaparti, B. Hinderliter, and D. Maskey, "Evaluation of Corrosion Growth on SS304 Based on Textural and Color Features from Image Analysis," *ISRN Corros.* vol. 2013, pp. 1–7, 2013.

[3] W. D. Callister, *Materials Science and Engineering: An Introduction*, vol. 6, no. 6058. 2007.

[4] J. H. P. Gerhardus H. Koch, Michiel P.H. Brongers, Neil G. Thompson, Y. Paul Virmani, "Corrosion Costs and Preventive Strategies in the United States," *Nace Int.*, 2002.

[5] A. B. Smith and R. W. Katz, "US billion-dollar weather and climate disasters: Data sources, trendistilled, accuracy and biases," *Nat. Hazardistilled*, vol. 67, no. 2, pp. 387–410, 2013.

[6] G. F. Hays, "Now is the Time," *World Corrosion. Organization.* pp. 1–2, 2013.

[7] C. M. Hansson, "The impact of corrosion on society," *Metall. Mater. Trans. A Phys. Metall. Mater. Sci.*, vol. 42, no. 10, pp. 2952–2962, 2011.

[8] H. Kaesche, "Pitting Corrosion," in *Corrosion of Metals SE - 12*, Springer Berlin Heidelberg, 2003, pp. 324–388.

[9] L. Tao, S. Song, X. Zhang, Z. Zhang, and F. Lu, "Image analysis of atmospheric corrosion of field exposure high strength aluminum alloys," *Appl. Surf. Sci.*, vol. 254, no. 21, pp. 6870–6874, 2008.

[10] D. M. Sherman and T. D. Waite, "Electronic spectra of Fe3+ oxides and oxide hydroxides in the near IR to near UV.," *Am. Mineral.*, vol. 70, no. 11–12, pp. 1262–1269, 1985.

[11] Hematite. (2015, July 20). In *Wikipedia, The Free Encyclopedia*. Retrieved 18:17, August 18, 2015,
from https://en.wikipedia.org/w/index.php?title=Hematite&oldid=672263080

[12] Wikipedia contributors, "Color of chemicals," *Wikipedia, The Free Encyclopedia.*, 2015. [Online].Available:https://en.wikipedia.org/w/index.php?title=Color_of_chemicals&oldid=669000017.

[13] W.-W. Yu, F. He, and P. Xi, "A rapid 3D seed-filling algorithm based on scan slice," *Computers & Graphics*, vol. 34, no. 4, pp. 449–459, Aug. 2010.

[14] L. Feng and S. H. Soon, "An effective 3D seed fill algorithm," *Computers & Graphics*, vol. 22, no. 5, pp. 641–644, Oct. 1998.

[15] Wikipedia contributors, "Flood Fill," *Wikipedia, The Free Encyclopedia*, 2015. [Online]. Available: https://en.wikipedia.org/w/index.php?title=Flood_fill&oldid=674549808.

[16] NASA-Kennedy Space Center, "Fundamentals of Corrosion and Corrosion Control," *Corrosion Technology Laboratory, NASA*. [Online]. Available: http://corrosion.ksc.nasa.gov/corr_fundamentals.htm.

[17] Wikipedia contributors, "Corrosion," *Wikipedia, The Free Encyclopedia*, 2015. [Online]. Available: https://en.wikipedia.org/w/index.php?title=Corrosion&oldid=681589017.

[18] World Steel Association, "Crude steel production 2014-2015," *2015*. [Online]. Available: https://www.worldistilledteel.org/statistics/crude-steel-production.html.

[19] E. Lee Bray, "Aluminum," *US Geological Survey Minerals Yearbook.* vol. 1, no. 703, pp. 16–17, 2014.

[20] Wikipedia contributors, "Iron," *Wikipedia, The Free Encyclopedia*, 2015. [Online]. Available: https://en.wikipedia.org/w/index.php?title=Iron&oldid=683310097.

[21] Aluminium Federation (ALFED), “Aluminium and Corrosion,” *Int. Alum. Inst. London*, vol. 44, no. 0, pp. 1 – 5.

[22] T. Ross and N. Lott, “A climatology of 1980-2003 extreme weather and climate events,” *Natl. Ocean. Atmos. Adm.*, no. 01, 2003.

[23] C. O. Obuekwe and D. W. S. Westlake, “Occurrence of bacteria in Pembina crude oil pipeline system and their potential role in corrosion process,” *Appl. Microbiol. Biotechnol.*, vol. 26, no. 4, pp. 389–393, 1987.

[24] Little, B. J., Mansfeld, F. B., Arps, P. J. and Earthman, J. C. 2007. Microbiologically Influenced Corrosion. Encyclopedia of Electrochemistry. .

[25] Bhopal disaster. (2015, September 26). In *Wikipedia, The Free Encyclopedia*. Retrieved 20:55, October 4, 2015, from https://en.wikipedia.org/w/index.php?title=Bhopal_disaster&oldid=682808422

[26] “Berlin_Kongresshalle.” https://upload.wikimedia.org/wikipedia/commons/8/8b/Berlin_Kongresshalle_BW_1.jpg.

[27] Aloha Airlines Flight 243. (2015, September 24). In *Wikipedia, The Free Encyclopedia*. Retrieved 22:37, October 4, 2015, fromhttps://en.wikipedia.org/w/index.php?title=Aloha_Airlines_Flight_243&oldid=682601296.

[28] R. Levinson, P. Berdahl, and H. Akbari, “Solar spectral optical properties of pigments—Part I: model for deriving scattering and absorption coefficients from transmittance and reflectance measurements,” *Sol. Energy Mater. Sol. Cells*, vol. 89, no. 4, pp. 319–349, Dec. 2005.

[29] J.-S. Han and J.-H. Park, “Detection of corrosion steel under an organic coating by infrared photography,” *Corros. Sci.*, vol. 46, no. 4, pp. 787–793, Apr. 2004.

[30] S. J. Palmer and R. L. Frost, “Characterisation of bauxite and seawater neutralised bauxite residue using XRD and vibrational spectroscopic techniques,” *J. Mater. Sci.*, vol. 44, no. 1, pp. 55–63, Dec. 2008.

[31] S. Wang, H. M. Ang, and M. O. Tadé, "Novel applications of red mud as coagulant, adistilledorbent and catalyst for environmentally benign processes," *Chemosphere*, vol. 72, no. 11, pp. 1621–1635, 2008.

[32] E. López, B. Soto, M. Arias, a Núñez, D. Rubinos, and M. T. Barral, "Adistilledorbent properties of red mud and its use for wastewater treatment," *Water Res.*, vol. 32, no. 4, pp. 1314–1322, 1998.

[33] C. Rémazeilles and P. Refait, "Fe (II) hydroxycarbonate Fe_2 (OH) $_2CO_3$ (chukanovite) as iron corrosion product: Synthesis and study by Fourier Transform Infrared Spectroscopy," *Polyhedron*, vol. 28, no. 4, pp. 749–756, Mar. 2009.

[34] F. L. Floyd, S. Avudaiappan, J. Gibson, B. Mehta, P. Smith, T. Provder, and J. Escarsega, "Using electrochemical impedance spectroscopy to predict the corrosion resistance of unexposed coated metal panels," *Prog. Org. Coatings*, vol. 66, no. 1, pp. 8–34, Sep. 2009.

[35] K. Darowicki, S. Krakowiak, and P. Ślepski, "Evaluation of pitting corrosion by means of dynamic electrochemical impedance spectroscopy," *Electrochim. Acta*, vol. 49, no. 17–18, pp. 2909–2918, Jul. 2004.

[36] M. Jez, M. Mitoraj, E. Godlewska, M. Jakubowska, and B. Bas, "Evaluation of corrosion behaviour of selected metallic samples by electrochemical noise measurements," *J. Solid State Electrochem.*, vol. 18, no. 6, pp. 1635–1646, 2014.

[37] J. Xiong, M. Y. Tan, and M. Forsyth, "The corrosion behaviors of stainless steel weldments in sodium chloride solution observed using a novel electrochemical measurement approach," *Desalination*, vol. 327, pp. 39–45, 2013.

[38] T.G.Gooch, Corrosion behavior of welded stainless steel, Weld. J.75 (1996) 135–154

[39] R. Levinson, P. Berdahl, and H. Akbari, "Solar spectral optical properties of pigments—Part I: model for deriving scattering and absorption coefficients from

transmittance and reflectance measurements," *Sol. Energy Mater. Sol. Cells*, vol. 89, no. 4, pp. 319–349, Dec. 2005.

[40] www.transtutors.com, "Passivity of Metals." [Online]. Available: http://www.transtutors.com/homework-help/engineering-chemistry/corrosion-/passivity-metals.aspx.

[41] ASTM, *Standard Guide for Examination and Evaluation of Pitting Corrosion*. Philadelphia: ASTM, 1988.

[42] H. H. U. J. Horvath, "Critical Potentials for Pitting Corrosion of Ni, Cr-Ni, Cr-Fe, and Related Stainless Steels," *Electrochem. Soc.*, vol. 115, no. 8, pp. 791–795, 1968.

[43] S. Mallat, *A Wavelet Tour of Signal Processing*. Elsevier Science, 1999.

[44] Shrivastava, Paul. "Rereading Bhopal: Anatomy of a crisis through a feminist lens." *Journal of Management Inquiry* 3.3 (1994): 278-285.

[45] F. Sen and W. G. Egelhoff, "Six Years and Counting: Learning from Crisis Management at Bhopal," *Public Relat. Rev.*, vol. 17, no. 1, pp. 69–83, 1991.

[46] Shrivastava, Paul, et al. "Understanding industrial crises [1]." *Journal of management studies* 25.4 (1988): 285-303.

[47] B. Bowonder and H. A. Linstone, "Notes on the Bhopal accident: Risk analysis and multiple perspectives," *Technol. Forecast. Soc. Change*, vol. 32, no. 2, pp. 183–202, 1987.

[48] United States. President's Commission on the Accident at Three Mile Island.*The need for change, the legacy of TMI: report of the President's Commission on the Accident at Three Mile Island*. The Commission, 1979.

[49] Union Carbide. (2015, October 30). In *Wikipedia, The Free Encyclopedia*. Retrieved 18:47, December 15, 2015, from https://en.wikipedia.org/w/index.php?title=Union_Carbide&oldid=688277998

[50] AZoM.com, “AISI 1008 Carbon Steel (UNS G10080),” 2015. [Online]. Available: http://www.azom.com/article.aspx?ArticleID=6538.

[51] Caproco, “Access & Retrieval System COUPONS / PROBES.” [Online]. Available: http://www.caproco.com/access/coupons.htm.

[52] ASTM, “Corrosion Standardistilled and Wear Standardistilled.” [Online]. Available: http://www.astm.org/Standardistilled/corrosion-and-wear-standardistilled.html#G01.04.

[53] NACE, “Standard Practices.” [Online]. Available: https://www.nace.org/uploadedFiles/Committees/List of NACE Standardistilled.pdf.

[54] Wikipedia contributors, “Manganese (II) oxide.” [Online]. Available: https://en.wikipedia.org/w/index.php?title=Manganese (II) _oxide&oldid=688609031.

[55] Iwaya, Kiyoshi, and Haruhiko Yamamoto. "The diagnosis of optimal harvesting time of rice using digital imaging." 農業気象 60.5 (2005): 981-984.

[56] F. Wang, H. Yamamoto, and Y. Ibaraki, “Measuring leaf necrosis and chlorosis of bamboo induced by typhoon 0613 with RGB image analysis,” J. For. Res., vol. 19, no. 3, pp. 225–230, 2008.

[57] Y. S. Jimenez, M. T. Gil, M. T. Guerra, L. S. Baltes, and J. C. M. Rosca, “Interpretation of Open Circuit Potential of Two Titanium Alloys For A Long Time Immersion In Physiological Fluid,” *Transilv. Univ. Brasov*, pp. 197–204, 2009.

[58] Y. Fang., “SIMULATION, MEASUREMENT AND IMAGE ANALYSIS OF CORROSION INITIATION AND GROWTH RATE OF ALUMIUM 2024 AND STEEL 304,” Virginia Commonwealth University, 2011.

[59] Alspi, “Corrosion Coupons,” vol. 2, no. 2, pp. 4–6.

[60] E. Thickness, M. Operating, and M. Operating, “Retrievable Electrical Resistance (ER) Probe Flush Mounting with Strip Element.”

[61] D. Itzhak and T. Zilberberg, “Pitting Corrosion Evaluation By Computer Image Processing *,” vol. 21, no. March 1980, pp. 17–22, 1981.

[62] E. N. Codaro, R. Z. Nakazato, a. L. Horovistiz, L. M. F. Ribeiro, R. B. Ribeiro, and L. R. O. Hein, “An image processing method for morphology characterization and pitting corrosion evaluation,” *Mater. Sci. Eng. A*, vol. 334, pp. 298–306, 2002.

[63] R. R. Ulmer, T. L. Sellnow, and R. Robert, “Consistent Ambiguity Crisis Communication : Jack in the Box as a Case Study of Questions in Organizational,” vol. 25, no. 2, pp. 143–155, 2012.

[64] J. B. Browning, “Jackson Browning Report - Union Carbide Corp.,” *Saf. Heal.*, pp. 1–15, 1993

[65] Ulmer, Robert R., and Timothy L. Sellnow. "Strategic ambiguity and the ethic of significant choice in the tobacco industry's crisis communication."*Communication Studies* 48.3 (1997): 215-233.

[66] Wikipedia contributors, “Bhopal,” *Wikipedia, The Free Encyclopedia*, 2016. [Online]. Available: https://en.wikipedia.org/wiki/Bhopal#Climate.Wikipedia contributors, “Bhopal,” *Wikipedia, The Free Encyclopedia*, 2016. [Online]. Available: https://en.wikipedia.org/wiki/Bhopal#Climate.

[67] B. Simon, “Dissolution rates of NaCl and KCl in aqueous solution,” *J. Cryst. Growth*, vol. 52, no. PART 2, pp. 789–794, 1981.

APPENDIX-A- Matlab Codes

1. RGB and grayscale conversion code

```
clear all

driveLocation = 'C:\Users\User\Documents\MATLAB\SplitColorImageToRGBChannel\';

input = imread(strcat('QD2_DISTILLED_day13.jpg'));

[x,y,z] = size (input);

Grayscale=rgb2gray(input);
red = input;
green = input;
blue = input

for k =1:z
   for i=1:x
      for j=1:y
         if k==1
            red(i,j,2:3) = 0;
         elseif k==2
            green(i,j,1:2:3) = 0;
         elseif k==3
            blue(i,j,1:2) = 0;
         end
      end
   end
end

imwrite (red, strcat('C:\Users\User\Documents\MATLAB\QD2_DISTILLED_day13_R.jpg'),
'jpg');
imwrite(green, strcat('C:\Users\User\Documents\MATLAB\QD2_DISTILLED_day13_G.jpg'),
'jpg');
imwrite(blue, strcat('C:\Users\User\Documents\MATLAB\QD2_DISTILLED_day13_B.jpg'),
'jpg');
imwrite(Grayscale,
strcat('C:\Users\User\Documents\MATLAB\QD2_DISTILLED_day13_Gray.jpg'), 'jpg');
```

2. Histogram code

```
clear all
a=imread('QD2_DISTILLED_day14.jpg');
M=rgb2gray(a);
K=imhist(M);
subplot(1,2,1); imshow(M);
```

```
subplot(1,2,2); imhist(M);
title('histogram day14');
```

APPENDIX-B- Experimental images

Stainless Steel SS 304 in distilled water experiment images

Day 0

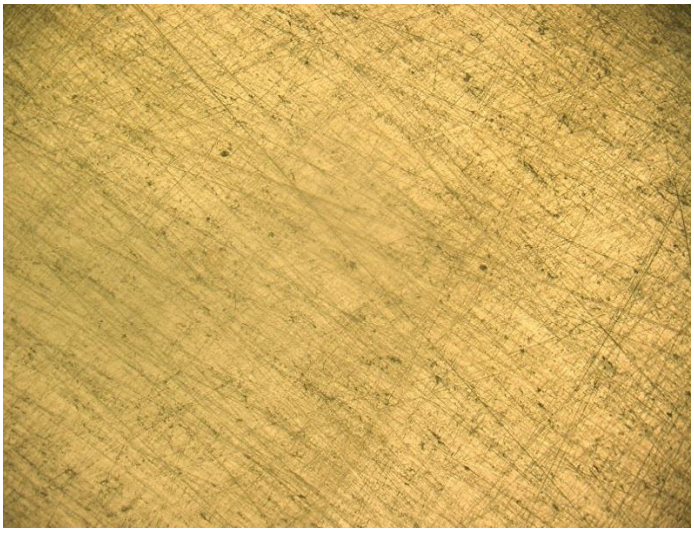

Day 0.04

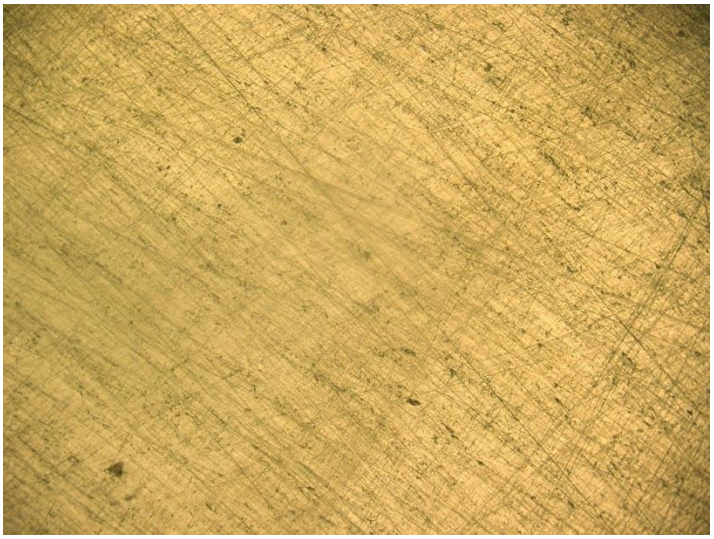

Day 0.08

Day 0.16

Day 0.24

Day 0.32

Day 0.45

Day 1

Day 2

Day 3

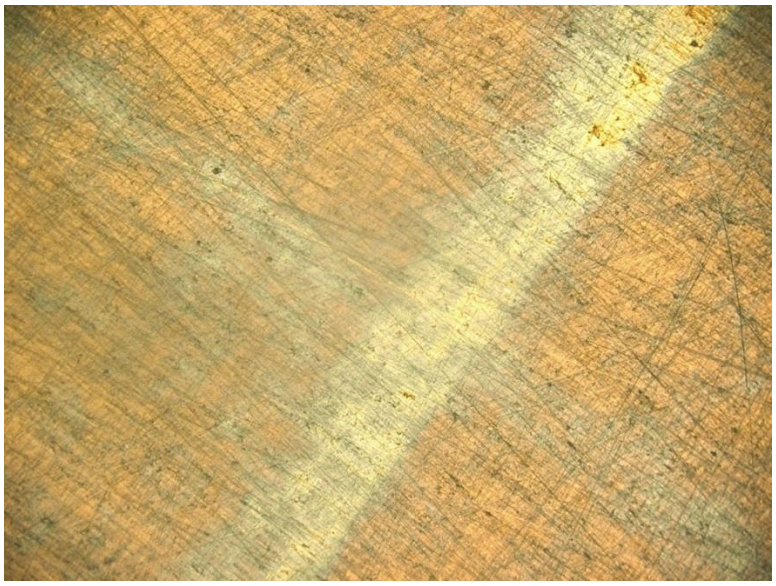

Day 10

Day 17

Day 26

Day 52

Day 92

Stainless steel SS 304 in Half-saturated NaCl solution experiment images

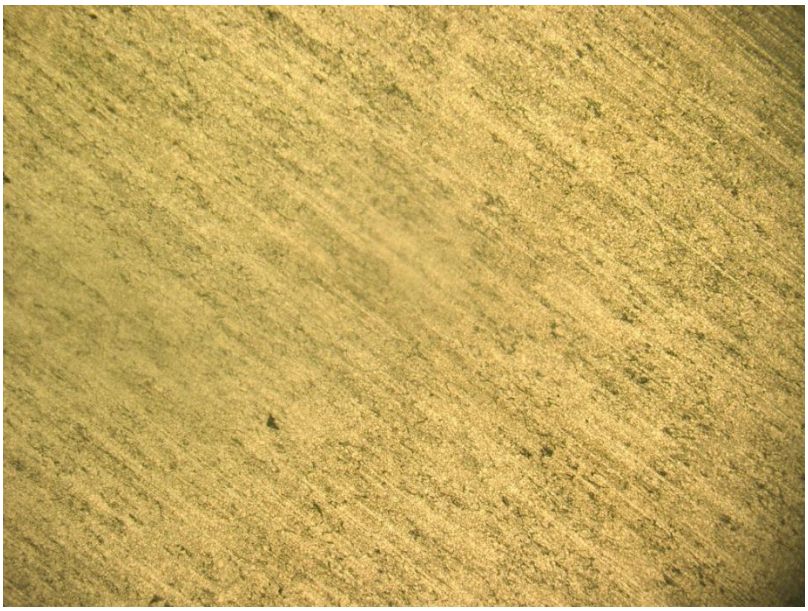

Min 0

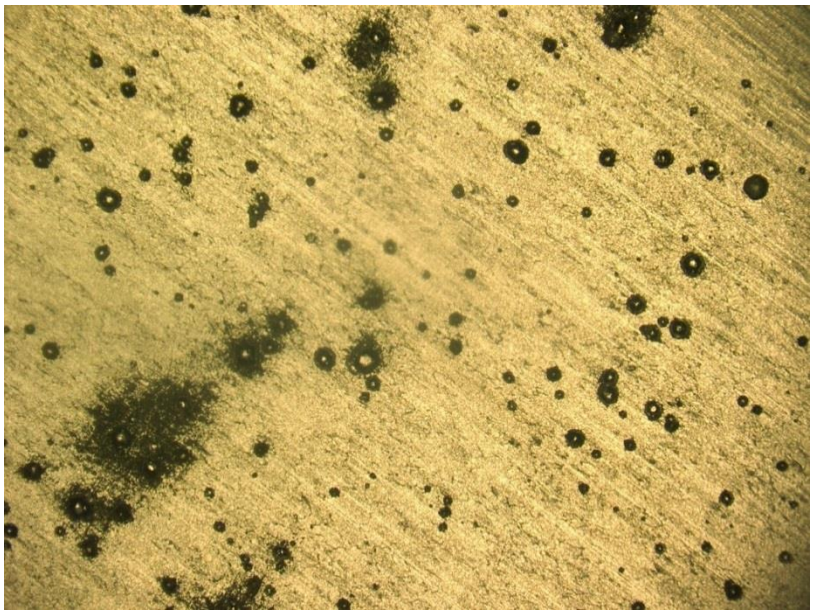

Min 15

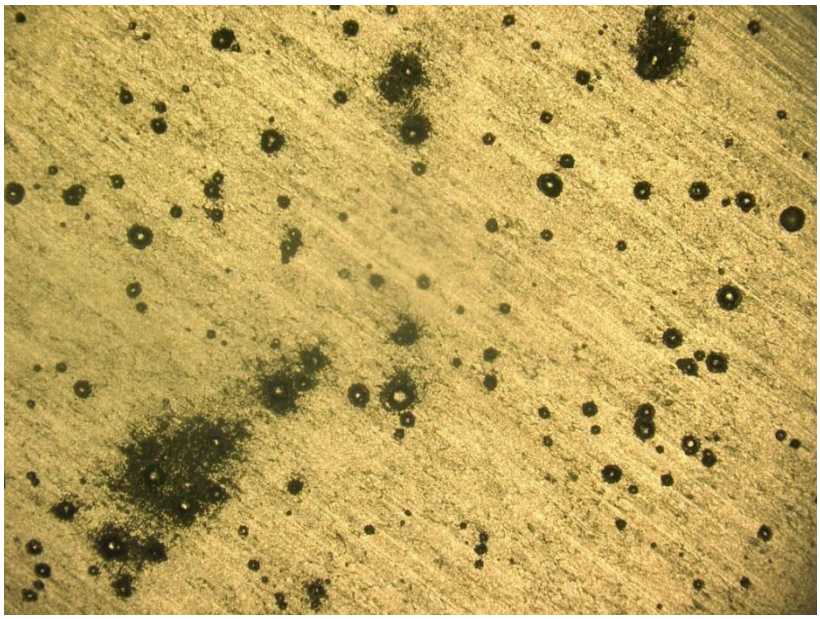

Min 30

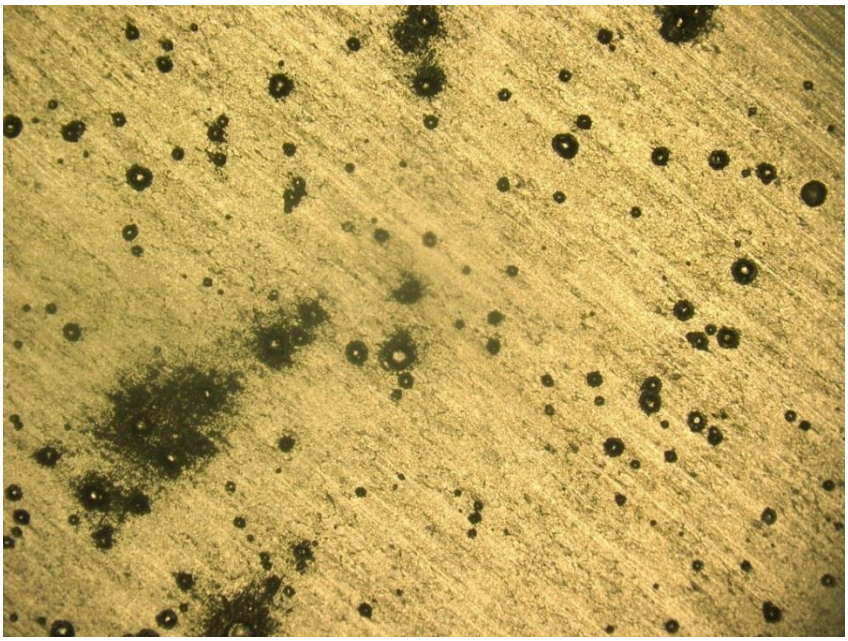

Min 45

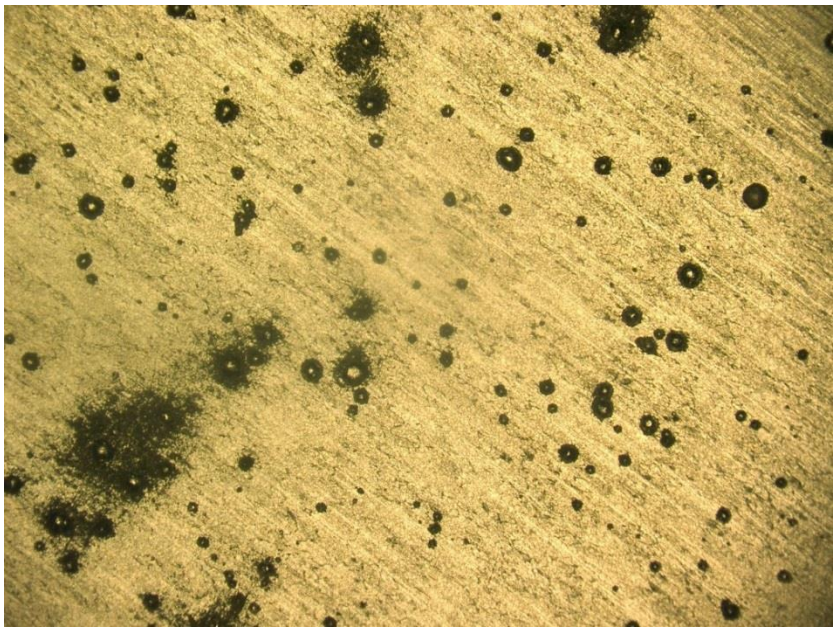

Min 60

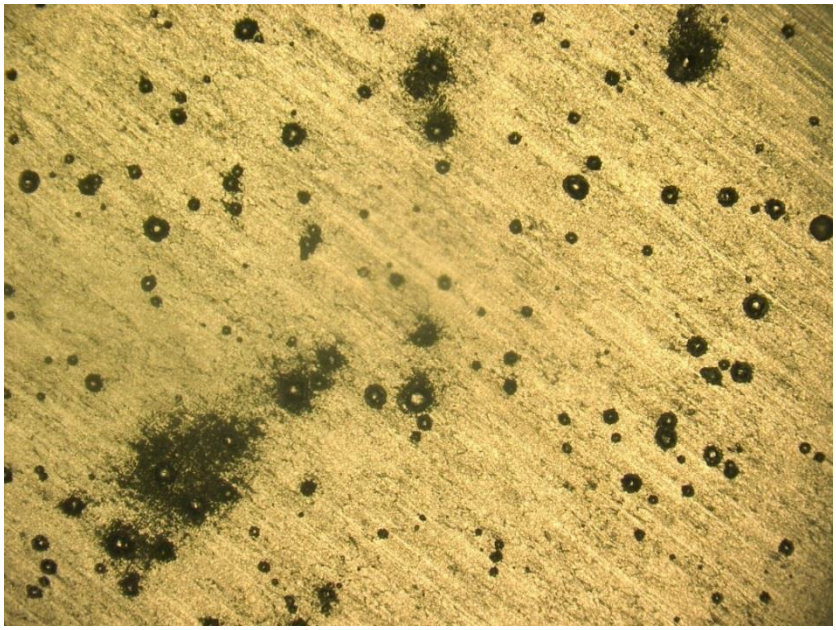

Min 75

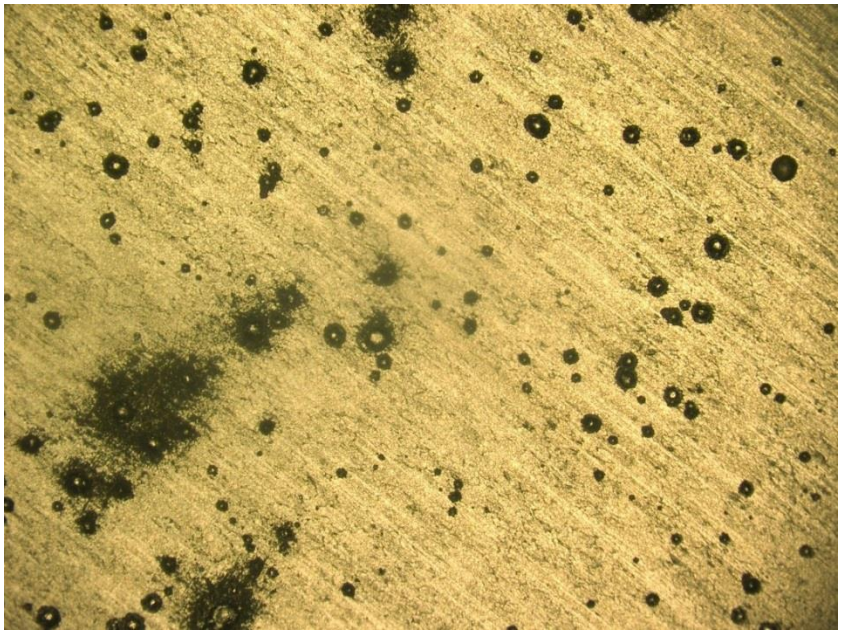

Min 90

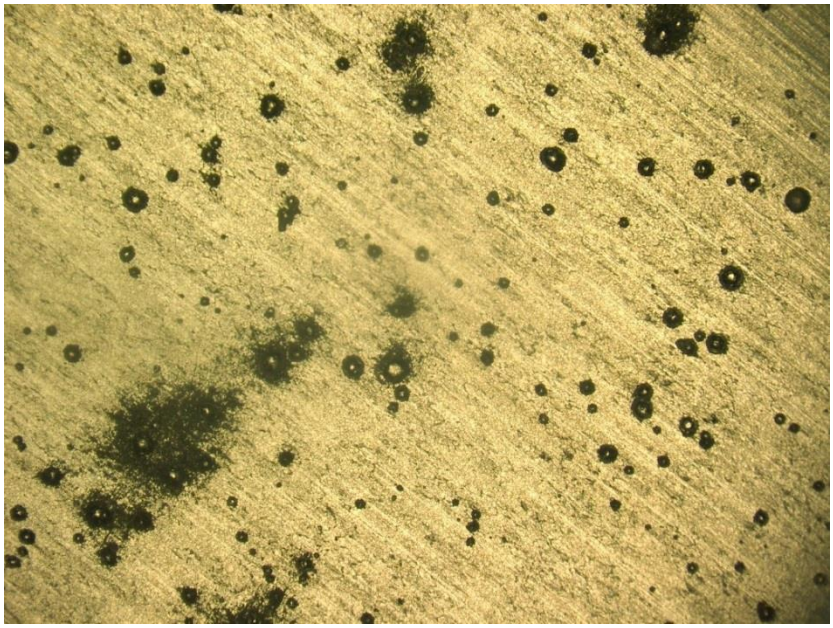

Min 105

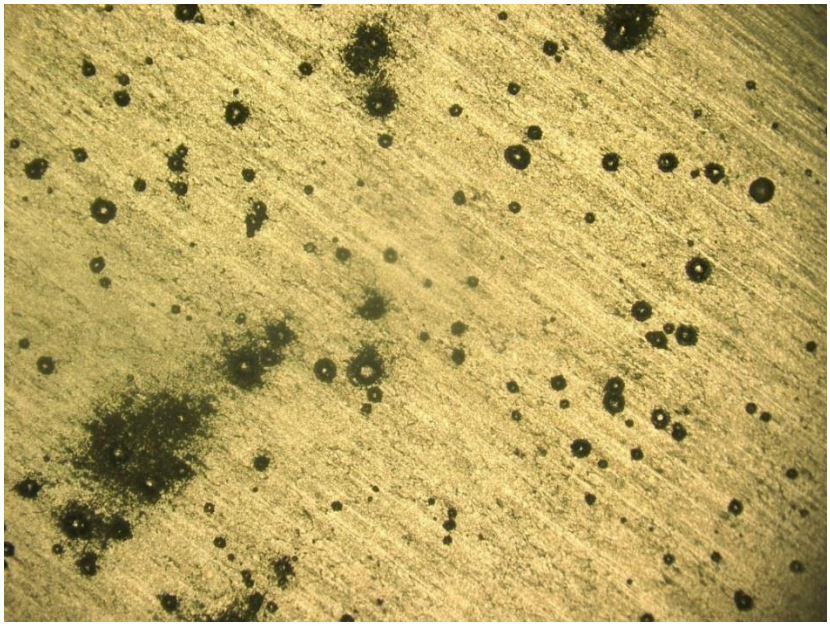

Min 135

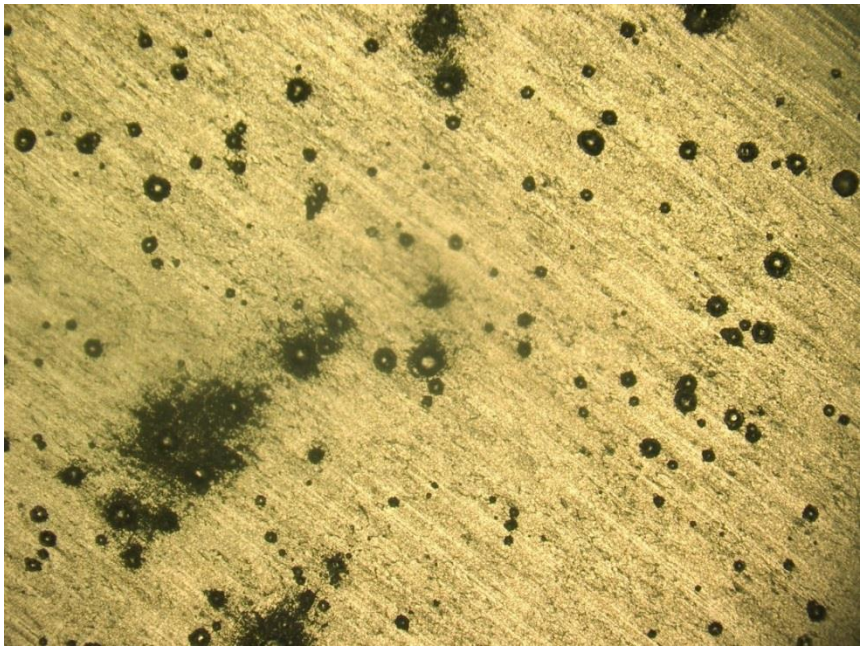

Min 165

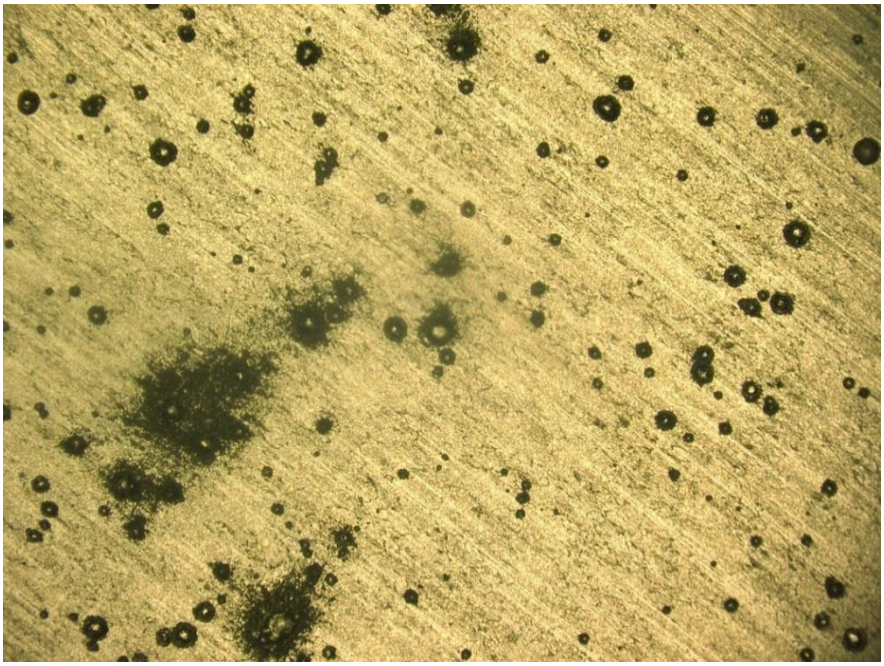

Min 195

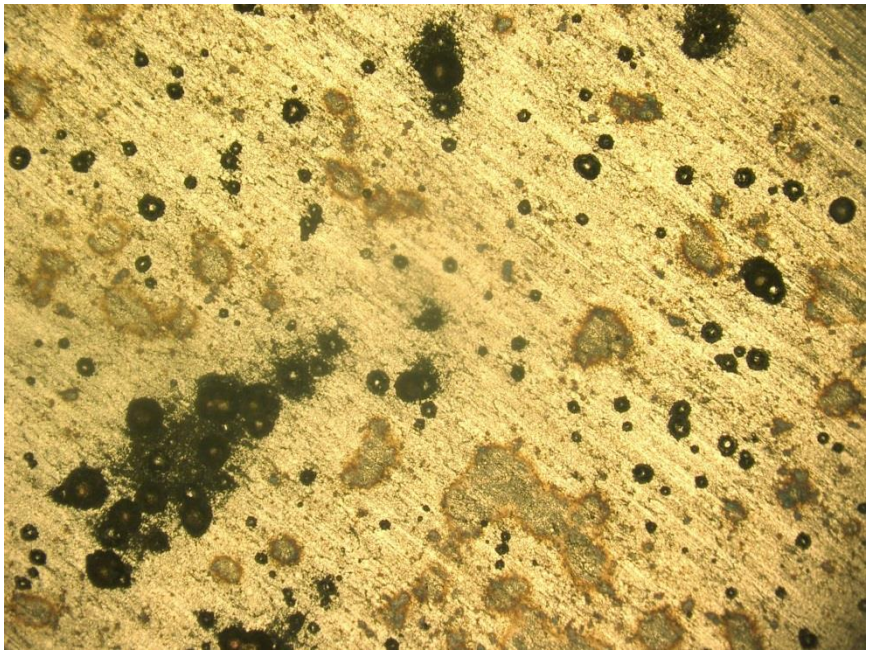

Min 225

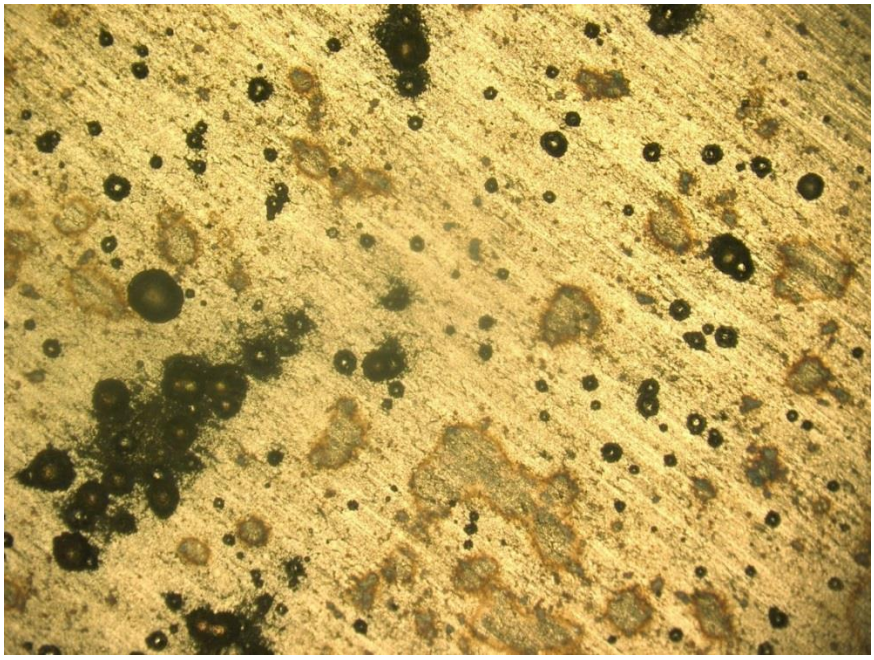

Min 255

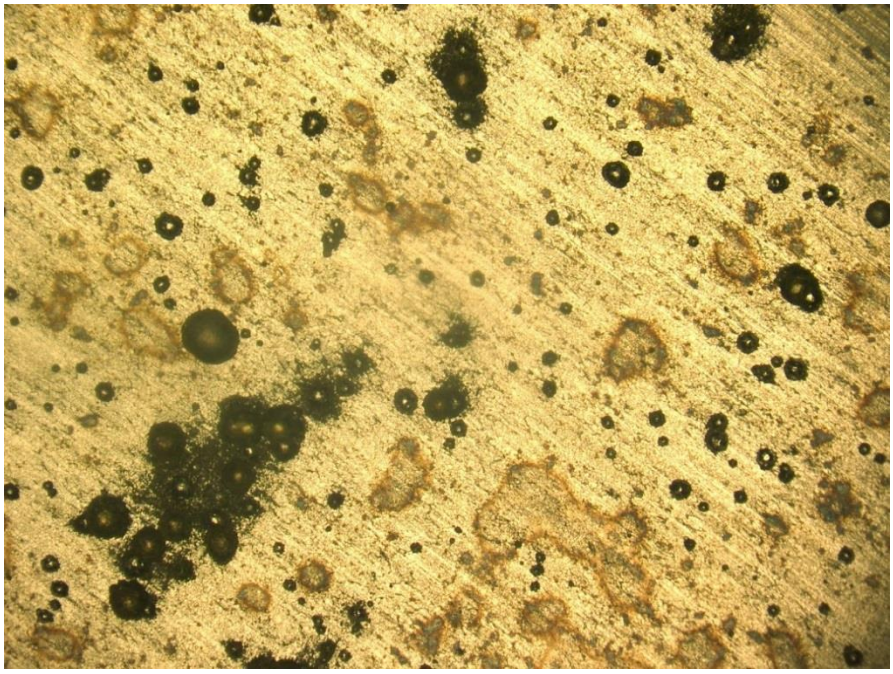

Min 285

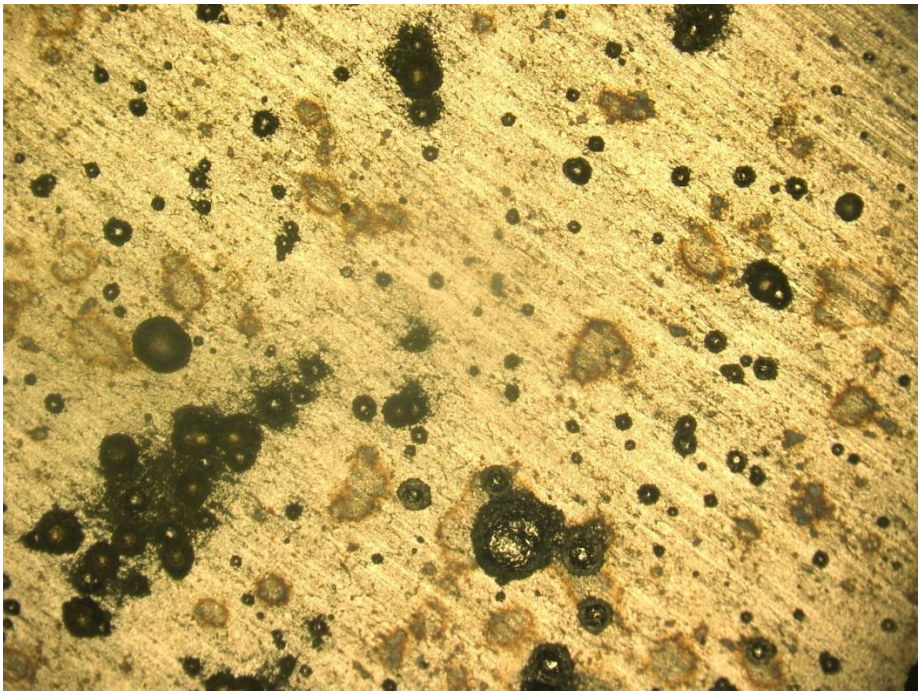

Min 315

Stainless steel SS 304 in Saturated NaCl solution experiment images

Day 0

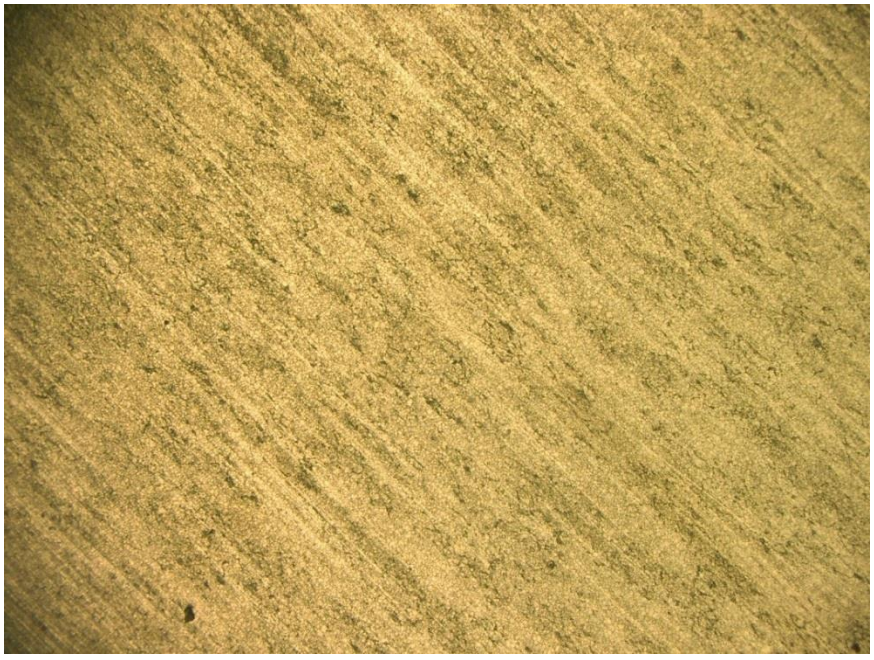

Day .02

Day 0.03

Day 0.08

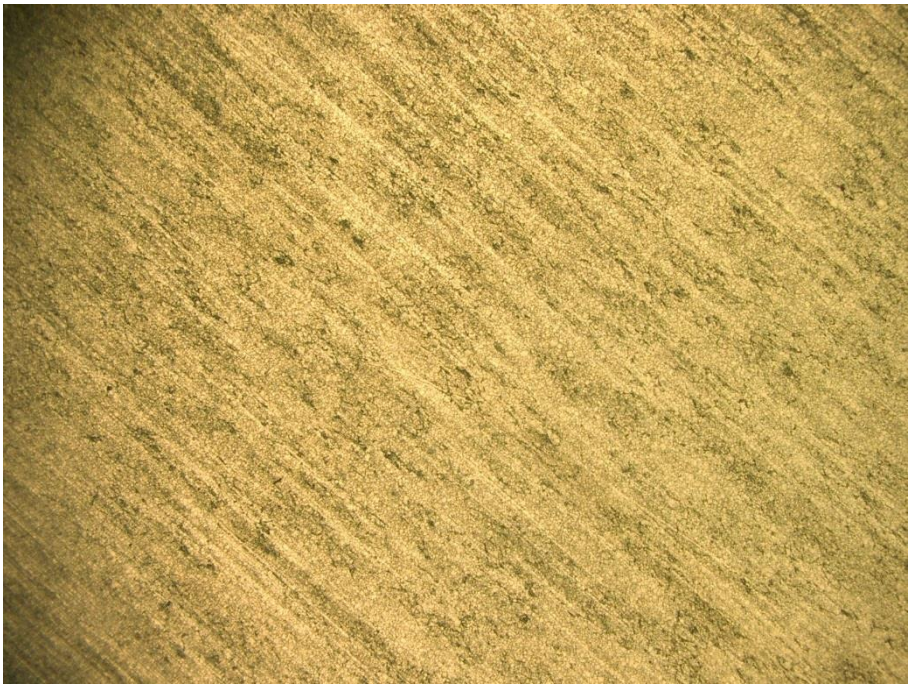

Day 0.16

Day 0.24

Day 3.24

Day 6.24

Day 11.24

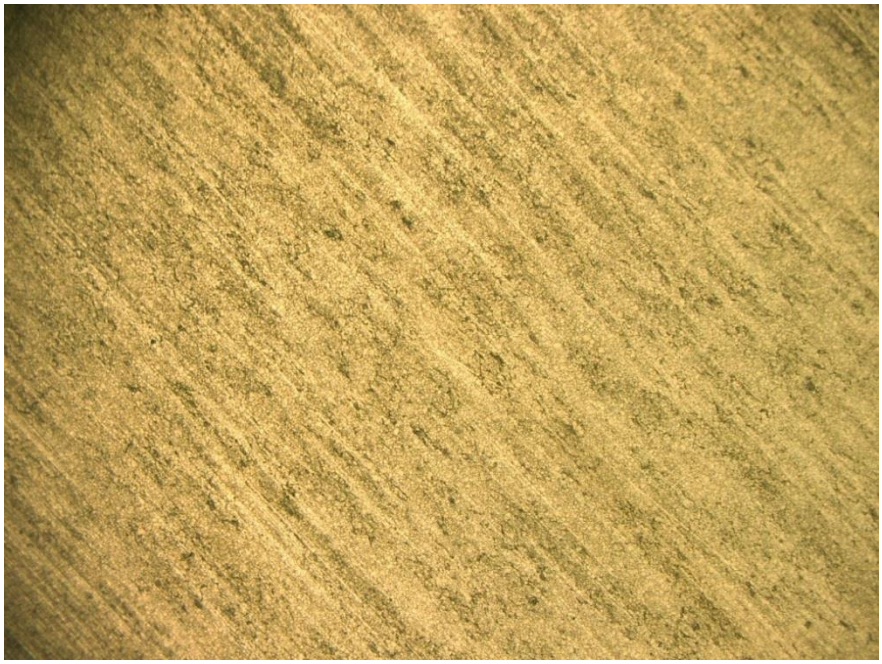

Day 19.24

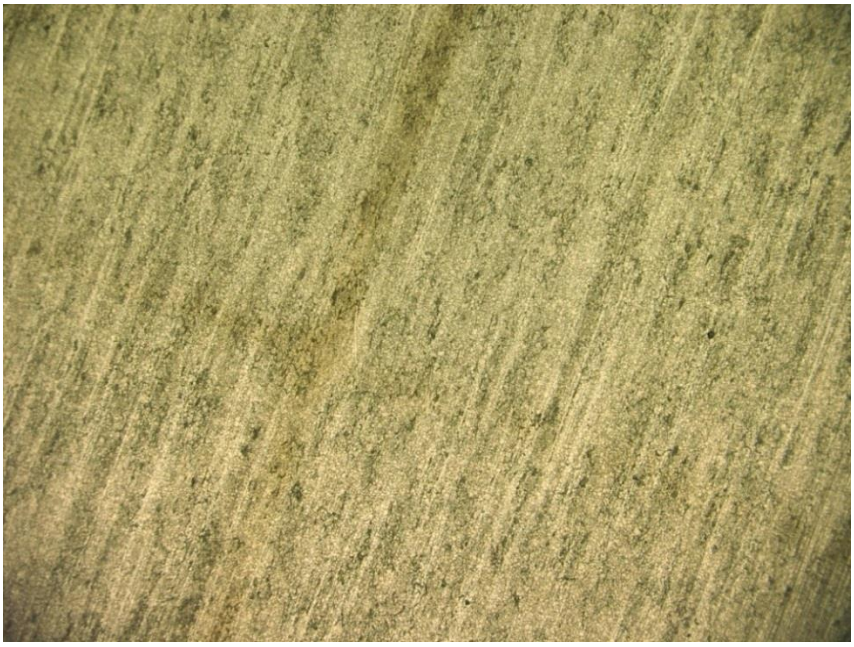

Day 29.24

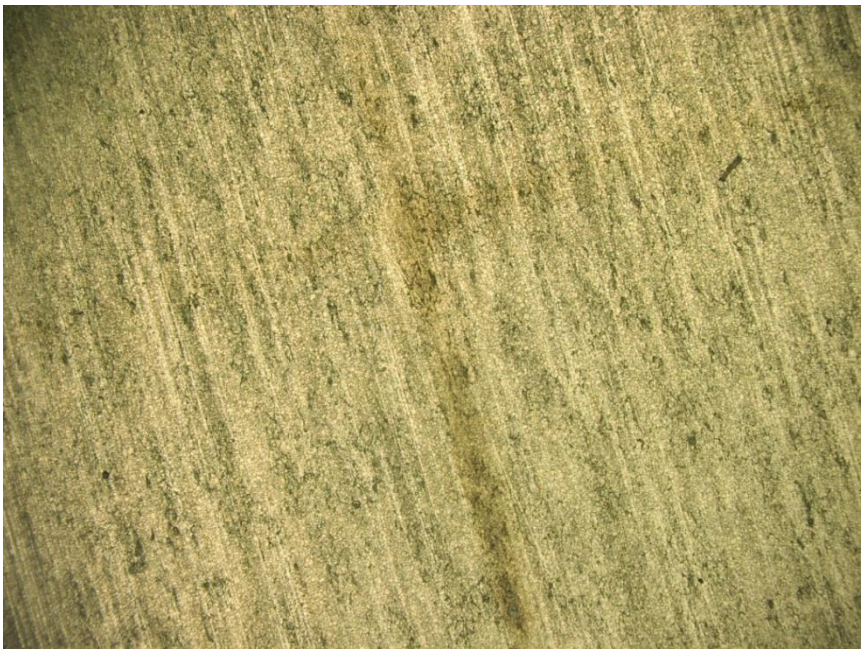

Day 41.24

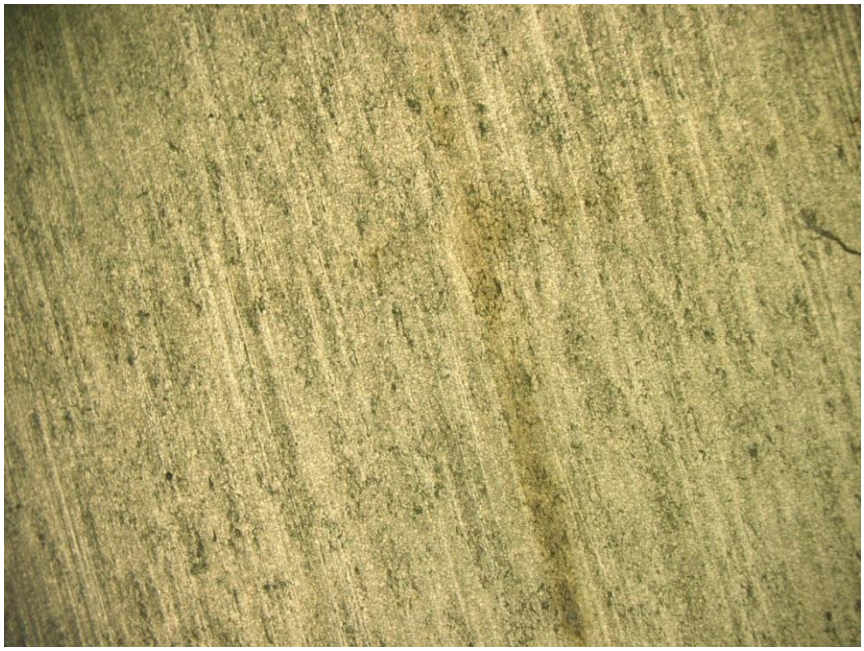

Day 55.24

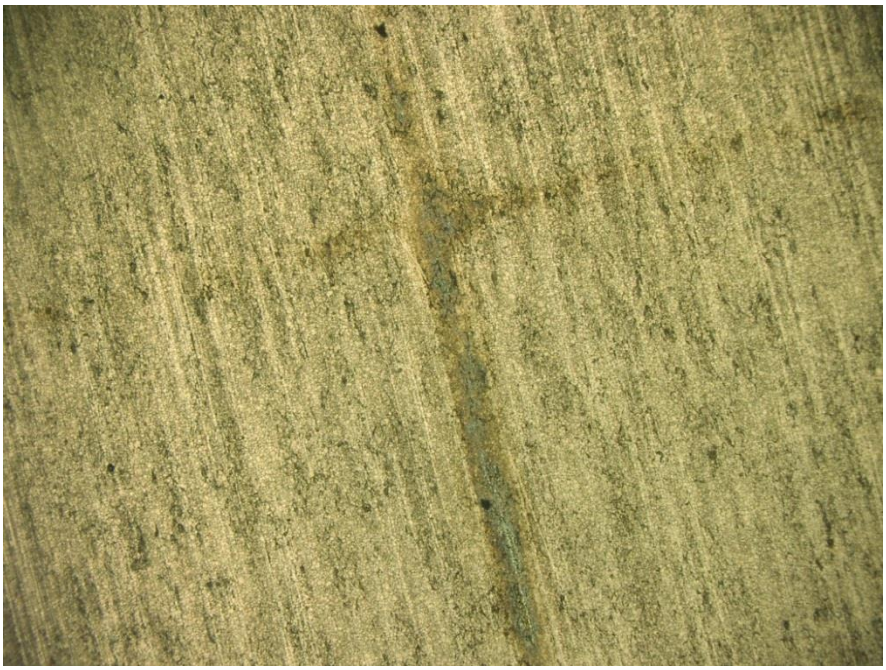

Day 81.24

Carbon steel QD1008 in distilled water experiment images

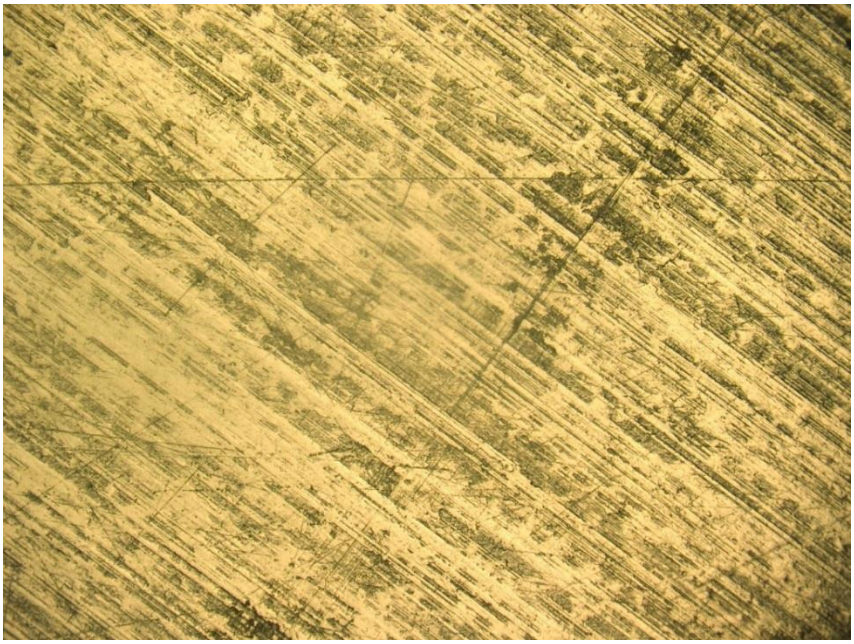

Day 0

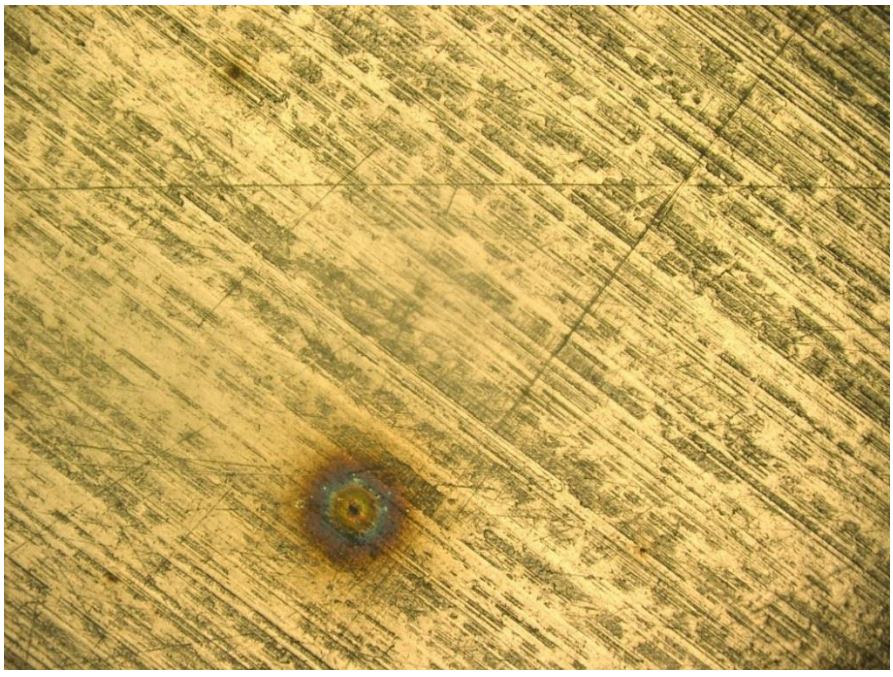

Day 0.01

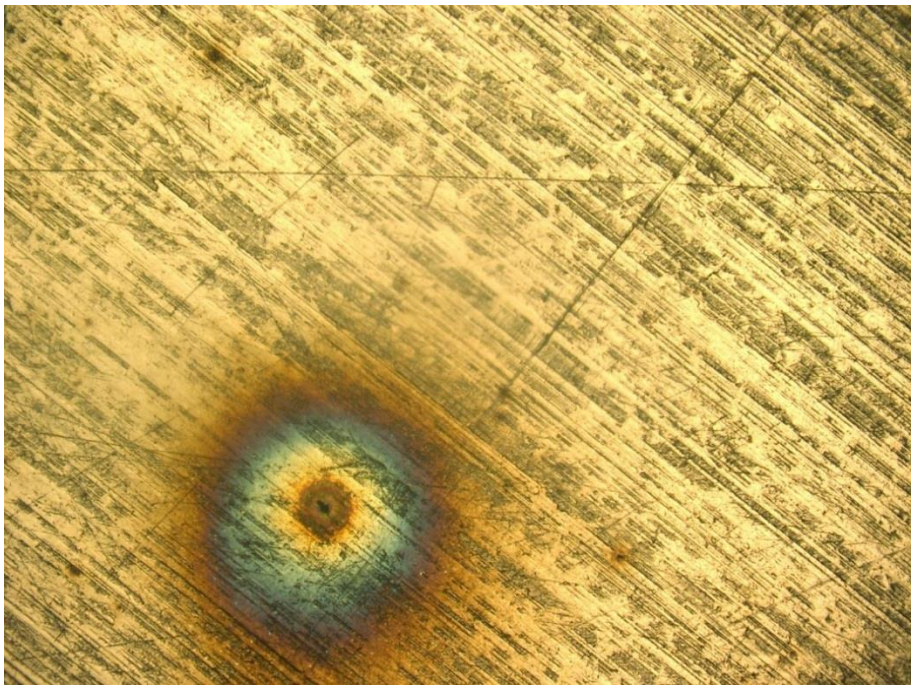

Day 0.02

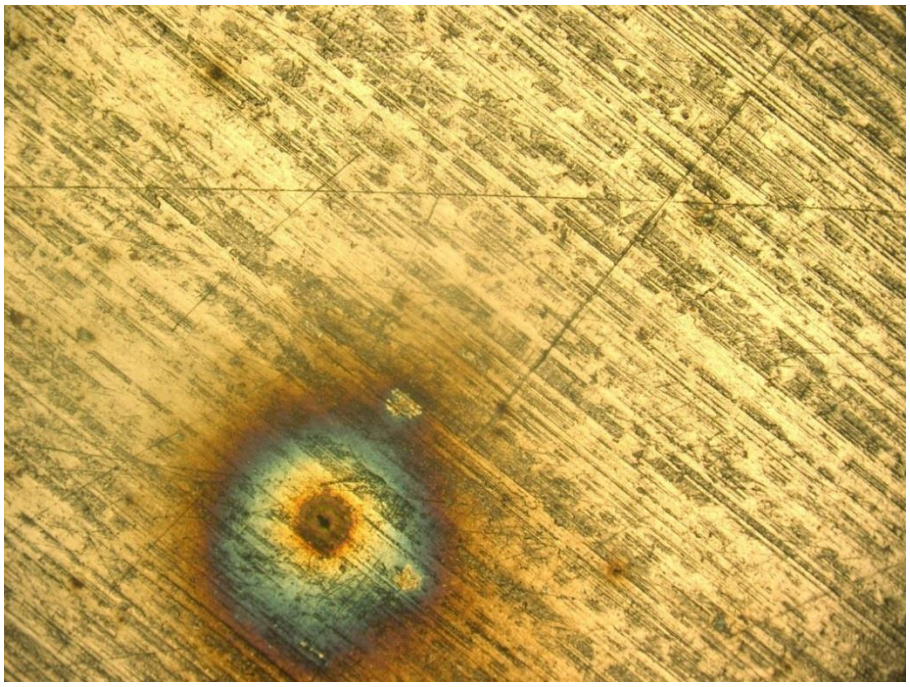

Day 0.03

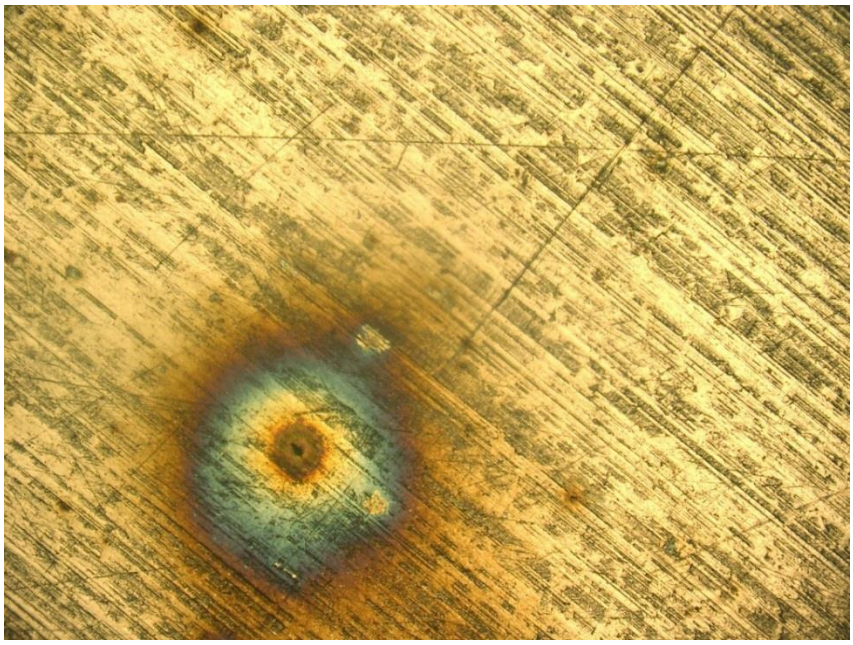

Day 0.04

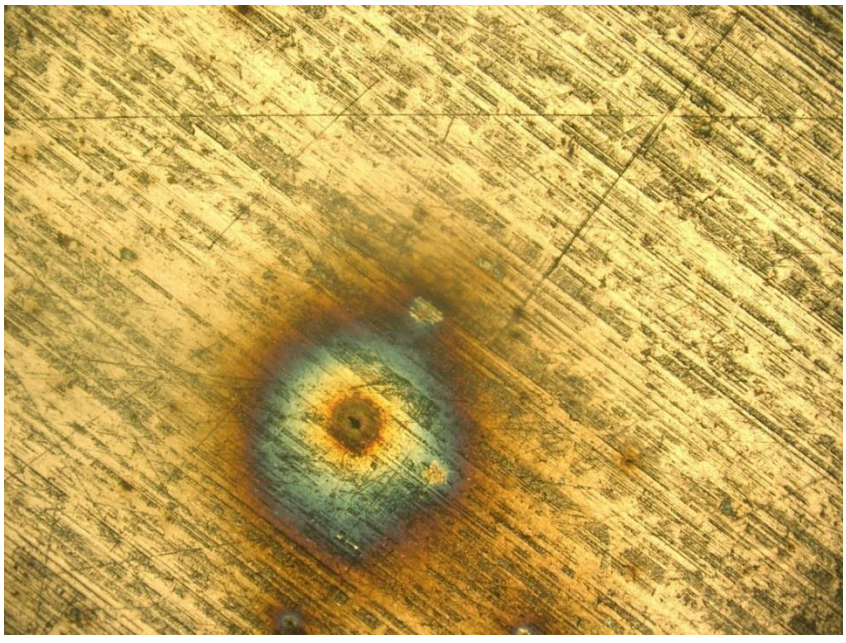

Day 0.06

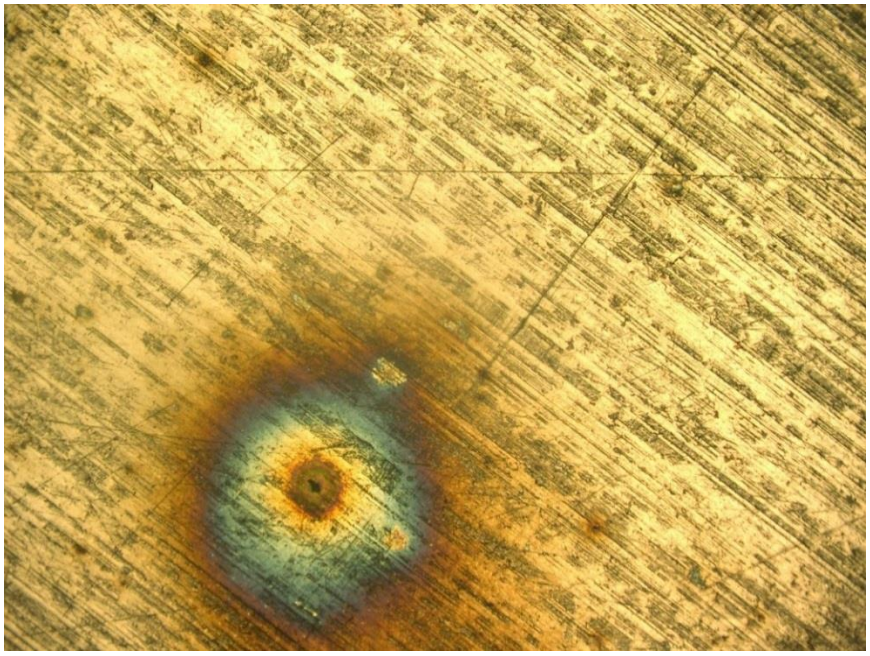

Day 0.08

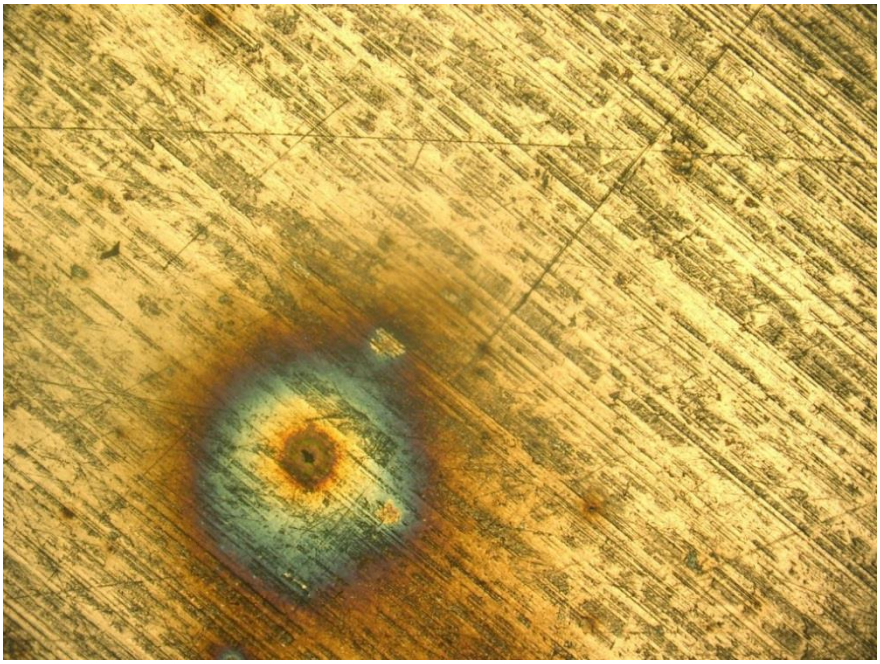

Day 0.1

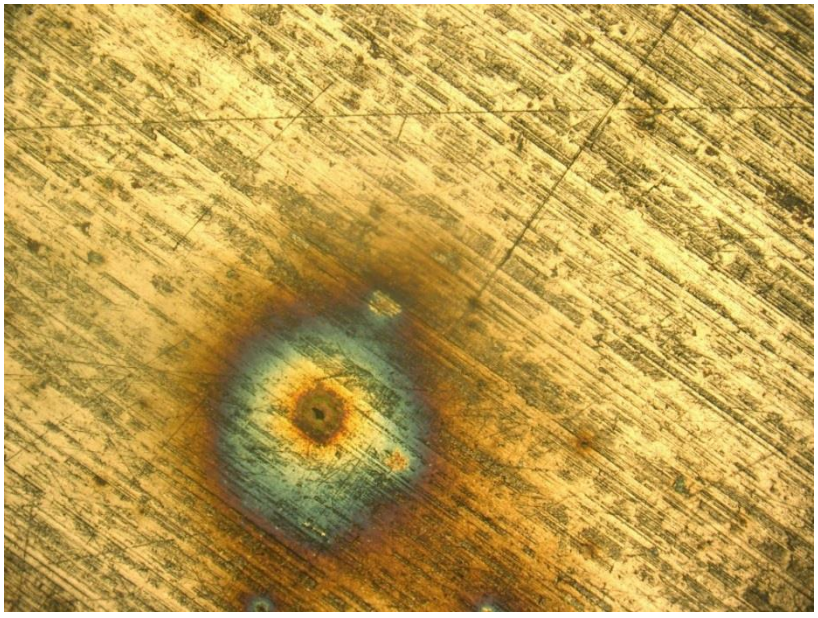

Day 0.12

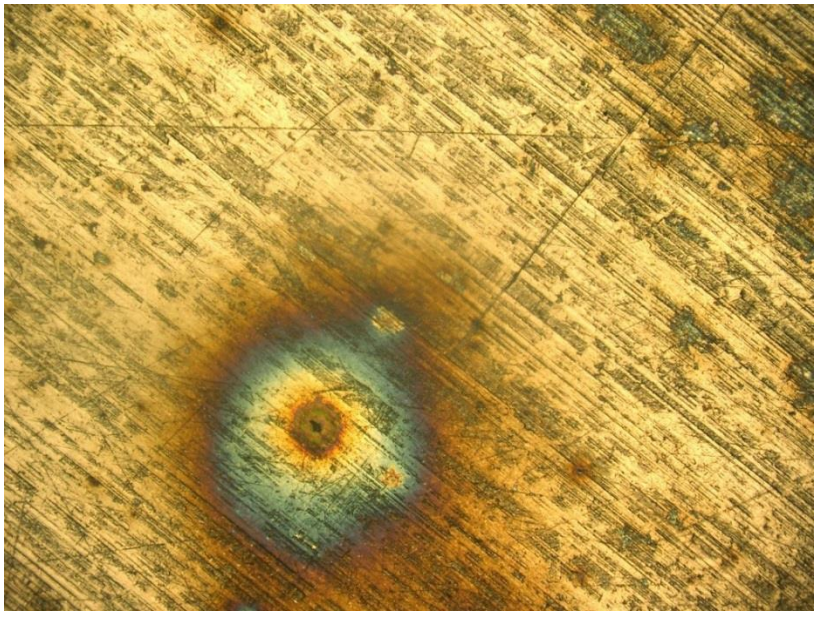

Day 0.14

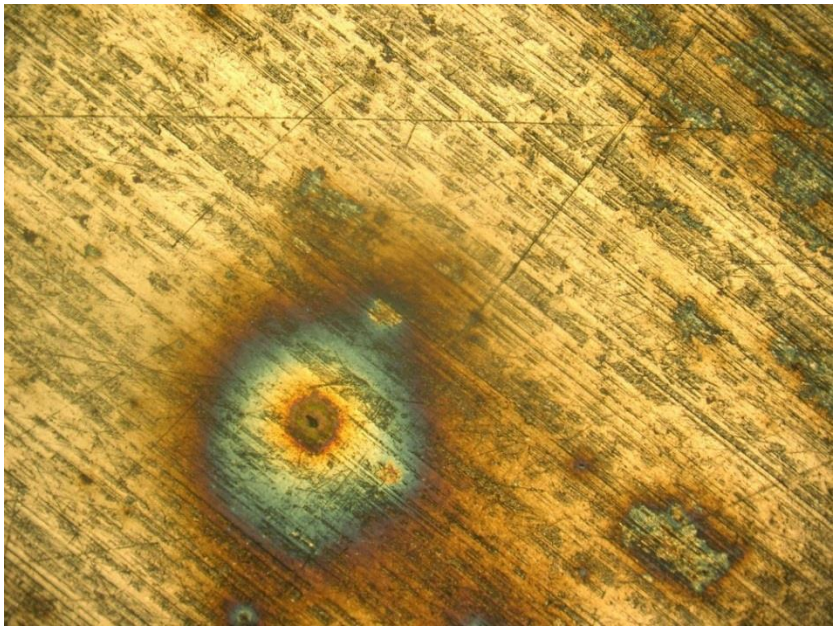

Day 0.16

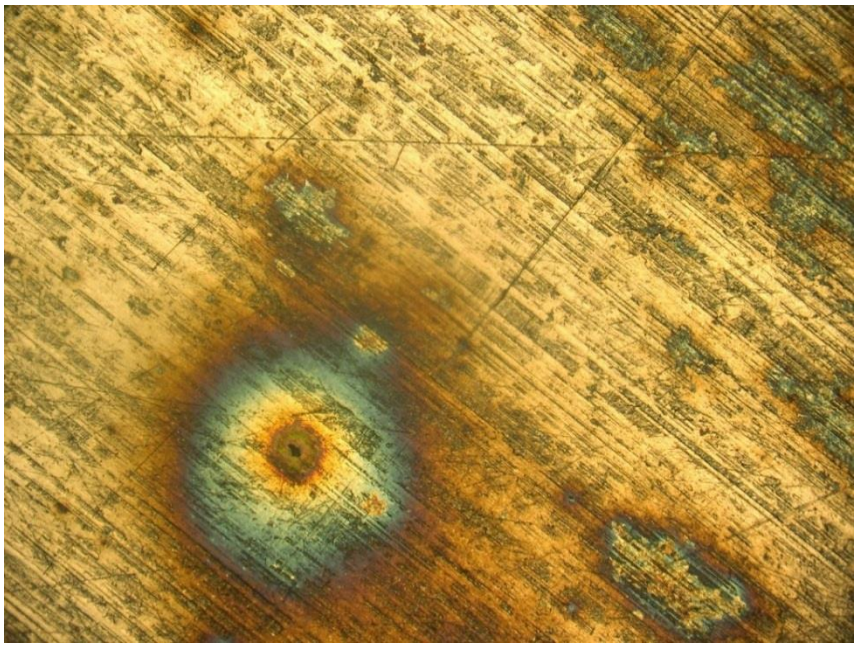

Day 0.18

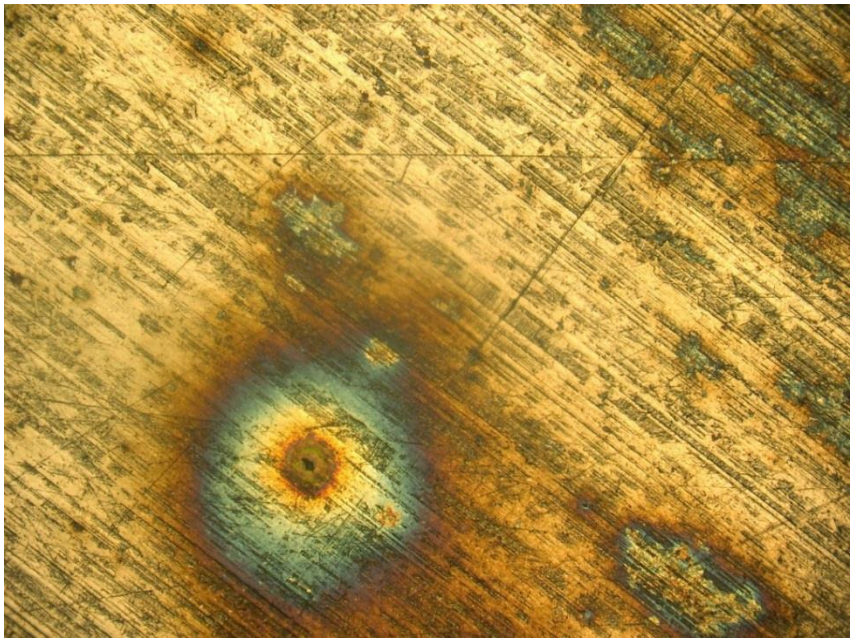

Day 0.22

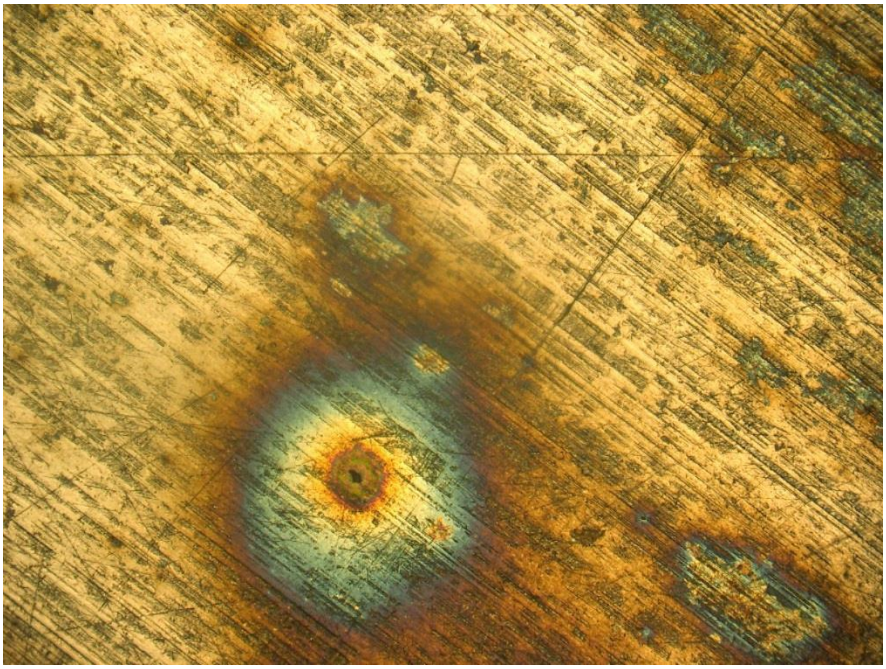

Day 0.3

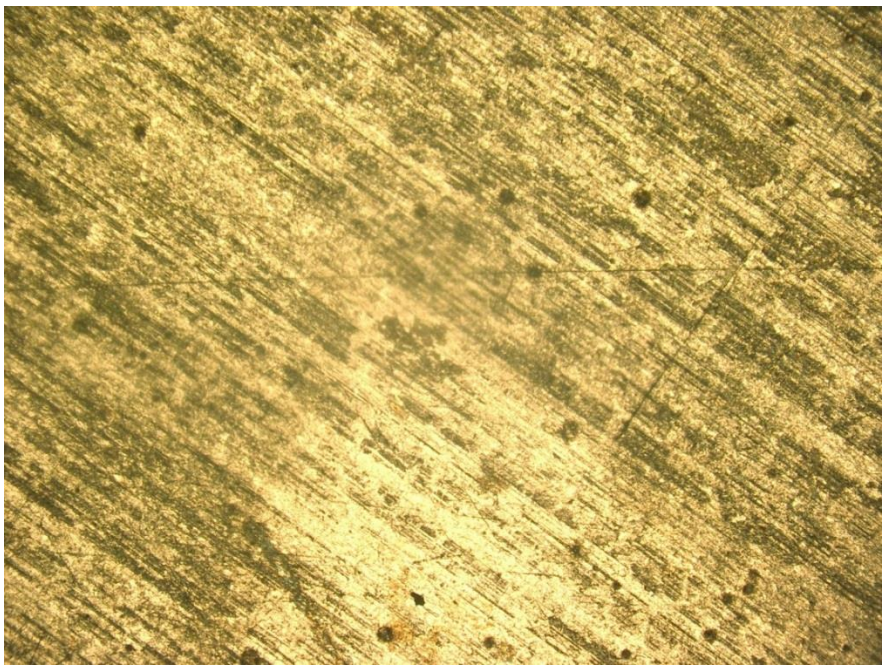

Day 2

Carbon steel QD1008 in Half-saturated NaCl experiment images

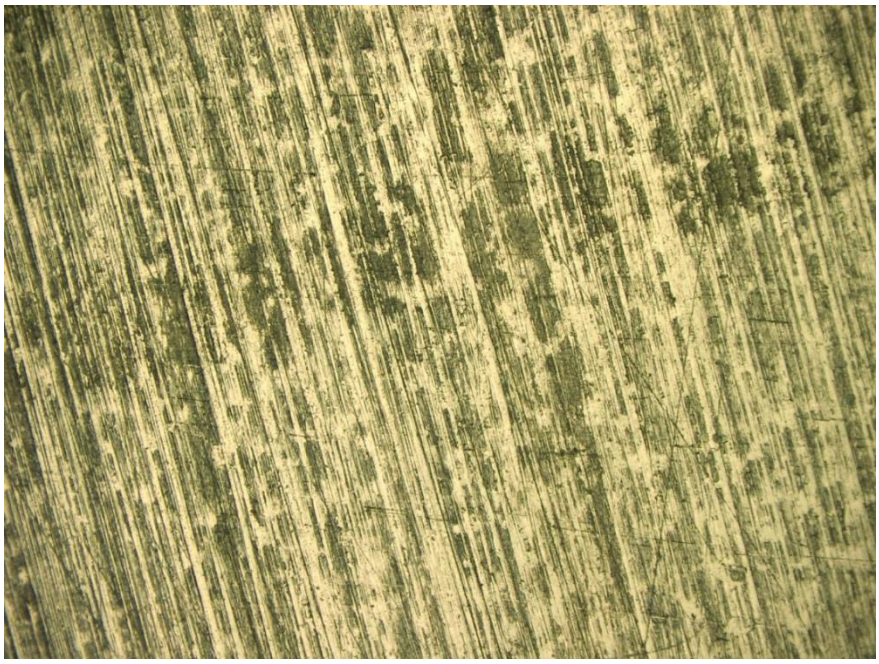

Day 0

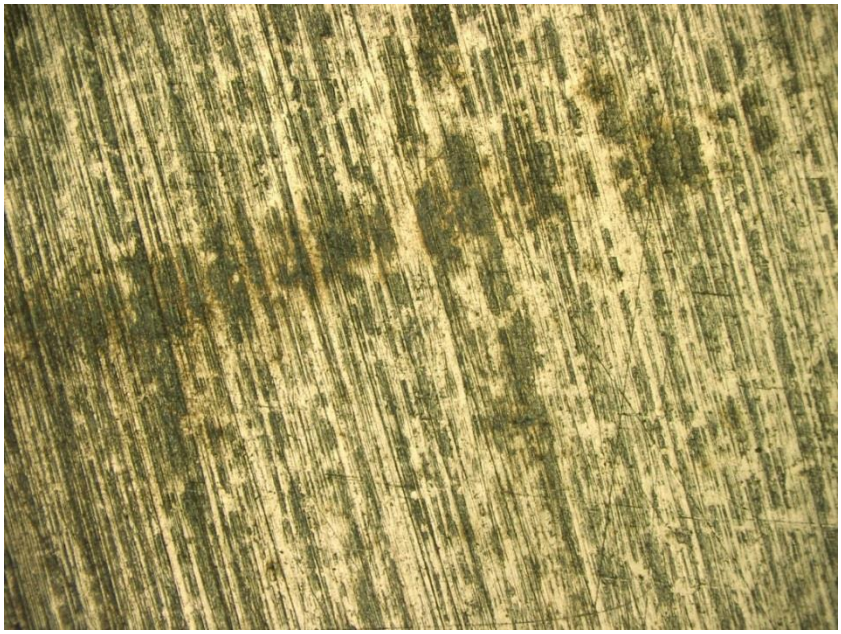

Day 0.02

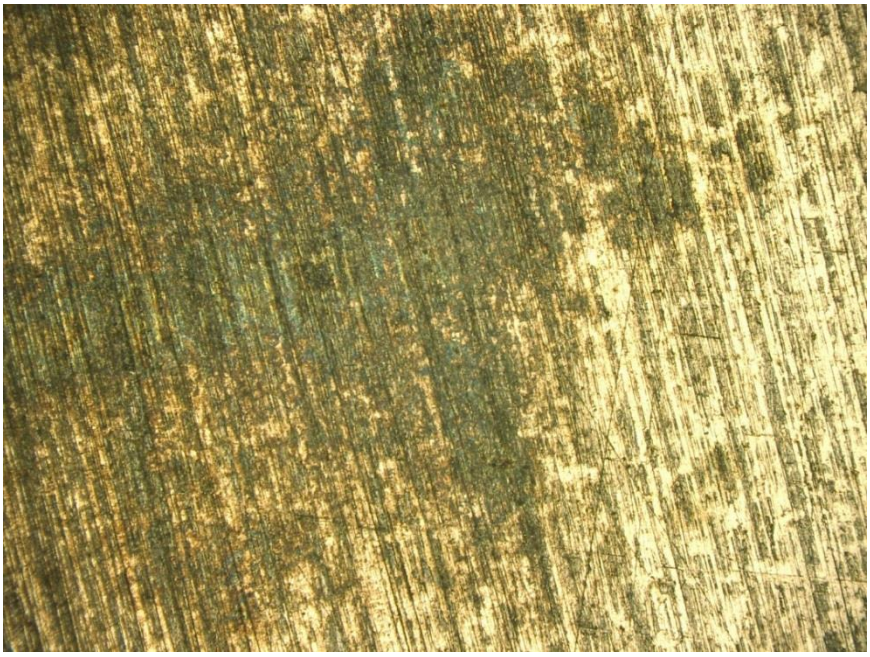

Day 0.04

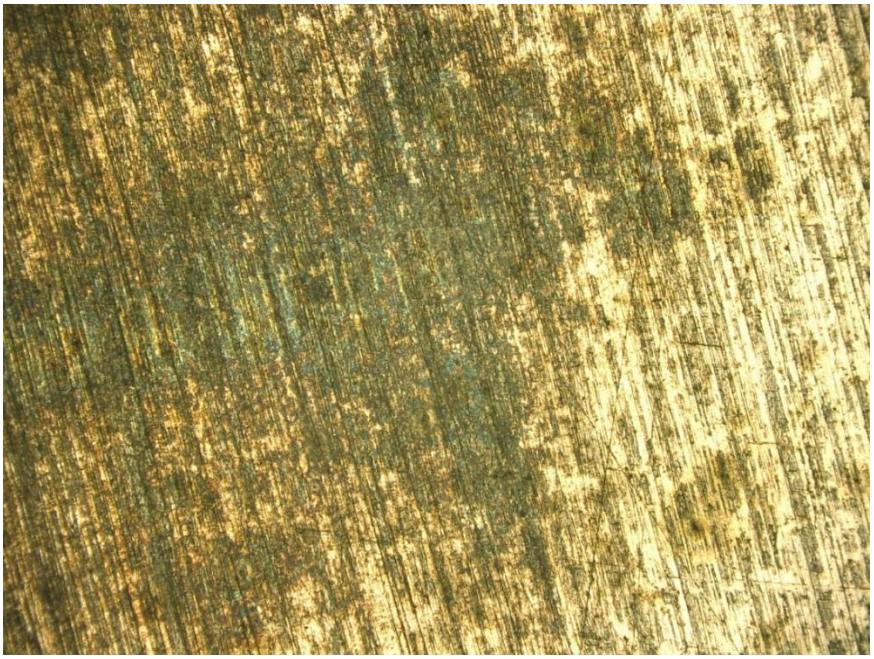

Day 0.06

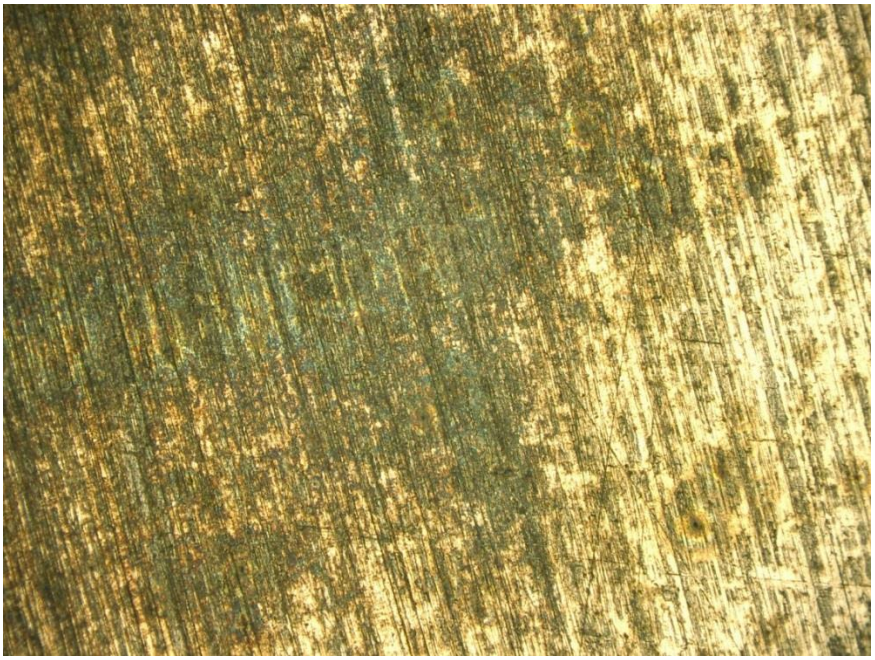

Day 0.1

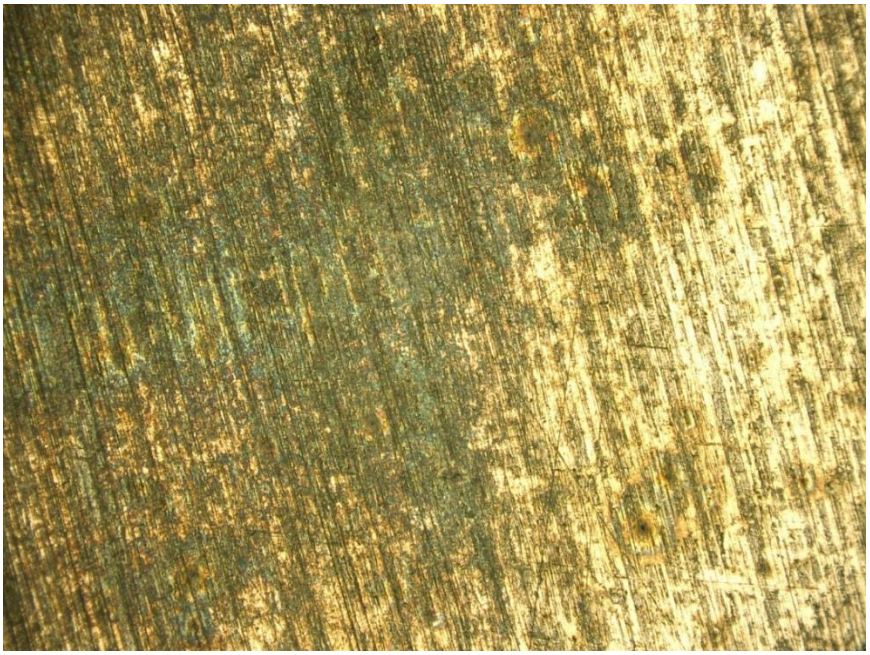

Day 0.14

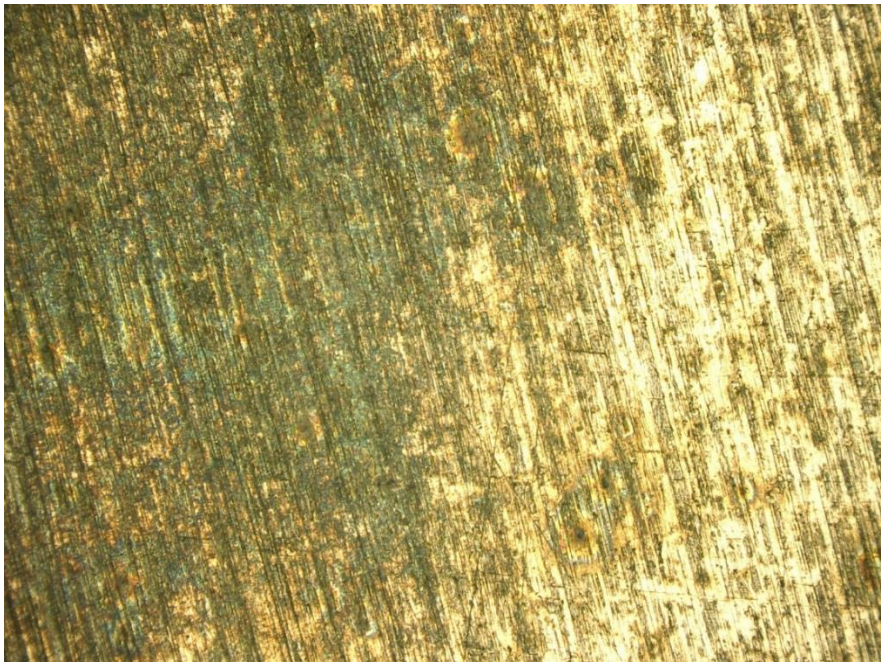

Day 0.18

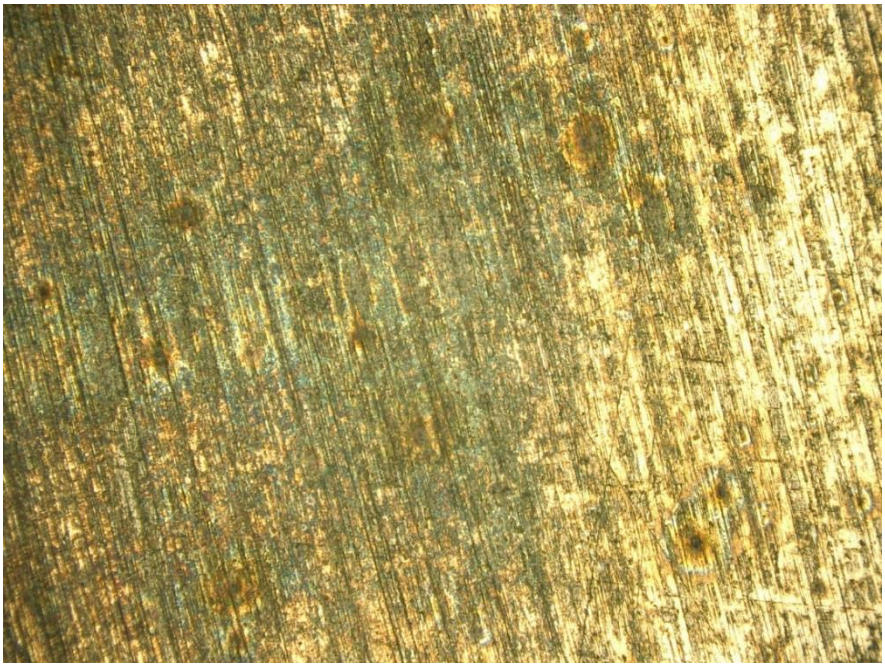

Day 0.22

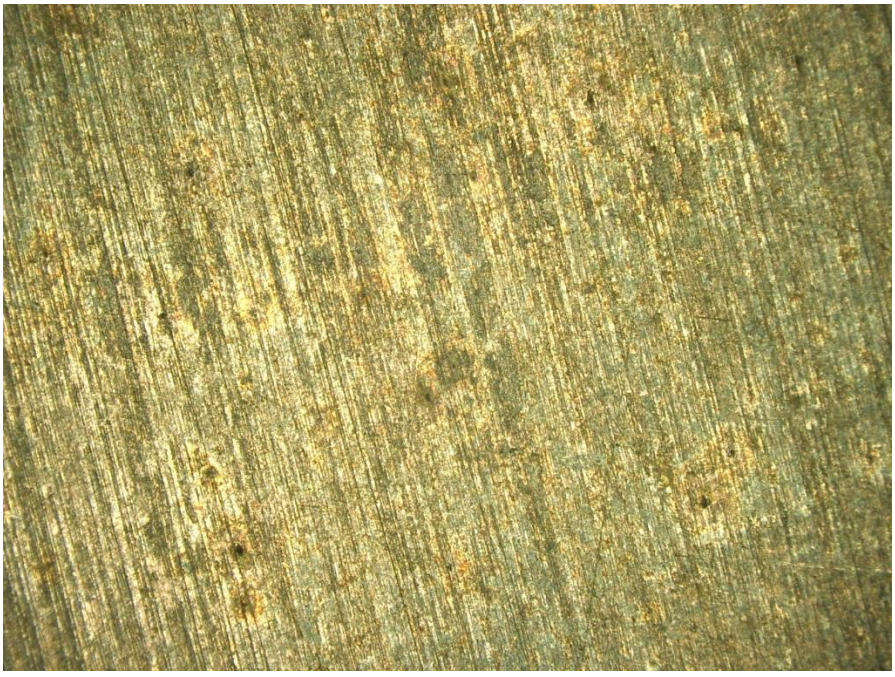

Day 3

Carbon steel QD 1008 in Saturated NaCl experiment images

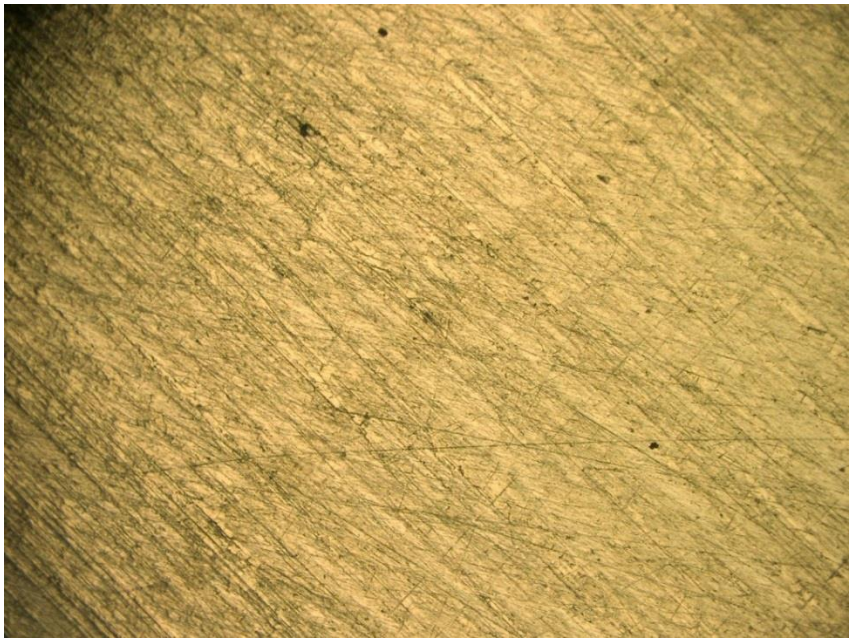

Day 0

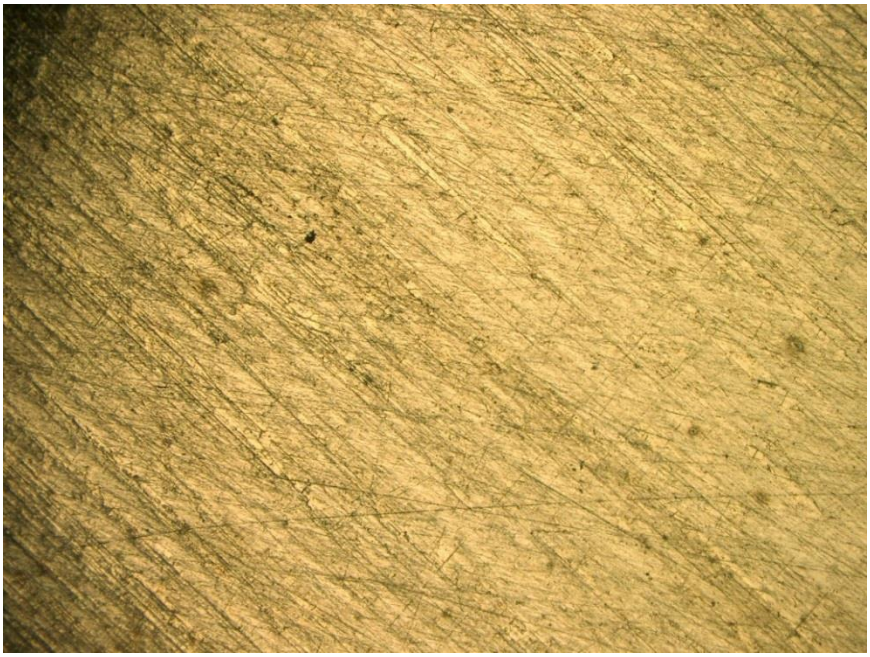

Day 0.01

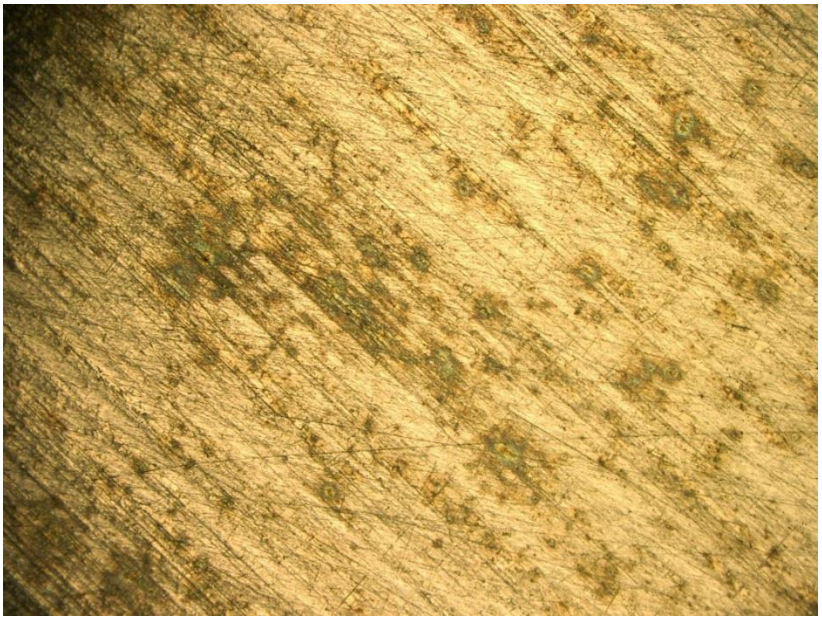

Day 0.02

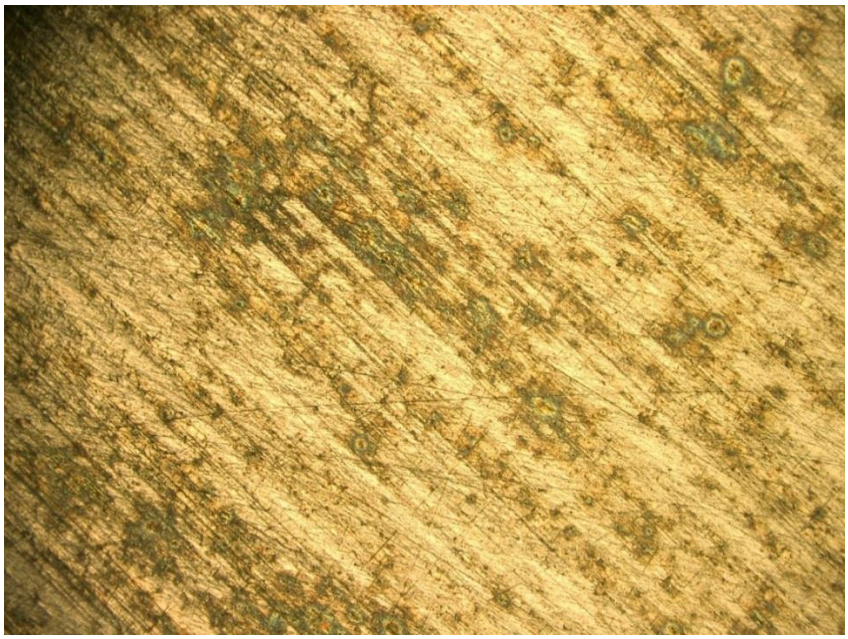

Day 0.03

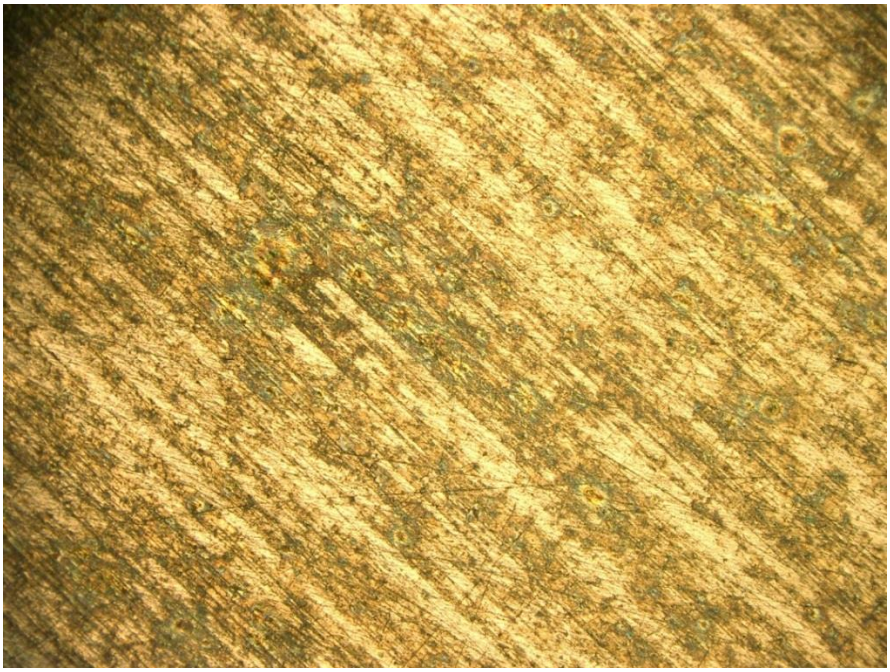

Day 0.07

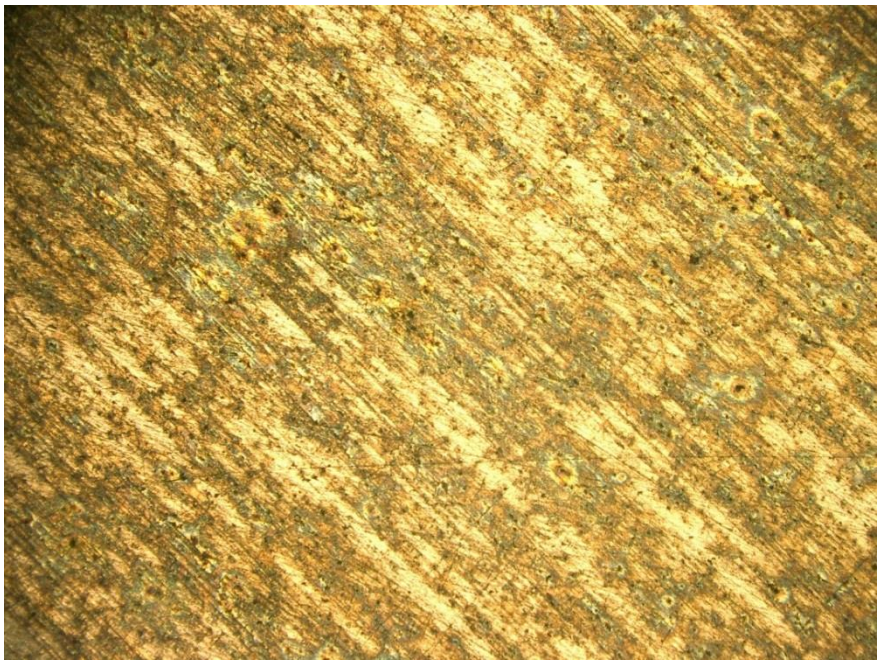

Day 0.15

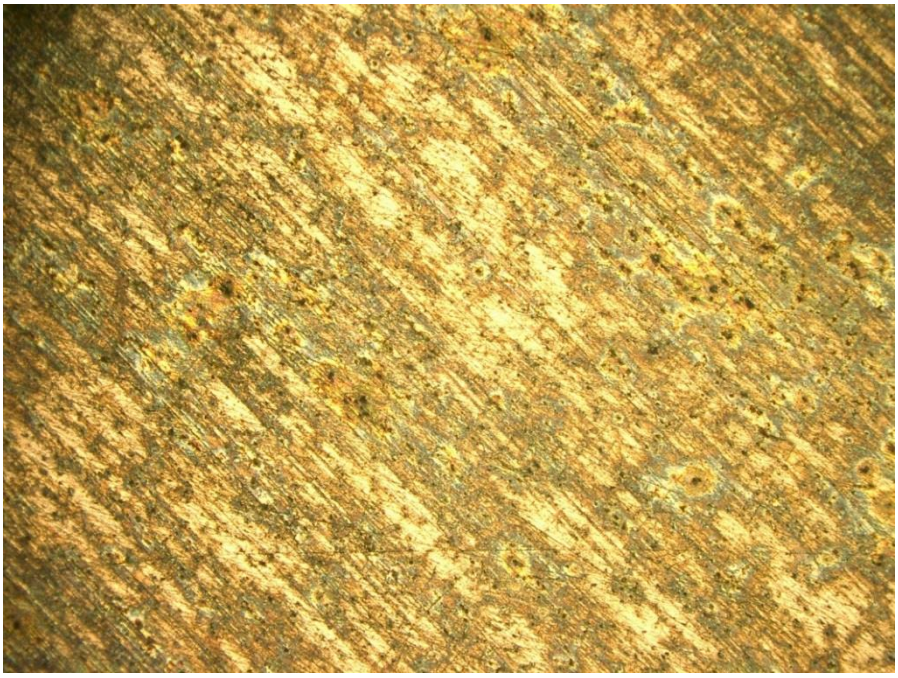

Day 0.23

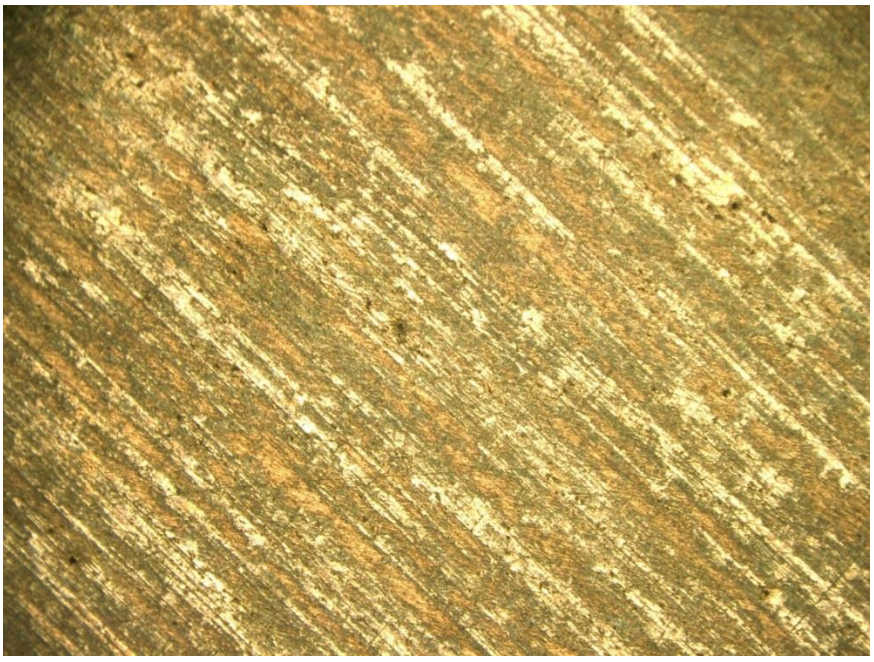

Day 3